



<https://theses.gla.ac.uk/>

Theses Digitisation:

<https://www.gla.ac.uk/myglasgow/research/enlighten/theses/digitisation/>

This is a digitised version of the original print thesis.

Copyright and moral rights for this work are retained by the author

A copy can be downloaded for personal non-commercial research or study, without prior permission or charge

This work cannot be reproduced or quoted extensively from without first obtaining permission in writing from the author

The content must not be changed in any way or sold commercially in any format or medium without the formal permission of the author

When referring to this work, full bibliographic details including the author, title, awarding institution and date of the thesis must be given

Enlighten: Theses

<https://theses.gla.ac.uk/>
research-enlighten@glasgow.ac.uk

An Analytical Investigation of Vortex Breakdown

by

Stephen G. Bryce, B.Sc.

Dissertation submitted to the Faculty of Engineering, University of
Glasgow, for the Degree of Doctor of Philosophy

December, 1987

© S.G. Bryce, 1987

ProQuest Number: 10970802

All rights reserved

INFORMATION TO ALL USERS

The quality of this reproduction is dependent upon the quality of the copy submitted.

In the unlikely event that the author did not send a complete manuscript and there are missing pages, these will be noted. Also, if material had to be removed, a note will indicate the deletion.



ProQuest 10970802

Published by ProQuest LLC (2018). Copyright of the Dissertation is held by the Author.

All rights reserved.

This work is protected against unauthorized copying under Title 17, United States Code
Microform Edition © ProQuest LLC.

ProQuest LLC.
789 East Eisenhower Parkway
P.O. Box 1346
Ann Arbor, MI 48106 – 1346

Contents

	Acknowledgements	i
	Abstract	ii
	Nomenclature	iv
Chapter 1	The Breakdown of Slender Wing Leading Edge Vortices	1
1.0	Introduction	1
1.1	The Slender Wing Flowfield	3
1.2	The Vortex Breakdown Flowfield	5
1.3	A Review of Theoretical Research	10
1.4	Catastrophe Theory	16
1.5	Computational Fluid Dynamics (C.F.D.)	18
1.6	Project Guidelines	20
Chapter 2	A Review of Existing Theoretical Models for the Flow Over a Delta Wing	21
2.0	Model Requirements	21
2.1	Slender Potential Models	22
2.2	Non-Slender Potential Models	32
2.3	Modelling the Vortex Core	35
2.4	The Method of Luckring: A Comprehensive Model for the Leading Edge Vortex	41
2.5	Survey Conclusions	43

Chapter 3	Development of the Flow Model	44
3.0	Introduction	44
3.1	The Point Vortex Model	46
3.2	Point Vortex Solution Method and Results	51
3.3	Selection of an Alternative Crossflow Model	53
3.4	The Vortex-Sink Model	54
3.5	Vortex-Sink Solution Method and Results	58
3.6	Modification of the Vortex-Sink Model	64
3.7	Conical Flow	67
3.8	Non-Conical Flow	69
3.9	Extension of the Model into Three Dimensions	78
3.10	A Summary of the Flow Model	81
Chapter 4	Application of the Flow Model to Vortex Breakdown Investigation	83
4.0	Introduction	83
4.1	The Test Case	85
4.2	The Investigative Procedure	89
4.3	Summary of the Flow Investigation	96
Chapter 5	Prospects for the Control of Vortex Breakdown	98
5.0	Introduction	98
5.1	Determination of the b_i - vs - α boundary curves	99
5.2	Applications of Leading Edge and Spanwise Blowing	101
5.3	Interpretation of Blowing and MODEL3D Results	106
5.4	Summary of Control Prospects	109

Chapter 6	Summary and Conclusions	110
	Appendices	115
Appendix 1	Laser Doppler Velocimetry	115
Appendix 2	Catastrophe Theory	119
Appendix 3	The Transformation from the Wing (Z) Plane to the Cylinder (Z_1) Plane	122
Appendix 4	Determination of the Governing Complex Potential in the Z_1 Plane for the Point Vortex Model	123
Appendix 5	Determination of the Stationary Vortex Boundary Condition	124
Appendix 6	Reduction of the Kutta Condition for the Point Vortex Model to One Real Equation	128
Appendix 7	Determination of the Stationary Vortex-Sink Boundary Condition	130
Appendix 8	Reduction of the Kutta Condition for the Vortex-Sink Model to One Real Equation	133
Appendix 9	The Non-Dimensional Form of the Kutta Condition for the Vortex-Sink Model	135
Appendix 10	Force Balance on the Vortex-Sink-Feeding Sheet Element	137
Appendix 11	A Conical Simplification of the Vortex-Sink- Feeding Sheet Force Balance	140
	References	141
	Tables	
	Figures	

Acknowledgements

The author wishes to express his gratitude to Professor Bryan Richards for his supervision of this work, to Mr. Stuart McDougall of British Aerospace Naval Weapons Division for his assistance as external supervisor, and to his parents for continued support and encouragement. Thanks also to my colleagues in J421 for their advice and sense of humour. The contributions of the following individuals are gratefully acknowledged:

Mr. David Pirie	}	Department of Aeronautics and Fluid Mechanics
Mr. Roy Bradley		
Miss Margaret Simpson		
Mrs. Linda M ^C Cormick	}	Computer Aided Engineering Centre
Mrs. Carol Carmichael		
Prof. R. Ogden	}	Department of Mathematics
Dr. A. Spence		
Mr. Stan Bizon	}	British Aerospace Naval Weapons Division, Bristol
Dr. Paul Dexter		
Mr. Bob Bignell		
Mr. J.H.B. Smith		R.A.E. Farnborough
Dr. Iain Stewart		Department of Mathematics, Warwick University
Mr. Stephan Hitzel		Dornier Aircraft Company Friedrichshafen, FRG

This work was funded by a Science and Engineering Research Council CASE award, in collaboration with British Aerospace Naval Weapons Division, Bristol.

Abstract

It is well-known that the separation of flow from the leading edges of a highly swept wing at a high angle of attack results in the creation of a well-ordered vortical flowfield above the upper surface of the wing; the sudden disruption of this flowfield that occurs at a critical angle of attack limits the flight regime for such a wing. Although considerable research effort has been directed towards this "vortex breakdown" phenomenon, there is as yet no widely accepted explanation for its occurrence, nor a consistently effective means for its prevention or control.

An analytical study, based on a complex potential representation of the vortex flow over a slender delta wing, was undertaken in an attempt to determine the parameter(s) governing vortex breakdown. This study indicated that the entrainment of flow into the vortex, as measured in the model by the ratio of sink-to-vortex strength, may play a dominant role in its subsequent breakdown. Further investigation revealed that control of this ratio, at some point close to the apex of the wing, can markedly delay the occurrence of vortex breakdown and that, as would be expected, the required control precision increases with angle of attack. It was considered that such control could be obtained in a real flow by the precise blowing of jets of air from the upper surface of the wing in a spanwise direction close to the leading edge. As has been found experimentally, the entrainment of these jets of air into the vortex does delay its breakdown, and it is hypothesised in this work that

the delay is a consequence of the effect of the jets on the overall entrainment level of the vortex. Comparison with experimental results provides evidence for such an enhancement mechanism, and it is concluded that a detailed experimental and numerical investigation should be undertaken of the role of entrainment in vortex breakdown.

Nomenclature

a	radius of circular cylinder in Z_1 -plane
b	entrainment coefficient = Q/Γ
b_c	critical entrainment coefficient
b_i	initial entrainment coefficient
C_1	constant of proportionality in singularity strength gradient relationship
C_{FZ}	coefficient of normal force in crossflow plane
C_{KE}	kinetic energy coefficient
C_L	lift coefficient
C_M	pitching moment coefficient
C_{PL}	pressure coefficient on the lower surface
C_{PU}	pressure coefficient on the upper surface
C_Q	air-blowing quantity coefficient
C_μ	blowing coefficient
F_Z	normal force in crossflow plane
G, Gamma	vortex strength in graphs
i	$\sqrt{-1}$
j	ordinate number
k	$\cot \Lambda$
M_∞	freestream Mach number
n	direction normal to particular geometry
P	freestream static pressure
Q	sink strength
r	radial coordinate in Z-plane
r_A	radial coordinate of vortex-sink in Z-plane
r_s	modulus of complex location on feeding sheet

S	bounding surface of K.E. calculation region
s	local wingspan
U_{S_1, S_2}	velocities along feeding sheet towards vortex-sink
U_∞	freestream velocity
U_c	crossflow component of freestream velocity
V_{ns}	non-singular crossflow velocity at vortex-sink centre minus the normal component of the freestream
V_*	non-singular crossflow velocity at singularity location
v	real component of complex velocity in Z-plane
v_a	velocity along axis of vortex
v_n	velocity normal to feeding sheet
v_r	radial velocity, +ve outwards from vortex centre
v_θ	circumferential velocity about vortex centre, +ve anti-clockwise
W	governing complex potential = $\Phi + i\Psi$
w	imaginary component of complex velocity in Z-plane
x, y, z	cartesian coordinate system
x_a	coordinate along axis of vortex
x_b	distance downwing of apex at which calculation fails
x_d	distance downwing of initial solution plane at which calculation fails
x_i	initial value of x
y, z	real and imaginary parts of Z
y_1, z_1	real and imaginary parts of Z_1
y_n, z_n	non-dimensionalised coordinates
Y_A, Z_A	coordinates of left-hand vortex-sink in Z-plane
Z	complex coordinate
\bar{Z}	conjugate of Z
Z_A, Z_V	location of left-hand vortex-sink in Z-plane

Z_1	complex coordinate in transformed (cylinder) plane
Z_{A1}	transformation of Z_A to Z_1 -plane
Z_S	complex location on feeding sheet in Z-plane
α	angle of attack
α_c	critical angle of attack
β	internal angle, at a point on a feeding sheet, between a line to the wing centreline and a line tangential to the sheet at that point.
Γ	vortex strength, +ve anti-clockwise
z	complex coordinate in transformed (vertical wing) plane
θ	angular coordinate in Z-plane
θ_A	angular coordinate of vortex-sink in Z-plane
Λ	angle of wing sweepback
ν	kinematic viscosity
ρ	freestream density
σ	coordinate along feeding sheet in Mangler and Smith model
ϕ	velocity potential
ψ	stream function

Subscript i relates to value in initial crossflow plane.

Subscript c denotes a critical value.

Chapter 1

The Breakdown of Slender Wing Leading Edge Vortices

1.0 Introduction

The flow past a slender flight vehicle at a high angle of attack is extensively vortex-dominated. Widespread flow separations, from both the body and wings of the vehicle, generate the strong vortices which are responsible for a considerable enhancement of lift and thence manoeuvrability. As a result, vortex flows are now routinely employed to improve the performance of slender combat aircraft and missile configurations. However, it is necessary to restrict the vehicle flight regime to ensure that the flow remains well-ordered and controllable.

A major limitation is imposed by the disruption of the wing leading-edge vortices which occurs at, and above, a critical angle of attack. This "vortex breakdown" phenomenon is accompanied by such a variation of aerodynamic coefficients that continued steady flight is impossible. If the resultant degradation of control was to occur during air combat or low level manoeuvring, then loss of the aircraft could result. Similarly, the occurrence of breakdown during missile flight must be avoided if the target is to be acquired and destroyed. It follows that in order to advance the capabilities of slender configurations the breakdown phenomenon must be prevented or controlled. Consistently effective prevention or control can only be

achieved by determining those parameters which cause or influence vortex breakdown. The primary aim of this study was, therefore, to obtain these parameters and thereafter to establish the effect of their variation on the subsequent development of the flow.

1.1 The Slender Wing Flowfield

To appreciate the significance of vortex breakdown, it is first necessary to understand the flow past a slender wing at a subcritical angle of attack. The important features are summarised below. For particular details, refs 1-5 should be consulted.

For simplicity, a wing of delta planform with aerodynamically sharp leading edges is considered. A schematic representation of the major features of the flowfield is shown in fig.1.1. For this configuration the two primary separation lines are fixed along the leading edges - if the edges were rounded these lines could lie along the upper surface. The shear layers leaving the wing at the edges roll up to form the two primary vortices indicated. The flow passing over the top of these vortices attaches to the wing upper surface at some point downstream. It then divides and strong spanwise boundary layer flows develop. These separate as a result of the strong adverse pressure gradients encountered underneath the primary vortices, and roll up to form two secondary vortices. Two further vortices, not shown in fig.1.1, are those formed downstream of the trailing edge as a result of the rolling up of the trailing vortex sheet. These are of opposite rotational sense to the primary vortices.

The pressure distribution for a cross-section of the wing is shown in fig.1.2. It is obvious that considerable lift enhancement is produced by the vortex flows. Furthermore, it is found that with increasing angle of attack α , the strengths of the vortices and

thereby the lift and nose-down pitching moment increase at low and moderate values of α , as indicated in fig.1.3.

It can be seen that there is a limit to this behaviour. At a high angle of attack vortex breakdown will occur, initially at some point downstream of the trailing edge. At this point the cores of the primary vortices suddenly increase in diameter or "burst", and the flow downstream becomes turbulent and diffuse. With further increases in α this breakdown point moves forward, until at some critical value α_c it crosses the trailing edge and the vortices breakdown above the wing upper surface. This is accompanied by the sudden decay in lift and pitching moment indicated for the higher angles of attack in fig.1.3. As α is increased still further the breakdown point moves towards the wing apex until eventually the flow above the wing is completely turbulent and has no regular structure.

Experimental evidence on the breakdown phenomenon is presented in more detail in the following section.

1.2 The Vortex Breakdown Flowfield

The first reported observation of vortex breakdown was made by Peckham and Atkinson¹ in 1957. During wind tunnel tests on a gothic wing the "belling-out" of a vortex core was noted, but given little attention. Subsequently the phenomenon has been extensively researched, breakdown having been found in a wide range of small and large scale, internal and external flows. It is hypothesised to play an important role in many fluid dynamic phenomena, for example boundary layer transition, and is thought to occur within geophysical swirling flows such as tornadoes and hurricanes.

As a result of this widespread interest, a large database of experimental evidence is available, much of which is relevant to the particular case of vortex breakdown above a delta wing in an incompressible flow. For this case, the main conclusions can be summarised as follows.

(i) There can be considered to be two basic forms of breakdown - the spiral and the bubble - although combinations of the two forms have been observed. Fig.1.4 shows schematically the behaviour of filaments of dye introduced along the axes of two leading edge vortices, as reported by Lambourne and Bryer⁶. Note that the upper vortex is undergoing breakdown of the spiral type, whilst the lower is displaying a bubble type. An additional form of breakdown, in which the filament of dye takes the form of a double helix, has been reported by Sarpkaya⁷ for a swirling flow in a mildly diverging cylindrical tube. However, such a

breakdown pattern has yet to be reported over a delta wing.

(ii) A feature of both forms of breakdown is the deceleration of flow along the vortex axis as a stagnation point is approached. Introducing a filament of dye along this axis is a common form of visualization for this type of flow. In the case of spiral breakdown, this tracer kinks after the stagnation point has been passed and takes up a spiral configuration which persists for an axial distance of 1-3 times the diameter of the upstream vortex core. This spiral rotates about a central stagnant region before the flow breaks down into large scale turbulence. From a cine film analysis performed in ref.6, it was found that the fluid particles do not follow a spiralling path, but take a curved path through the central stagnant region, as shown in fig.1.5. In the fully developed bubble form of breakdown, the tracer of dye appears to spread and fill this zone. The axial extent of this bubble is of the same order as that of the spiralling configuration. In most cases the flow becomes completely turbulent immediately downstream of this region, although it has been found that under certain conditions a new vortex core emerges from the rear of the bubble and then undergoes a breakdown of the spiral form.

(iii) The form of breakdown which occurs appears to depend to a large extent on the ratio of swirl-to-axial velocities in the vortex. It has been found from investigations of vortex breakdown in pipe and channel flows that this velocity ratio must reach a certain value before a breakdown of any type occurs⁸.

Thereafter the spiral form is favoured until the swirl reaches such a level that it is replaced by the bubble form. There may be some vacillation between the two forms until the bubble becomes established. In the majority of cases for the delta wing, it is the spiral type which is found.

(iv) One of the primary vortices may break down slightly in advance of the other, probably as result of small asymmetries in the flow. Therefore, the effect of breakdown is not limited to the longitudinal aerodynamic coefficients and lateral stability problems may ensue⁹.

(v) An adverse pressure gradient along the axis of a vortex moves the breakdown point upstream¹⁰. Conversely, the application of downstream axial suction can delay, if not prevent, breakdown. For example, the adverse pressure gradient produced by the deflection of a plain trailing edge flap moves breakdown upstream¹¹, fig.1.6. Deflection of a leading edge flap reduces the pressure peak near the leading edge, and therefore the breakdown point is moved downstream¹², fig.1.7.

(vi) It is possible to delay vortex breakdown by increasing the angle of leading edge sweepback¹², fig.1.8.

(vii) The location of breakdown is only very slightly dependent on Reynolds' number. In ref.6, over a Reynolds' number range of 0.01×10^6 to 4.6×10^6 the breakdown point moved upstream by a maximum of 15% of the root chord, fig.1.9. The breakdown

phenomenon can therefore be considered as essentially inviscid.

Until the advent of laser doppler velocimetry (LDV), conclusion (v) precluded detailed study of the structure of vortex breakdown. The sensitivity of the flow to pressure gradient is such that any intrusive method of measurement, e.g. a pressure probe, moves the breakdown point upstream. However, the basic principle of LDV is that it is possible to measure the velocity of a particle from the shift in frequency of a light beam that is incident upon it. It is therefore possible to study a flowfield in a non-intrusive manner and so the applicability of LDV to vortex breakdown investigation is obvious. (The LDV equipment available in the Department of Aeronautics and Fluid Mechanics at the University of Glasgow is discussed in Appendix 1). Detailed research has been carried out over slender wings¹³⁻¹⁷ using LDV systems, but problems still remain, for example the difficulty of obtaining information from near the vortex core where there are few light-scattering particles.

An alternative non-intrusive method of flow measurement which may prove of value in the future is that of Particle Image Velocimetry (P.I.V.)¹⁸ At present this technique can provide an instantaneous two-dimensional velocity map of a flowfield by recording a double exposure photograph of a thin sheet of light in a seeded flow. A pulsed laser is used as a light source in order to ensure that the flow is "frozen" during each exposure, and to provide sufficient light energy to record the images of the flow particles. When the photographic negative is interrogated at any point by a laser beam, Young's fringes are produced. The orientation and spacing of these

fringes are dependent on the local displacement of a particle, and hence its velocity vector. Therefore it is possible to build up a velocity map of the flowfield.

As with L.D.V., certain problems exist with the application of P.I.V. to vortical flows, for example the lack of light-scattering particles in areas of high vorticity, and the requirement for a powerful laser. In addition, its present restriction to two-dimensional measurement would be of limited value in the highly three-dimensional vortex breakdown flowfield. Nevertheless, future experimental investigations of vortex breakdown should be based on some form of non-intrusive measurement in order to be worthwhile.

1.3 A Review of Theoretical Research

At present, a widely accepted explanation for the cause of vortex breakdown does not exist. As stated by Hall¹⁹, the available explanations for the phenomenon belong, in the majority of cases, to one of three main groups: those which view breakdown as being analogous to the separation of a two-dimensional boundary layer, those which regard the phenomenon as resulting from hydrodynamic instability, and those which require the existence of a "critical state" in the flow before breakdown can occur.

1.3.1 The Boundary Layer Analogy

The boundary layer analogy can be considered to offer a simple explanation. It has been found that well upstream of breakdown the axial gradients in a vortex are small compared with the radial gradients (i.e. $d/dx_a \ll d/dr$). The stream surfaces are almost cylindrical, and so the vortex core is described as being quasi-cylindrical. The approximated (quasi-cylindrical) equations of motion for steady, laminar, incompressible, axisymmetric flow are, as derived in ref.20,

$$\frac{\partial v_r}{\partial r} + \frac{v_r}{r} + \frac{\partial v_a}{\partial x_a} = 0 \quad (1)$$

$$\frac{v_\theta^2}{r} = -\frac{1}{\rho} \frac{\partial P}{\partial r} \quad (2)$$

$$v_r \frac{\partial v_\theta}{\partial r} + \frac{v_r v_\theta}{r} + v_a \frac{\partial v_\theta}{\partial x_a} = \nu \left[\frac{\partial^2 v_\theta}{\partial r^2} + \frac{1}{r} \frac{\partial v_\theta}{\partial r} - \frac{v_\theta}{r^2} \right] \quad (3)$$

$$v_r \frac{\partial v_a}{\partial r} + u \frac{\partial v_a}{\partial x_a} = - \frac{1}{\rho} \frac{\partial p}{\partial x_a} + \nu \left[\frac{\partial^2 v_a}{\partial r^2} + \frac{1}{r} \frac{\partial v_a}{\partial r} \right] \quad (4)$$

By application of suitable boundary conditions and assuming initial upstream velocity profiles for v_r , v_θ and v_a , a solution can be obtained by stepping downstream in the axial direction (as for a boundary layer). The appearance of large axial gradients in the flow results in the failure of the quasi-cylindrical approximation; the vortex is assumed to break down at this point¹⁹ (cf boundary layer separation).

There are serious drawbacks to such an approach: the constraint of upstream axisymmetric flow is a major limitation, no knowledge can be obtained of the flow downstream of breakdown and, most importantly, it provides no explanation of several critical features of breakdown.

1.3.2 Hydrodynamic Instability

A theoretical criterion for vortex breakdown as a consequence of hydrodynamic instability was derived by Ludwig²¹ on the basis of his study of the flow between two coaxial rotating cylinders. Ludwig stated that a helical flow is unstable if

$$(1 - C_\phi) (1 - C_\phi^2) - (1.667 - C_\phi) C_z^2 < 0 \quad (5)$$

$$\text{where } C_{\theta} = \frac{r}{v_{\theta}} \frac{\partial v_{\theta}}{\partial r} \quad C_z = \frac{r}{v_{\theta}} \frac{\partial v_a}{\partial r}$$

A typical stability diagram is shown in fig.1.10.

If the flow is unstable, then the amplification of spiral disturbances may eventually lead to stagnation on the vortex axis. In addition, there will be an abrupt expansion of the vortex core (which has become asymmetric as a result of the disturbances). This is taken to indicate vortex breakdown.

Ludwig's approach is not valid for the axisymmetric bubble form of breakdown and therefore the possible vacillation between spiral and bubble forms is unexplained. The presence of instabilities within a vortical flow close to breakdown is extremely likely, given the range of velocities and velocity gradients present. Whether these actually cause breakdown is difficult to establish. In addition, as stated by Harvey²², the fact that in certain conditions a vortex reforms downstream of a bubble-type breakdown indicates that the phenomenon is reversible and unlikely to be the result of instability.

Bossel²³ also investigated the possible amplification of disturbances in a swirling flow. He derived a criterion for such amplification which proposed a critical swirl angle (= $\text{atan}(v_{\theta}/v_a)$) of 54.8° . There is some experimental evidence which shows breakdown occurring close to this value. However, Bossel's criterion provides no further detail on, or explanation of, vortex breakdown.

1.3.3 The Critical State

The critical state for a vortex flow has been defined as the condition at which an infinitesimal stationary disturbance (or standing wave) of infinite wavelength just becomes possible. If a flow is subcritical then the wavelength of the disturbance reduces. If, however, the flow is supercritical, no such disturbances can be supported.

Various explanations have been put forward for the role, if any, of the critical state in vortex breakdown. Squire²⁴ stated that a subcritical flow would allow downstream disturbances to propagate upstream and cause breakdown. On this basis he equated a criterion for subcriticality to a criterion for breakdown of a vortex. Such an approach leaves major features of the phenomenon unexplained.

Benjamin^{25,26} advanced a more complex argument in which he drew an analogy between breakdown and the hydraulic jump found in open channel flow. He considered breakdown to mark the transition between two conjugate flows, the flow being supercritical upstream and subcritical downstream. Conservation of momentum required the appearance downstream of small standing waves. Benjamin considered the leading wave to represent breakdown. However, his case was founded upon small perturbations of the flow; this is clearly invalid at breakdown of a vortex.

Escudier and Keller^{27,28} postulated that vortex breakdown was characterised by three flow regimes connected by two fundamentally

different transitions. An inviscid analysis of the first transition, considered to be the non-dissipative diversion of an isentropic flow around a region of stagnant flow, showed that this transition occurred between two supercritical flow states, and provided a breakdown criterion based on a requirement for the conservation of momentum. (This first transition is followed by a dissipative transition to the downstream state; however, no detailed analysis of this transition was attempted). Realistic representations have been obtained for the bubble-type of breakdown in pipes and channels; however, the analysis relates only to this type of breakdown.

Much related work has been performed by Leibovich^{8,29-31} in the areas of wave propagation, flow stability and criticality classification. His "synthetic theoretical breakdown scenario" is of interest, but remains unestablished.

Solutions to a linear equation of motion were obtained by Bossel for a bubble type of breakdown between prescribed upstream and downstream flow profiles and boundary conditions. He considered that breakdown was a required characteristic of the solution of the equations of motion for an upstream supercritical flow when these conditions were imposed. This approach is obviously very restrictive, being dependent on a priori knowledge of the flow upstream and downstream.

Hall¹⁹ attempted to identify the failure of the quasi-cylindrical approximation with the critical state. He applied the approximation to a supercritical flow tending to critical and showed that this

tendency produces a retardation of the axial flow. Close to criticality, the axial gradients become very large, and the quasi-cylindrical approximation fails. The critical state is used to explain the sudden change in the vortex core and the importance of the swirl level in breakdown. However, it has been shown by Shi³² that the critical state corresponds to a singularity, on opposite sides of which the flows are in contradistinction. Shi considered that the flow behaviour close to criticality reported by Hall was a result of the quasi-cylindrical approximation itself rather than physically realistic.

1.4 Catastrophe Theory

From the preceding section it should be clear that an acceptable theoretical explanation will be extremely difficult to obtain. However, it appears that the recent mathematical innovation of catastrophe theory may provide a means of realising such an explanation. Only the possible application of catastrophe theory to vortex breakdown is considered here. Further details of the theory are given in Appendix 2.

If a governing potential function for the flow past a delta wing can be determined, then study of this function may indicate the existence of multiple potential minima, i.e. more than one stable flow state is possible. Gradual variation of the control parameters such as pressure gradient and leading edge sweep may alter the stable states in a discontinuous way, such discontinuities being "catastrophes". The required sudden changes in the flow could then cause breakdown of the vortices (cf the separation of a boundary layer as it passes through the discontinuity of a shock). By determination of the control parameters governing the catastrophe, it would be possible to develop a new criterion for breakdown.

The involved nature of catastrophe theory mathematics^{33, 34} coupled with the complexity of the breakdown scenario, makes its application to this flow phenomenon too difficult to attempt by purely theoretical means. An alternative method of developing the catastrophe surfaces discussed in Appendix 2 must be found. The problem has been studied experimentally to a limited extent by

Gersten et al³⁵, who showed the existence of hysteresis between flow states. A comprehensive experimental research programme considering in turn the effect on breakdown of varying each possible control parameter would yield the required catastrophe surfaces. However, it would be beneficial if particular parameters of interest could first be established by analytical means. As stated in the Introduction, the identification of these parameters is a primary aim of this study.

1.5 Computational Fluid Dynamics (C.F.D.)

The recent advances in supercomputer technology have made feasible the numerical solution of the Navier-Stokes equations for a fully three-dimensional vortical flow. Preliminary solutions for leading edge vortex breakdown have been obtained³⁶ but are subject to a programme of validation and comparison with experimental data. Computational studies of an unconfined viscous vortex, for example refs.37-39, have indicated that axisymmetric bubble breakdown patterns can be calculated. However, the low Reynolds' number range (<1000) required for such solutions renders them of no practical importance in the vortex breakdown phenomenon as found in the external flow past an aerospace vehicle.

Although solutions to the Euler equations for the flow past a delta wing cannot predict viscous separations, they do capture the primary leading edge vortices, for reasons which have not yet been fully established. It has been shown⁴⁰ that the dominant terms in the Navier-Stokes equations applied to a leading edge vortex are convective rather than diffusive, except in a very small region close to the vortex core. In addition, as discussed in section 1.2, experimental evidence has indicated the relatively minor role of viscosity in vortex breakdown. Therefore the use of the Euler equations in a study of the breakdown phenomenon can be justified.

Euler solutions⁴¹ have shown typical features found experimentally for the breakdown region, for example the reversal of axial flow downstream and the widening of the vortex core. As for

the Navier-Stokes solutions, however, such results require careful validation.

In an application, such as vortex breakdown, where the flow is not fully understood, it would be hazardous to rely only on results from C.F.D. codes . The concept of the synergy of analytical, experimental and computational fluid flow modelling⁴² is particularly valid in vortex breakdown research. C.F.D. on its own will not provide a unifying solution to the breakdown problem.

1.6 Project Guidelines

It was decided that any worthwhile experimental investigation could not be accomplished within a three year timescale and/or a reasonable budget. The Laser Doppler Velocimetry equipment available at the University of Glasgow is unproven, and in any case is unsuitable for an application to the vortex breakdown problem.

C.F.D. based research is best suited to centres where Navier-Stokes and Euler codes are well established and suitable guidance exists for their application to an already highly involved problem. The computational time required for any such study would be impractical in an university environment

A computer based analytical investigation of breakdown held most promise. A suitable model for the flow past a delta wing was to be developed, with the requirement that it was to be sufficiently simple to ensure that the dominant parameters in the flow could be readily identified as it proceeded to break down. The effect of the variation of these parameters would then be established. Subsequently, recommendations could be made for further investigation of those parameters which appeared to control breakdown.

Chapter 2

A Survey of Existing Theoretical Models for the Flow Over a Delta Wing

2.0 Model Requirements

A survey was performed of existing models for the well-ordered flow past a delta wing, to discover which, if any, were suitable for, or could be modified to allow, application to an investigation of vortex breakdown. It was stipulated that:

- (1) the model should adequately represent the major features of the flow
- (2) it should be possible to readily assess the contribution of each control parameter to the development of the flow
- (3) excessive computational time should be avoided.

Available flow models were considered with regard to these requirements.

2.1 Slender Potential Models

The four inviscid, irrotational models discussed in this section make the slender wing assumption, namely that the flow in any crossflow plane is governed by the two-dimensional Laplace equation

$$\frac{\partial^2 \Phi}{\partial y^2} + \frac{\partial^2 \Phi}{\partial z^2} = 0 \quad (6)$$

Therefore, a complex potential representation for the crossflow is possible, which considerably simplifies analysis. The additional requirement of a conical flow pattern (i.e. one where the flow quantities over the wing are constant along a ray drawn from the apex) is imposed on the first three models and provides further simplification. However, it should be noted that a conical flow pattern cannot satisfy a Kutta condition at the trailing edge.

2.1.1 The Method of Legendre

For a delta wing flow, similar to that of fig.1.1, Legendre⁴³ considered that the crossflow could be represented by two symmetrically placed vortices, of equal but opposite strength, in the presence of a finite wing, as shown in fig.2.1. The complex potential W could not be obtained directly in the Z -plane, and so a transformation to the ζ -plane

$$\zeta^2 = Z^2 - s^2 \quad (7)$$

was employed, indicated in fig.2.2. Since the wing now lay along the axis of symmetry, in this case the imaginary axis, there was no image vortex problem. However, asymmetric flow could not be investigated in this plane. It was found for small angles of attack that

$$W = Ux - i\alpha U\zeta - \frac{i\Gamma}{2\pi} \ln \frac{\zeta - \zeta_v}{\zeta + \overline{\zeta_v}} \quad (8)$$

A Kutta condition was imposed in the Z-plane at the leading edges, $Z = \pm s$, to represent flow separation there, i.e.

$$\frac{dW}{dZ} = \frac{dW}{d\zeta} \frac{d\zeta}{dZ} = \frac{Z}{\zeta} \left[-i\alpha U - \frac{i\Gamma}{2\pi} \left(\frac{1}{\zeta - \zeta_v} - \frac{1}{\zeta + \overline{\zeta_v}} \right) \right] = 0 \quad (9)$$

and so, by requiring the square-bracketed term to equal zero

$$\frac{\Gamma}{2\pi\alpha U} = \frac{\zeta_v \overline{\zeta_v}}{\zeta_v + \overline{\zeta_v}} \quad (10)$$

Thus the vortex strength could be determined in terms of its position. Legendre required that the vortex align itself with the local flow direction in order that it could be force free, i.e. the velocity V_* normal to the vortex, in the limit as Z tended to Z_v , was equal to zero. This was more easily satisfied by reference to the conjugate velocity V_* , for which it followed that

$$\overline{V^*} = -U \left[\frac{d\overline{Z_V}}{dx} + i\alpha \frac{Z_V}{\zeta_V} - \frac{i\Gamma}{2\pi U} \left(\frac{Z_V}{\zeta_V(\zeta_V + \overline{\zeta_V})} + \frac{s^2}{2Z_V\zeta_V^2} \right) \right] = 0 \quad (11)$$

Given the assumption of conical flow

$$\frac{d\overline{Z_V}}{dx} = \frac{\overline{Z_V}}{x} \quad (12)$$

and taking $s = kx$, it was found that eqn.11 reduced to

$$\frac{\overline{Z_V}}{s} + i \frac{\alpha Z_V}{k \zeta_V} - \frac{i\Gamma}{2\pi kUs} \left(\frac{sZ_V}{\zeta_V(\zeta_V + \overline{\zeta_V})} + \frac{s^3}{2Z_V\zeta_V^2} \right) = 0 \quad (13)$$

The Kutta condition was then expressed as

$$\frac{\Gamma}{2\pi kUs} = \frac{\alpha \zeta_V \overline{\zeta_V}}{k s(\zeta_V + \overline{\zeta_V})} \quad (14)$$

Conical solutions to (7), (13) and (14) have been obtained in which Z_V/s , ζ_V/s and Γ/kUs were constants and dependent only on the incidence parameter α/k , which is found to play the dominant role in all four models of this section.

This summary of Legendre's method is due to Smith⁴⁴ (as the original version was unobtainable), who considered that the solutions showed the main qualitative features of the flow, i.e. vortices of the correct sign lying inboard of the leading edge and

above the upper surface, and a non-linear lift curve. However, he found that the quantitative results were inaccurate. The vortices were located at too great a distance from the wing, and the non-linear lift was overpredicted. In addition, this approach violates Kelvin's theorem for the constancy of circulation as a result of the increase in vortex strength downstream.

2.1.2 The Method of Brown and Michael

Brown and Michael⁴⁵ adopted a similar approach to Legendre, with the exception that the growth in circulation downstream was accounted for by the introduction of two feeding vortex sheets joining the leading edges to the point vortices, as shown in fig.2.3. Their apparently arbitrary selection of sheet shape has been found to be justified. The geometry of the physical and transformed planes was in accordance with that of Legendre. However, where Legendre considered that the point vortices should be force free, Brown and Michael imposed the force free condition on the point vortex-feeding sheet combinations.

An element Δx of the starboard feeding sheet sustains a force equivalent to

$$F_{fs} = i\rho U \frac{d\Gamma}{dx} (Z_v - s) \Delta x \quad (15)$$

For an element Δx of the point vortex the force is expressed as in eqn.16 overleaf,

$$F_v = -i\rho V_* \Gamma \Delta x \quad (16)$$

where V_* is once again the limiting complex velocity as Z tends to the vortex location.

Since

$$F_v + F_{fs} = 0 \quad (17)$$

it was found that

$$V_* = -\frac{U}{\Gamma} \frac{d\Gamma}{dx} (Z_v - s) \quad (18)$$

Evaluating V_* as before gave

$$\frac{d\bar{Z}_v}{dx} + \frac{(\bar{Z}_v - s)}{\Gamma} \frac{d\Gamma}{dx} + i\alpha \frac{Z_v}{c_v} - \frac{i\Gamma}{2\pi U} \left(\frac{Z_v}{c_v(c_v + \bar{c}_v)} + \frac{s^2}{2Z_v c_v^2} \right) = 0 \quad (19)$$

This was simplified, as in section 2.1.1, to

$$2 \frac{\bar{Z}_v}{s} - 1 + i \frac{\alpha Z_v}{k c_v} - \frac{i\Gamma}{2\pi k U s} \left(\frac{s Z_v}{c_v(c_v + \bar{c}_v)} + \frac{s^3}{2Z_v c_v^2} \right) = 0 \quad (20)$$

The Kutta condition, eqn.14, remained valid, and solutions to eqns.

7, 14 and 20 again gave solutions for which Z_v/s , c_v/s and Γ/kUs were constants and dependent only on the incidence parameter. Momentum

considerations then permitted simple calculation of the resulting lift, and thence pitching moment.

The introduction of feeding sheets by Brown and Michael improved on the realism of Legendre's model and fixed the locations of the pressure discontinuities in the flow. However, slender wing theory requires that only the crossflow plane be considered, and therefore the addition of vortices acting out of this plane is a violation. Quantitative results were more accurate than those of Legendre, but the lift and the spanwise coordinate of vortex location were again overpredicted.

2.1.3 The Method of Mangler and Smith

Mangler and Smith^{46,47} removed the requirement for out-of-plane vortices whilst attempting to calculate the shape and strength of a feeding sheet. The flow pattern assumed for the crossflow plane was as shown in fig.2.4. It can be seen that the vortex core has been replaced by a point vortex, which is joined to the outer spiral by a cut (across which the pressure is discontinuous). Again a zero total force condition was applied, in this case to the combination of point vortex and cut. Five boundary conditions were imposed:

- (a) no flow disturbance at infinity
- (b) zero normal flow velocity on the wing surface
- (c) smooth separation at the leading edge
- (d) no discontinuity in pressure across the feeding sheet
- (e) the feeding sheet was a streamsurface of the three dimensional flow.

However, slender wing considerations required that these conditions be formulated in the two-dimensional crossflow plane. Conditions (d) and (e) are inherently three-dimensional, but after manipulation it was found that (d) could be satisfied by requiring that

$$\Delta\phi = \left(r_s \frac{dr_s}{d\sigma} - \frac{sv_{tm}}{2kU} \right) \Delta \frac{d\phi}{d\sigma} \quad (21)$$

where Δ indicates a jump in ϕ on going from inside to outside the sheet, r_s is the modulus of a complex location Z_s on the feeding sheet, σ is the coordinate along the sheet and v_{tm} is the mean of the tangential velocities on opposite sides of the sheet. Condition (e) was expressed in two dimensions as

$$v_n = - \left(\frac{2kU}{s} \right) r_s \sin\beta \quad (22)$$

where β is the internal angle, at the point Z_s , between a line to the wing centreline and a line tangential to the sheet at that point.

Eqn.(22) indicates that the trace of the three-dimensional streamsurface in the crossflow plane does not form a streamline.

Initially conditions (21) and (22) could only be applied to the sheet at one or two points. However, from the improved method of Smith⁴⁸, it is now possible to satisfy (21) and (22) at a distribution of points along the sheet.

A transformation to the ζ -plane by eqn.(7) again removed the

image vortex problem. Considerable algebraic manipulation was required to obtain the transformed boundary conditions, and for full details of these and the solution procedure for the resulting equations ref. should be consulted. A summary of the major results is given below.

It was found that close to the apex of the wing, where the real flow was near conical, good agreement with experimentally measured pressure distributions and hence lift could be obtained. However, on moving down the wing the theoretical predictions became less accurate as a result of the increased effect of secondary separations and the trailing edge in the real flow. As for the preceding two models, the quantitative predictions of overall lift and pitching moment were inaccurate. Nevertheless, the good representation of the position and shape of the primary vortex obtained by the improved method of Smith has resulted in its application to a wide range of problems in slender wing aerodynamics.

2.1.4 The Multi-Vortex Model of Peace

Using a crossflow geometry similar to that of Smith, Peace⁴⁹ modelled a feeding vortex sheet by a distribution of line vortices and used an isolated vortex to represent the core. By shedding discrete vortices at intervals downwing along the leading edge, it was found that these vortices would wrap around the "core" vortex and thereby describe the rolling up of the vortex sheet. Peace considered that initially a shed vortex had zero strength and that it then obtained its circulation along a cut joining it to the leading

edge (cf Brown and Michael). When this feeding process was terminated by the shedding of the next vortex, the first vortex then aligned itself with the local flow direction in order to be force free. Chaotic behaviour close to the core with an increasing number of discrete vortices was avoided by amalgamating vortices with the core whenever their angular separation exceeded a pre-assigned value.

Solutions for the flow were obtained by marching between downwing stations, and the method is therefore non-conical. However, no trailing edge effect was considered.

This flow model has been applied by Peace to several wings. For the case of a flat plate delta wing, the results were in close agreement with those from the Smith method. In consequence the predicted crossflow pattern was in good agreement with that found experimentally but the overall loading was not accurately predicted. The major advantage the multi-vortex model has over the vortex sheet model is its ability to handle flows where more than one vortex system is present, e.g a double delta wing.

2.1.5 Applicability of Slender Potential Models to Vortex Breakdown Investigation

It is obvious that the assumption of a conical flow pattern precludes any study of the vortex breakdown phenomenon. Furthermore, the appearance of the large axial gradients in the flow that accompany breakdown renders slender wing approximations invalid. However, as for the quasi-cylindrical approximation, in certain cases

it may be possible to relate the failure of the slender wing approximation to the onset of breakdown.

Of the four methods detailed in the preceding sections, it was considered that the Brown and Michael model offered the best balance of simplicity and physical realism. However, it would require to be set within a non-conical framework, and to provide a more complete description of flow within the vortex core region, if it were to provide the basis for a vortex breakdown investigation.

2.2 Non-Slender Potential Models

To obtain a completely three-dimensional description of the flow past a delta wing it is necessary to consider that disturbances can propagate both upstream and downstream, i.e. a trailing edge Kutta condition is required and slender approximations are not valid. The governing equation for a potential flow is then the Prandtl-Glauert equation

$$(1 - M_\infty^2) \frac{\partial^2 \Phi}{\partial x^2} + \frac{\partial^2 \Phi}{\partial y^2} + \frac{\partial^2 \Phi}{\partial z^2} = 0 \quad (23)$$

Several approaches have been made to the solution of this equation, the majority of which have been based on the single line vortex, multi-vortex or vortex-sheet models. It should therefore be apparent that these are inherently more complex than those of subsections 2.1.1 to 2.1.4. Nevertheless, it was considered worthwhile to study the methodology of a typical model to assess both its suitability as an investigative tool and the degree of physical realism achieved.

2.2.1 A Panel Method for the Solution of the Leading Edge

Vortex Flow

The inviscid flow model employed by Johnson et al⁵⁰ represented a highly swept wing of arbitrary geometry by a distribution of source and/or doublet singularity panels. Doublet panels alone were used to represent the rolled-up vortex sheets and the wake. It can be seen

in fig.2.5 that the core was once again replaced by a line vortex, which was joined by a cut to the feeding sheet (cf Smith). The boundary conditions imposed were:

- (a) zero normal flow velocity on the wing surface, feeding sheet and wake.
- (b) zero pressure difference across the feeding sheet and wake.
- (c) the total force on the line vortex and cut was required to be parallel to the line vortex.
- (d) Kutta conditions along the leading, side and trailing edges of the wing.

(Condition (c) requires the normal force on the representation of the vortex core to equal zero. It should be noted that it is no longer necessary for the normal direction to lie in the crossflow plane.)

The required singularity distributions and the geometry of the feeding sheets were then calculated iteratively from a starting solution based either on the user's experience or Smith's conical solutions. Careful consideration of the numerical methods employed was required to optimise the method run time and to ensure that any numerical instabilities were properly damped.

Results obtained for a delta wing show good agreement with experimental measurements, although secondary vortex effects cannot be calculated. However, Johnson and his co-workers concluded that considerable work was required to obtain a reliability similar to that of an attached potential method.

2.2.2 Applicability of Non-Slender Potential Models to Vortex Breakdown Investigation

The additional requirement to satisfy the Kutta condition at the trailing edge led to a considerable increase in complexity of models for the leading edge vortex flow. From the first model of Nangia and Hancock⁵¹, to the most recent work by Hoeijmakers⁵², this has produced a need for computational resources that is unmatched by slender models. Even so, the representation of flow near the core remains poor. Any attempted modification of such a method to accurately simulate flow within the core region and to reproduce the breakdown phenomenon would so increase the complexity of the model as to make it almost unworkable. This feature, coupled with the detailed validation program required by even the most up-to-date potential-based panel methods, renders such models unsuitable for use in an investigation of vortex breakdown.

2.3 Modelling the Vortex Core

It is widely believed that the vortex breakdown phenomenon may originate from the core of a leading edge vortex. To assess the validity of this hypothesis, it is necessary to include some representation of the core regions in a model of the flow past a delta wing. In the models of sections 2.1 and 2.2, this was attempted by reducing a core to a line vortex. While such a representation provides an approximate simulation of the effect of the core on the outer flow, its indication of singular behaviour at the centre of the core is unrealistic. In addition, the importance of features such as the entrainment of flow into the core cannot be determined.

Considerable effort has been directed to overcoming these restrictions, most notably by researchers at R.A.E. Farnborough in the 1960's. The major features of their work are detailed in the following subsections.

2.3.1 The Inviscid Rotational Vortex

The experimental results of Harvey, as summarised by Hall⁵³ indicated that, for a leading edge vortex, within one convolution of the spiral it was not possible to distinguish the feeding shear layer (or vortex sheet) as it became progressively more diffuse. From this feature, Hall concluded that a rotational model based on distributed vorticity was more physically realistic than one based on vorticity concentrated along feeding sheets in an otherwise

irrotational flow. However, to simplify the model, Hall was required to make certain restricting assumptions:

- (1) the flow was to be axisymmetric and incompressible
- (2) the velocity field was to be conical
- (3) the effects of viscous diffusion were to be neglected.

Hall named his model the "Euler Vortex" since, with these assumptions, the Euler equations govern the flow.

It is known, from the work of Earnshaw², that at the centre of a leading edge vortex there exists a small viscous subcore, within which the effects of viscosity are dominant. Furthermore, in a real flow there is a progressive departure from axial symmetry as the distance from the vortex axis is increased. Therefore, the "Euler Vortex" is only valid within a limited region of the flow close to the core, but outwith the viscous subcore.

Solutions obtained by Hall show good general agreement with experiment, in particular the high axial velocities and low pressures within the core. In addition, the sensitivity of flow within the vortex to external boundary conditions has also been confirmed experimentally. Hall hypothesised that this sensitivity could partly explain the vortex breakdown phenomenon.

2.3.2 An Improved Representation of Flow Within the Core

Hall⁵⁴ improved his representation of the flow within the leading edge vortex core through inclusion of a model for the viscous subcore. The outer part of the core was again represented by the

"Euler Vortex", which provided the edge boundary conditions for the subcore. Further extensions to Hall's theory for the subcore were made through collaboration with Stewartson⁵⁵, and it is their modified theory which is summarised overleaf.

As a first stage in obtaining a solution for the subcore (the inner solution), the flow was assumed to be laminar and boundary layer type approximations were made to the governing Navier-Stokes equations. Subsequently, suitable independent flow variables were identified, and the outer solution expressed in terms of these variables. An asymptotic expansion for the subcore solution was then obtained and substituted in the approximated governing equations. An order of magnitude analysis of these equations then yielded a set of ordinary differential equations which, when coupled with suitable boundary conditions, resulted in an inner solution which approached the solution for the outer core with increasing distance from the vortex axis.

The results obtained from this method have shown good qualitative agreement with experiment. However, quantitative comparison highlighted some shortcomings which may have been a consequence of the laminar, instead of turbulent, representation of the subcore. It has been shown that substitution in the governing equations of an eddy viscosity, of approximately five times the magnitude of the kinematic viscosity, produces acceptable agreement with experimental results.

2.3.3 Two Further Models for the Flow Near a Vortex Core

Subsequent to the work of Hall, Mangler and Weber⁵⁶ determined a non-slender potential representation of the flow near a vortex core. As assumed by Smith, they considered that the vorticity in the flow was concentrated on a thin sheet, and that elsewhere the flow was inviscid, incompressible and conical. However, slender wing approximations were made in only one case, for the purpose of comparison with the non-slender model.

Results from this method indicated that, as would be expected, the required shape of the sheet was a tightly wound spiral and that high axial velocities existed within the spiral. The differences between slender and non-slender representations were also highlighted, in particular for the values of the circumferential and radial velocities as the centre of the spiral was approached. In the limit, the circumferential velocity in the slender solution tended to a finite value, whereas that in the non-slender solution tended to infinity. For the slender solution, it was found that the mean value of radial velocity was always zero whilst that of the non-slender solution only tended to zero at the centre. In both solutions the axial velocity tended to infinity.

A detailed comparison with experimental results was not attempted by Mangler and Weber. Nevertheless, it is apparent that such a method is inapplicable within the viscous subcore and close to the wing leading edge.

It appears that the three-dimensional vortex filament method developed by Leonard⁵⁷ may yield useful results for flow behaviour within the core. The basic assumption made by Leonard was that it is possible to represent a vorticity field by a distribution of vortex filaments (within each of which the vorticity distribution is non-singular). The development of the flow is calculated from the dynamic interaction between the individual filaments. This method was applied by Nakamura et al to simulate the axisymmetric breakdown of an isolated vortex.

Nakamura⁵⁸ found that it was possible to reproduce several of the characteristics associated with axisymmetric vortex breakdown, including changes in the vortex core as breakdown was approached. These included the deceleration of the axial flow and an increase in the swirl angle. Furthermore, with the provision of suitable upstream boundary conditions from experiment, it was possible to show the occasionally observed feature of a recovery zone behind the initial axisymmetric breakdown followed by a second breakdown of the spiral type.

However, the application of the vortex filament method to the breakdown of a leading edge vortex represents a more complex task. Such an application has not yet been attempted.

2.3.4 Applicability of Core Models to Vortex Breakdown

Investigation

It is considered that the vortex core has a considerable role to play in the breakdown phenomenon. However, it is unclear whether breakdown originates from within the core or is, alternatively, a consequence of the effect of the core on the outer flow. It was therefore vital that an investigation of the breakdown of the leading edge vortex should be performed on a model that included detailed representation of the core flow. Such an approach was adopted by Luckring and is discussed in the following section.

2.4 The Method of Luckring: A Comprehensive Model for the Leading Edge Vortex

Luckring⁵⁹ developed a composite representation for the three-dimensional leading edge vortex flow in an attempt to obtain a fuller understanding of the flow within the core and the breakdown phenomenon.

The major features of this model are shown in fig.2.6. The three-dimensional panel method of Johnson et al, summarised in section 2.2.1, was selected to represent the outer part of the flow. This was matched to an inner solution of the quasi-cylindrical Navier-Stokes equations of section 1.3.1, where the numerical solution procedure was that developed by Hall. As discussed in section 1.3.1, such a representation for the inner flow requires a starting solution. In this case, the inner flow in the initial plane was provided by a solution of the core representation detailed in section 2.3.2.

Calculations were performed for delta wings with a leading edge sweep angle ranging from 55° to 85°, and over an angle of attack range of 5° to 50°. Particular arrow and diamond wings were also analysed. All cases were considered for incompressible flow at a Reynolds' Number of the order of one million, based on the wing root chord.

Comparison of theoretical results with the experimental results of Earnshaw has indicated that reasonable agreement is achieved

throughout the core, with the exception that the centreline axial flow is not well predicted. It was considered that, in addition to experimental inaccuracies, a major cause of this error was the assumption of a laminar, incompressible flow within the viscous subcore. As discussed in section 2.3.2, a turbulent model of the subcore appears more appropriate. In addition, the local maximum in velocity on the vortex axis can result in compressibility effects in this area for an incompressible freestream.

From consideration of the experimental results of Wentz and Kohlman, Luckring found a close correlation, for all wings studied, between the occurrence at the trailing edge of vortex breakdown and a particular constant swirl angle ($= \text{atan}(v_\theta/v_a)$) within the vortex. The fact that at this condition the theoretical results did not exhibit any of the features associated with breakdown, was attributed by Luckring to the approximated representation of the viscous subcore. However, the ability of this composite method to model the vortex breakdown phenomenon remains unproven.

2.5 Survey Conclusions

From the methods of modelling the leading edge vortex flow considered in this chapter, it was found that none were directly applicable to a simple, flexible investigation of vortex breakdown. The majority of the methods studied were deemed unsuitable for reasons of complexity and excessive computational requirements. It was concluded that the development of a basic model of the flow, designed to meet the requirements of section 2.0 and intended primarily for the study of vortex breakdown, should be undertaken.

Chapter 3

Development of the Flow Model

3.0 Introduction

As discussed in Chapter 2, many extensive models have been developed for the high angle of attack flow past a delta wing. Although several of these models provide detailed representations of the vortex flow, it was considered that an investigation of the inherently complex vortex breakdown problem would be best performed with a simple, yet physically realistic, analytical model. Such a model would represent the essential aspects of the flow whilst facilitating identification of the dominant control parameters. The effect on the flow of a variation of these parameters could then be studied in an attempt to establish their importance, if any, in the vortex breakdown phenomenon.

The development of a suitable flow model was undertaken in two stages; initially a model was developed for the crossflow, this model being subsequently extended into three dimensions. In order to determine a representation for the crossflow which provided sufficient realism, whilst retaining simplicity, it was necessary to adopt a "building-block" approach. In this way it was possible to proceed from the simplest possible point vortex model, through a first vortex-sink model, to the modified vortex-sink model which represents the entrainment of flow into the vortex (neglected in

earlier analytical models), and also provides the basis for a quasi-three-dimensional study of the flow.

Application of a Kutta condition to the leading edges of the wing reveals a previously unreported result: it appears that the ratio of sink-to-vortex strength, a measure of the entrainment effect, plays a major controlling role in the crossflow. If this ratio falls below a critical value, then the crossflow exhibits behaviour which may well be related to vortex breakdown in three dimensions, thus indicating the possible importance of the entrainment effect of the vortex in the phenomenon.

The chapter concludes with the method chosen for extension of the model into three dimensions which, on the basis of the results for the crossflow plane, was chosen such that the importance of the entrainment-related parameter could be fully investigated.

3.1 The Point Vortex Model

The simplest possible representation for the crossflow past a delta wing is that of two point vortices in the presence of a flat plate, as shown in fig.3.1. As stated in Chapter 1, vortex breakdown is largely an inviscid phenomenon, and therefore an inviscid model for the crossflow is acceptable. Furthermore, with the concentration of the rotationality of the flow at two points, a governing complex potential can be derived. Obviously no representation of the flow within the vortex core is possible with such a model. As discussed in Chapter 2, there is no conclusive evidence on the role of the core in vortex breakdown. Therefore it was decided to simplify analysis of the phenomenon by considering only the core's effect on the outer flow, as modelled by a complex potential representation.

For the flow representation of fig.3.1, image vortices are required to ensure that the wing remains a solid boundary, and this problem cannot be resolved in the complex Z -plane. A conformal transformation to an additional complex plane is required.

In previous work, e.g. refs 45 and 46, the transformation employed has been such that the wing lies along an axis of symmetry of the flow and therefore no images are required. However, as such an approach precluded the possibility of extending the model to investigate asymmetric distributions of the leeside vortices, an alternative transformation (as employed by Pullin in ref.60) was considered.

By transforming the wing to a circular cylinder in the Z_1 -plane, fig.3.2, it was possible to resolve the image vortex problem by application of the Circle theorem, as detailed in ref.61. The required transformation, derived in Appendix 3, is an inverse formulation of the Kutta-Joukowski transformation, and is given by

$$Z_1 = -0.5i (Z + \sqrt{ Z^2 - 4a^2 }) \quad (24)$$

As shown in Appendix 4, the governing complex potential for the flow in this plane is of the form

$$W(Z_1) = \Phi + i\Psi = U_C \left(Z_1 + \frac{a^2}{Z_1} \right) - \frac{i\Gamma_1}{2\pi} \ln \left[\frac{Z_1 (Z_1 - Z_{A1})}{a^2 - Z_1 \overline{Z_{A1}}} \right] - \frac{i\Gamma_2}{2\pi} \ln \left[\frac{Z_1 (Z_1 - Z_{B1})}{a^2 - Z_1 \overline{Z_{B1}}} \right] \quad (25)$$

Through eqn.24 it is then possible to obtain the value of the complex potential for all points in the Z -plane.

3.1.1 Boundary Conditions

Three boundary conditions were imposed initially:

- (a) the flow in the Z -plane was to be symmetric about the imaginary axis in order to simplify the analysis

(b) the complex velocity in the limit as a vortex centre was approached was to be zero i.e. the vortex was to be stationary

(c) a Kutta condition was necessary at the wing leading edges to ensure finite velocities there.

Condition (a) obviously requires symmetrically placed vortices of equal strength. The complex potential of eqn.25 then reduces to

$$W(Z_1) = \phi + i\Psi = U_C \left[Z_1 + \frac{a^2}{Z_1} \right] - \frac{i\Gamma_1}{2\pi} \ln \left[\frac{(Z_1 - Z_{A1})(a^2 - Z_1 Z_{A1})}{(Z_1 - Z_{B1})(a^2 - Z_1 Z_{B1})} \right] \quad (26)$$

To invoke condition (b), it was first necessary to note that a vortex induces no velocity at its own centre. As proven in Appendix 5, it can then be deduced that the vortex will be stationary if

$$\left[W_1 \frac{dZ_1}{dZ} \right]_{Z=Z_A} - \frac{i\Gamma_1}{4\pi} \left[\frac{d^2 Z_1}{dZ^2} / \frac{dZ_1}{dZ} \right]_{Z=Z_A} = 0 \quad (27)$$

$$W_1 = U_C \left[1 - \frac{a^2}{Z_{A1}^2} \right] - \frac{i\Gamma_1}{2\pi} \left[\frac{-Z_{A1}}{a^2 - Z_{A1}^2} - \frac{1}{Z_{A1} - Z_{B1}} + \frac{-Z_{B1}}{a^2 - Z_{B1}^2} \right] \quad (28)$$

$$\frac{d^2 Z_1}{dZ^2} / \frac{dZ_1}{dZ} = \frac{-4a^2}{(Z^2 - 4a^2)(Z + \sqrt{Z^2 - 4a^2})} \quad (29)$$

The Kutta condition (c) required that

$$\frac{dW}{dz} = 0, \quad z = \pm \frac{s}{2} \quad (30)$$

which is equivalent to requiring in the Z_1 -plane that

$$\frac{dW}{dZ_1} = 0, \quad Z_1 = \mp ai \quad (31)$$

From (26), it can be found that this leads to the condition

$$\frac{dW}{dZ_1} = U_c \left[1 - \frac{a^2}{Z_1^2} \right] - \frac{i\Gamma_1}{2\pi} (W_2) = 0, \quad Z_1 = \mp ai \quad (32)$$

$$W_2 = \left[\frac{1}{Z_1 - Z_{A1}} - \frac{Z_{A1}}{a^2 - Z_1 Z_{A1}} - \frac{1}{Z_1 - Z_{B1}} + \frac{Z_{B1}}{a^2 - Z_1 Z_{B1}} \right] \quad (33)$$

which can be expressed, for a solution in the left half Z -plane, as

$$2U - \frac{i\Gamma_1}{2\pi} W_3 = 0 \quad (34)$$

where

$$W_3 = \left[\frac{1}{ai - Z_{A1}} - \frac{Z_{A1}}{a^2 - aiZ_{A1}} - \frac{1}{ai - Z_{B1}} + \frac{Z_{B1}}{a^2 - aiZ_{B1}} \right] \quad (35)$$

It would appear that the two boundary conditions (b) and (c) have provided four governing equations with only three unknowns: y_{A1} , z_{A1} , and Γ . Thus the problem would be overdetermined. However, as shown in Appendix 6, W_3 can be expressed as the wholly imaginary function given below

$$W_3 = i \left[\frac{-a^3 + az_{A1}^2 + ay_{A1}^2}{(a^2 - az_{A1})^2 + a^2y_{A1}^2} + \frac{a^3 - az_{A1}^2 - ay_{A1}^2}{(a^2 + az_{A1})^2 + a^2y_{A1}^2} \right] \quad (36)$$

and so the Kutta condition reduces to one real equation. Therefore, there are only three equations in terms of three unknowns and a solution, if one exists, is possible.

3.2 Point Vortex Solution Method and Results

The problem of the simultaneous satisfaction of eqns.27 and 34 has previously been addressed by Coe⁶², and also by Clark and Smith⁶³. Coe found a locus of possible solutions for vortex position and strength; however, in ref.63 it was shown that Coe's derivation of the governing equations was incorrect and that no non-zero solutions were possible. On this basis, Clark and Smith stated that stationary vortices could not exist behind a two-dimensional flat plate.

It was considered that verification of this result was necessary, by an alternative means to the algebraic approach employed in ref.63. The Numerical Algorithm Group's⁶⁴ (NAG) C05NBF algorithm, as implemented on the VAX11/750, was used in a numerical attempt to determine simultaneous solutions for eqns.27 and 34. This algorithm seeks the zero of a system of n nonlinear, well-behaved, functions in n variables by a modified Powell Hybrid method. The user is required to provide an estimate of the solution together with the desired convergence tolerance, which for this investigation was set at the recommended value of the square root of machine precision.

On the basis of flow symmetry, solutions were sought only for the left-half Z -plane. The crossflow velocity U_c and the wingspan s were fixed at 1.0 m/s and 1.0 m respectively. The initial estimated solutions are shown together with the results in Table 1. It can be seen that in no case was a converged solution obtained, as indicated by the typical results in figs.3.3 and 3.4. It was considered that

this provided numerical verification of the result of Clark and Smith. The Kutta condition and the requirement for a stationary vortex cannot be met simultaneously. Therefore the point vortex model cannot provide a realistic model for the crossflow past a delta wing.

Utilising the "building-block" approach discussed in the introduction to this chapter, it was considered that the introduction of a sink to both vortices of the point vortex model would enhance the realism of the model, by representing the entrainment of flow into the vortices, and might permit satisfaction of the imposed boundary conditions. This possibility is investigated in the following section.

3.3 Selection of an Alternative Crossflow Model

From the results of section 3.2, it is obvious that the point vortex model is unsuitable for the well-ordered delta wing crossflow, and cannot therefore be used in an investigation of vortex breakdown. The development of an alternative model for the crossflow became necessary. A logical progression from the point vortex model can be obtained by addition of a sink to both point vortices of the point vortex model, as this will provide representation of the entrainment effect of the cores of the leading edge vortices whilst requiring only slight modification of the original model.

Fig.3.5 shows the streamline pattern, in the crossflow plane of a delta wing, determined by Verhaagen⁵ from a topological analysis of experimental data. For comparison, fig.3.6 shows the pattern as obtained from the point vortex model, where the Kutta condition (but not the stationary condition) was satisfied. This highlights the failure of the point vortex model to show the spiralling nature of the crossflow, although it must be stated here that there is a view that any spiralling of the crossflow streamlines is minimal, and that spiralling is chiefly a feature of the three-dimensional streamlines. Nevertheless, it was judged that such crossflow spiralling, however small, had to be included in the model in order that its effect on the vortex flow could be established. The development of the necessary vortex-sink model is fully described in the following section.

3.4 The Vortex-Sink Model

The modified representation for the delta wing crossflow is shown in fig.3.7. This was also the representation selected by Coe⁶⁵ in his vortex entrainment model. (It should be noted that the vortex-sink model developed by Mourtos⁶⁶ was for the chordwise, rather than crossflow, plane). As can be seen, two sinks of equal strength have been added to the point vortex model. Transformation to the Z_1 -plane was again required to resolve the image problem, fig.3.8, and the governing complex potential for symmetric flow was found to be of the form

$$\begin{aligned}
 W(Z_1) = U_C \left[Z_1 + \frac{a^2}{Z_1} \right] - \frac{i\Gamma}{2\pi} \ln \frac{(Z_1 - Z_{A1})(a^2 - Z_1 Z_{A1})}{(Z_1 - Z_{B1})(a^2 - Z_1 Z_{B1})} \\
 - \frac{Q}{2\pi} \ln \frac{(Z_1 - Z_{A1})(Z_1 - Z_{B1})}{(a^2 - Z_1 Z_{A1})(a^2 - Z_1 Z_{B1}) Z_1^2 |Z_{A1}|^2} \quad (37)
 \end{aligned}$$

It was noted at this point that Q and Γ are dimensionally equivalent i.e. both have units of m^2s^{-1} , and it was stated that

$$Q = b\Gamma \quad (38)$$

where b is a real number, and was defined as an "entrainment coefficient". Eqn.38 is used to simplify the later analysis.

3.4.1 Boundary Conditions

The three boundary conditions imposed were those of the point vortex model:

- (a) symmetric flow
- (b) the vortex-sink was to be stationary
- (c) a Kutta condition was to be satisfied at the leading edges.

Condition (a) is automatically satisfied by the symmetric formulation of eqn.37.

As shown in appendix 7, condition (b) will be met if

$$\left[(W_1 + W_4) \frac{dZ_1}{dZ} \right]_{Z=Z_A} - \frac{(i+b)\Gamma}{4\pi} \left[\frac{d^2Z_1}{dZ^2} / \frac{dZ_1}{dZ} \right]_{Z=Z_A} = 0 \quad (39)$$

where W_4 is expressed as

$$W_4 = \frac{b\Gamma}{2\pi} \left[\frac{Z_{A1}}{a^2 - Z_1 Z_{A1}} - \frac{1}{Z - Z_{B1}} + \frac{Z_{B1}}{a^2 - Z_1 Z_{B1}} + \frac{2}{Z_1} \right] \quad (40)$$

For this model the Kutta condition, as expressed in eqns.30 and 31, reduced to the condition that

$$\frac{dW}{dZ_1} = U_C \left[1 - \frac{a^2}{Z_1^2} \right] - \frac{i\Gamma}{2\pi} W_2 - \frac{b\Gamma}{2\pi} W_5 = 0, \quad Z_1 = \mp ai \quad (41)$$

where W_2 is given by eqn.33 and W_5 is given by

$$W_5 = \frac{1}{z_1 - z_{A1}} - \frac{z_{A1}}{a^2 - z_1 z_{A1}} + \frac{1}{z_1 - z_{B1}} - \frac{z_{B1}}{a^2 - z_1 z_{B1}} - \frac{2}{z_1} \quad (42)$$

Eqn.41 can be expressed as

$$iW_2 + bW_5 = \frac{4\pi U_C}{\Gamma} \quad (43)$$

As shown in appendix 8, at $z_1 = ai$, W_5 reduces to the wholly real function

$$W_5 = \frac{-2y_{A1}}{a^2 - 2az_{A1} + z_{A1}^2 + y_{A1}^2} - \frac{-2y_{A1}}{a^2 + 2az_{A1} + z_{A1}^2 + y_{A1}^2} \quad (44)$$

and so given that W_2 reduces to the wholly imaginary function W_3 shown in eqn.36, it can be seen that the Kutta condition is again a real equation. The non-dimensional form of the equation is derived in appendix 9, and is found to be

$$\frac{z_n - z_n^3 - y_n^2 z_n - by_n - by_n z_n^2 - by_n^3}{1 - 2z_n^2 + 2y_n^2 + z_n^4 + 2y_n^2 z_n^2 + y_n^4} = \frac{\pi U_C a}{\Gamma} \quad (45)$$

$$y_n = y_{A1}/a \quad , \quad z_n = z_{A1}/a \quad (46)$$

It can be seen that the Kutta condition is controlled by the parameters $U_C a/\Gamma$ and b .

The boundary conditions have again provided three equations.
However, in this case there are four unknowns: y_{A1} , z_{A1} , Γ and b .

3.5 Vortex-Sink Solution Method and Results

The simultaneous solution of eqns.39 and 41 was attempted using the algorithm described in section 3.2. Again solutions were sought only for the left half Z-plane. The problem of the additional unknown was overcome by specifying a value for b , which was varied between 0.0 and -1.0 in steps of -0.01 over a series of runs. Since Γ is defined as negative for the left-hand vortex and Q defined as positive for a sink, a negative value of b was required to ensure that a solution of the proper sense was obtained.

Initially, U_c and s were set at 1.0 m/s and 1.0m respectively, in order to correspond with the point vortex investigation. For this case the initial estimated solution was $y_A = -0.5$, $z_A = 0.5$, and $\Gamma = -5.0$. As b was decreased, the estimated solution for a program run was the actual solution of the preceding run, if such existed. Otherwise, the last available solution was used.

The case $b = 0$ corresponds to the vortex alone case and, as would be expected, no solution was found. In addition, no solution was found for $b = -0.01$.

In the interval $-0.02 \geq b \geq -0.71$ solutions of the proper sense were obtained in the upper left half plane. (No solutions were possible in the lower left half plane over the whole b range.) As can be seen in fig.3.9, initially the required vortex-sink locations are far removed from the wing. However, as b is progressively decreased, there is an allied inboard and downward movement of the

vortex-sink; for $-0.15 \geq b \geq -0.71$ it lay inboard of the leading edge. As b tends towards -0.71 the solution locations become more compressed. When compared with the experimental results of Verhaagen⁵ (for four angles of attack close to the apex of a slender delta wing), in all cases the vortex-sink is either located too far inboard, or at too great a distance from the wing to provide even an approximately realistic representation of the position of a leading edge vortex core. However, as shown in fig.3.10, the inboard and downward movement of the vortex-sink is initially accompanied by a decrease in clockwise vortex strength, as is found in reality. This behaviour is reversed when the vortex-sink moves inboard of approximately the thirty-five percent semi-span point, well inboard of any core locations found by experiment.

It should be noted that no solutions were possible for $-0.72 \leq b$. This can be explained by reference to fig.3.11, where the required value of vortex strength at each solution location is plotted against the ratio b . As b tends from 0 to -0.28 , $d\Gamma/db$ becomes progressively less negative. At $b = -0.28$ a maximum of Γ occurs (indicating a minimum of clockwise vortex strength), and thereafter $d\Gamma/db$ becomes progressively more positive, until $d\Gamma/db$ tends to infinity as $b = -0.71$ is approached. The resulting extremely high values of Γ preclude further solutions in the region of practical interest close to the wing.

The solution behaviour for this first case was only one of four types found.

The solution for $U = 2.0$ m/s and $s = 1.0$ m is typical of the second type of behaviour. For the starting solution $y_A = -0.5$ m, $z_A = 0.5$ m and $\Gamma = -5.0$, the solution locations shown in fig.3.12 were found over the range $-0.02 \geq b \geq -1.0$. As b was decreased, there was an inboard and upward movement of the vortex-sink solution, with the accompanying increase in the clockwise vortex strength indicated in fig.3.13. The variation of vortex strength with b is shown in fig.3.14. In this case, comparison with the Verhaagen results shows that the vortex-sinks are located too far outboard. However, the degree of physical realism achieved is considerably higher than that for the first case, and so it was considered that streamline and equipotential plots should be obtained.

The streamlines and lines of equal velocity potential for the crossflow plane could be determined for each solution point by use of the NAG contouring routine J06GBF. The resulting plots for one of the vortex-sink locations are shown in figs.3.15 and 3.16, and are typical of those found over the range of solutions. As a result of the periodic nature of the streamfunction for a sink in isolation

$$\psi = \frac{Q}{2\pi} \theta \quad (47)$$

and also that of the velocity potential for a vortex in isolation

$$\phi = - \frac{\Gamma}{2\pi} \theta \quad (48)$$

all streamline and equipotential plots exhibit two lines of discontinuity, one from each vortex-sink to the boundary of the plane for the streamline plots, and one from each vortex-sink to the wing for the equipotential plots. Although the values of Ψ and Φ change across the lines of discontinuity, the gradients of Ψ and Φ are unaffected, and so the crossflow velocities v and w are unaffected across these discontinuities. (The magnitude of the jumps in Ψ and Φ are shown in the three-dimensional plots of Ψ and Φ against y and z in figs. 3.17 and 3.18).

The third type of behaviour is typified by that for the case $U_c = 4.0$ m/s and $s = 1.0$ m. For the starting solution $y_A = -0.5$ m, $z_A = 0.5$ m and $\Gamma = -5.0$, it was found that solutions again existed over the range $-0.02 \geq b \geq -1.0$. However, in this case the vortex-sink locations always lay inboard of the leading edge and below the wing, as shown in fig.3.19. As b was decreased, there was an inboard and downward movement of this location, accompanied by the increase in clockwise vortex strength of fig.3.20. Obviously such solutions bear no resemblance to the real crossflow.

The fourth type of solution behaviour is typically that found for the case $U_c = 1.0$ m/s and $s = 5.0$ m, with the starting solution $y_A = 0.5$ m, $z_A = 0.5$ m and $\Gamma = -5.0$. Here no converged solutions were found for any value of b in the range $-0.01 \geq b \geq -1.0$.

It can be seen from Table 2 that there was no pattern to suggest which type of behaviour would be found. One interesting point is that where the first type was found, the vortex-sink location always

moved inboard of the leading edge at $b = -0.15$, and the boundary beyond which no solutions could be found always lay at $b = -0.71$. This indicates that the parameter b plays the dominant controlling role in the flow. However, the reason why this is not the case in the three other types of behaviour is not clear.

It should be noted that Coe also found solutions for such a vortex-sink model, with no reported difficulties. However, these solutions were obtained for specified locations determined from experimental results, no purely theoretical study being attempted.

It was considered that the unpredictable solution behaviour necessitated the rejection of the vortex-sink model in the form discussed in this section. However, comparison of the streamline plot of fig.3.15 with fig.3.5, the crossflow streamline pattern of Verhaagen, shows that the model does provide an adequate representation of the crossflow streamlines. In addition, there appears to be a dependence of the solution for the model on the ratio of sink-to-vortex strength. For both the above reasons, it was desired to retain the governing complex potential in the form given in eqn.37. Therefore the next development of the flow model could only be obtained by modification of one or more of the imposed boundary conditions. As discussed in the following section, the requirement for a stationary vortex-sink was replaced by a force-free condition on a vortex-sink-feeding sheet combination. Not only does this approach improve on the realism of the model, but it also provides the basis for the extension of the model into three dimensions, as the feeding sheet concept provides a mechanism for

growth of the vortex and sink strengths in the downstream direction.

3.6 Modification of the Vortex-Sink Model

As was stated in section 3.5, the lines of discontinuity in the equipotential plot of fig.3.16 indicate the existence of a potential jump. In section 2.1.3 and eqn.21, it was shown that such a jump exists across the trace in the crossflow plane of the three-dimensional feeding sheet. It was therefore decided that a line of discontinuity in potential should be taken to represent such a trace. With the assumption that the discontinuity runs from the leading-edge to the vortex-sink (which is approximately correct and must be imposed to avoid excessive computational time), a force-free condition, similar to that of Brown and Michael, could then be applied to a vortex-sink-feeding sheet combination. This would replace the stationary vortex-sink condition, which is inapplicable as the vortex-sink is effectively "tethered" to the leading edge by the feeding sheet. However, the requirements for symmetric flow and a Kutta condition at the leading edges were again invoked.

It should be clear that the feeding sheet is not directly imposed on the flow, but rather is a function of the potential jump. Therefore the governing complex potential and the Kutta condition are unchanged from eqns.37 and 41. The force-free condition is detailed fully in the following subsection, and is based on the three-dimensional coordinate system of fig.1.1.

3.6.1 The Force-Free Condition

An element Δx of the vortex-sink-feeding sheet combination is

shown in fig.3.21. This differs from Brown and Michael's model in that not only has a sink been added to the point vortex, but there is also a component, $(d\Gamma/dx)_1$, of the feeding sheet circulation lying in the plane of the sheet. As can be seen in fig.3.22, this was used to represent a difference in velocities towards the vortex-sink along the sheet. For simplicity it was assumed that this difference in velocities could be directly related to the change in sink strength in the downwing (x) direction, and so it was stated that

$$\frac{dQ}{dx} = C_1 \left(\frac{d\Gamma}{dx} \right)_1 \quad (49)$$

where C_1 is a real constant.

It is shown in Appendix 10 that an approximate force balance on this element leads to the equation below.

$$\frac{1}{C_1} \frac{dQ}{dx} + i \frac{d\Gamma}{dx} = \frac{- \left[U_\infty \frac{dZ_A}{dx} + V_{ns} \right] (Q + i\Gamma)}{U_\infty (Z_A + s/2) \cos \alpha} \quad (50)$$

where U_∞ is the freestream velocity, α is the angle of attack and V_{ns} is the non-singular component of crossflow velocity at the vortex-sink minus the normal component of the freestream. As stated in Appendix 10, the accuracy of this force balance decreases with increasing angle of attack.

Although a conical solution for the vortex-sink model, modified by the inclusion of this force-free condition, would be of no importance in a study of vortex breakdown, its possible existence was investigated as detailed overleaf for the purpose of completeness.

3.7 Conical Flow

From eqn.50 it can be seen that the force-free condition is essentially three-dimensional. However, making the assumptions of conical flow, namely

$$\frac{d\bar{z}_A}{dx} = \frac{\bar{z}_A}{x} \quad (51)$$

$$\frac{dQ}{dx} = \frac{Q}{x} \quad (52)$$

$$\frac{d\Gamma}{dx} = \frac{\Gamma}{x} \quad (53)$$

eqn.50 reduces, as proven in Appendix 11 for $C_1 = 1$, to the condition that

$$V_{ns} + U_\infty \left[\left[\frac{z_A}{x} + \cot \Lambda \right] \cos \alpha + \frac{\bar{z}_A}{x} \right] = 0 \quad (54)$$

where Λ is the angle of wing sweepback. For a specified value of x the condition is effectively two-dimensional.

Such a conical formulation obviously cannot yield information of interest on vortex breakdown, since the conicity of the flowfield precludes any three dimensional behaviour. However, it was considered worthwhile to study any possible conical solutions before proceeding to a non-conical investigation., as in reality a region of

near conical flow is found over a delta wing away from the trailing edge.

3.7.1 Modified Vortex-Sink Solution Method and Results (Conical)

The simultaneous solutions of eqns.54 and 41 was again attempted by use of the NAG C05NBF algorithm. The freestream velocity U_∞ and the wingspan s were fixed at 1.0 m/s and 1.0 m respectively for the values of Λ and α given in Table 3. To obtain a solution of the proper sense, b was once more required to be negative. The spanwise vortex-sink coordinate, y_A , was varied between $-1.5s$ and 0.0 to find solutions in the variables z_A , b and Γ in the left half plane.

As shown in Table 3, the solution behaviour was unpredictable over the range of freestream velocities and wing parameters investigated. In six cases no solutions could be obtained. Where a solution was possible, for example where

$$\Lambda = 70^\circ, \quad \alpha = 20^\circ$$

it can be seen from fig.3.23 that all the possible vortex-sink locations lay outboard of the leading edge. The variations of b and Γ with y_A are also shown. Such a lack of physical realism, coupled with the non-existence of a solution in particular cases, rendered the conical vortex-sink model of little value. Its application was not pursued further. Full details of the non-conical investigation of the crossflow are given in the following section.

3.8 Non-Conical Flow

By considering the flowfield to be non-conical, as it must be if vortex breakdown is to occur, further simplification of the force-free condition, eqn.50, is not possible. The equation remains three-dimensional, and yields no information on the flow in the crossflow plane. Therefore the crossflow problem is highly indeterminate, with only one real equation, the Kutta condition, in four unknowns: y_A , z_A , Γ and b .

In section 3.5, it was shown that the parameter b appeared to play a significant role in the crossflow under certain conditions. It was considered that it would be worthwhile to study the effect of a variation in b on the required value of Γ for a fixed vortex-sink location (and therefore for constant y_{A1} and z_{A1} in the transformed plane). In addition, from the Kutta condition, eqn.45, it is obvious that for fixed values for b and Γ , a locus of solution points for the vortex-sink exists. This behaviour was also to be studied.

3.8.1 Variation of the "Entrainment Coefficient" b

A series of locations was specified for the vortex-sink in the left half Z -plane. These locations were then transformed to the Z_1 -plane, and the parameter b varied between -1.0 and 1.0 in steps of 0.01 . The required variation of Γ , and thence Q , could then be obtained. The non-dimensional formulation of the Kutta condition is such that the only effect of crossflow velocity and wingspan is to factor the vortex strength, whilst all other features of the solution

behaviour are unaffected. Therefore U_c and s were fixed at 1.0 ms^{-1} and 1.0 m respectively.

Shown in fig.3.24 is the mesh indicating the 2401 vortex-sink locations investigated. For each location the solution behaviour with b was the same, as typified by the four cases shown in fig.3.25.

It was necessary for Γ to be negative and Q positive, i.e b negative, for the vortex-sink to be of the proper sense, and so it was the behaviour of Γ and Q for $-1.0 \leq b \leq 0.0$ that was of particular interest. In all cases a discontinuity in the solution was found within this range at some value of b equal to b_c , the "critical entrainment coefficient", shown in fig.3.25. For $-1.0 \leq b \leq b_c$, Γ was positive and Q negative. As b_c was approached, the magnitudes of Γ and Q became extremely high. (It is assumed that these values would be well damped in a model where viscous effects within the vortex core were represented). These remained high, but reversed in sense, as b_c was passed. Thereafter, for $b_c \leq b \leq 0.0$, a vortex-sink of the proper sense was possible, and the magnitudes of Γ and Q quickly fell to what were considered reasonable values for the imposed flow conditions. As b passed through zero and became positive, Q fell through zero to become negative whilst Γ remained negative. Although solutions of the proper sense were impossible for $0.0 \leq b \leq 1.0$, no discontinuities were present.

On the basis of the interesting nature of this solution behaviour, it was considered that a study of the associated variation

of normal force, F_z , would be of interest. Although several methods exist for such a calculation, a simple approach was sought which would minimise computational time.

It was initially considered that F_z could be calculated by application of the theorem of the Blasius

$$F_y - iF_z = \frac{1}{2} \rho i \int_c \left(\frac{dW}{dz} \right)^2 dz \quad (55)$$

where c is a contour around the wing, vortex-sinks and feeding sheets. However, such an approach would calculate the force acting on both the wing and the vortex-sink-feeding sheet combinations. This could not be reconciled with the requirement that only the wing can sustain force and that the vortex-sink feeding sheet combinations should be force-free. As a result, any calculated normal forces would be excessive.

An alternative method was developed based on the pressure distribution close to the wing surface. In the crossflow plane the wing is represented by a line of zero thickness, and therefore the pressure distribution directly on the wing could not be considered. An artificial thickness, as shown in fig.3.26, was required.

The pressure coefficient C_p at any point in the crossflow is given by eqn.56 overleaf.

$$C_p = 1 - \left[\frac{v^2 + w^2}{U_c^2} \right] \quad (56)$$

On the wing surface where w is required to be zero, this can be expressed as

$$C_p = 1 - \left[\frac{\operatorname{Re} \left[\frac{dW}{dz} \right]}{U_c} \right]^2 \quad (57)$$

The pressure distribution for

$$y_A = -0.4, \quad z_A = 0.2, \quad \Gamma = -4.0, \quad b = -0.1$$

is typical and shown in fig.3.27. Unexpectedly, there is a region of positive pressure coefficient on the upper surface. The region of higher suction inboard of the leading edge occurs underneath the vortex-sink location. The pressure jump at the leading edge is a consequence of the introduction of the artificial thickness; from the equipotential plot of fig.3.16 it can be seen that the lines of equal ϕ will be more closely spaced on the artificial upper surface than on the artificial lower surface, and so a pressure discontinuity is to be expected at the artificial leading edge, despite the fact that a Kutta condition is satisfied at the real leading edge.

From the pressure distribution, it is possible to calculate the normal force acting on the wing from the relation

$$F_z = \frac{1}{2} \rho U_c^2 \int_{-s/2}^{s/2} (C_{p1} - C_{pu}) dy \quad (58)$$

where C_{p1} and C_{pu} are the pressure coefficients on the upper and lower surfaces respectively. A normal force coefficient C_{Fz} was defined as

$$C_{Fz} = \int_{-s/2}^{s/2} (C_{p1} - C_{pu}) dy \quad (59)$$

The required integration was performed numerically using the NAG algorithm D01GAF, which employs third order finite difference formulae with error estimates according to a method due to Gill and Miller. The variation of C_{Fz} with b for the four cases of fig.3.25 is shown in fig.3.28. As b falls from zero towards the critical value b_c , there is an increase in normal force. Close to b_c this increase becomes large and C_{Fz} tends to an extremely high value. A maximum of C_{Fz} exists at b_c , followed by an abrupt decrease as b is further reduced. This decrease in C_{Fz} becomes more gradual as the value of b tends to -1.0.

The critical dependence of the Kutta condition and normal force on b , and the flow behaviour at b_c , indicate that the entrainment coefficient is the dominant control parameter in this crossflow model. Fig.3.29 shows two views of a three-dimensional plot of b_c against y_A and z_A , where b_c has been determined by an inverse solution of eqn.43, with the vortex strength set at $\Gamma = -10000$ to

correspond to the asymptotic behaviour typified in fig.3.25. (It should be noted that the region of constant b_c outboard of the leading edge does not exist in reality, but is a consequence of the truncation of the values of very low, i.e. highly negative, values of b_c in this region. This truncation was required to ensure that a meaningful plot could be obtained for the remainder of the region considered). It can be seen that outwith a region close to the wing, an inboard and upward movement of the vortex-sink produces an increase in the value of b_c , i.e it becomes less negative.

There are three features of the controlling role of b that indicate the possible importance of the entrainment of flow into a leading edge vortex core in the subsequent breakdown of that vortex.

Firstly, if the entrainment varies such that b falls below b_c , i.e. $-1.0 \leq b \leq b_c$, the required flow change is that the vortex should reverse its direction of rotation, and outflow should replace inflow as Q becomes negative. It was considered that this may be related to the spiralling of the vortex axis and the subsequent "bursting" of the vortex at breakdown.

Secondly, the existence of a critical sink-to-vortex strength ratio b_c , the critical entrainment, indicates the existence of a critical radial-to-swirl velocity ratio. In three dimensions, the axial flow along a vortex core is largely controlled by entrainment into the core, and therefore to a certain extent by the radial velocity field. The experimentally deduced critical swirl-to-axial velocity ratio (see section 1.2 of Chapter 1) may be further

related to a critical swirl-to-radial, or radial-to-swirl, velocity ratio. This would be qualitatively in agreement with the critical nature of b found for this vortex-sink model of the crossflow.

Thirdly, although the values of normal force become extremely high close to b_c (as a consequence of the extremely high values of Q and Γ), the behaviour of C_{Fz} as b is decreased below b_c is similar to that which occurs for the lift acting on a delta wing with increasing angle of attack. As the angle of attack of the wing is increased towards a critical value, there is a non-linear growth in lift, followed by a sudden reduction as the critical value is passed, marking the onset of vortex breakdown above the wing.

(As an aside, it is considered that it may also be possible to determine the role of b in the breakdown of a vortex flow within a circular pipe. This could be attempted by studying the crossflow within the cylinder in the Z_1 -plane, with a no-slip condition imposed at the cylinder wall).

3.8.2 Variation of Vortex-Sink Locii with Γ and b

The Kutta condition, eqn.45, produces a locus of possible vortex-sink solution points for specified values of Γ and b . For a fixed value of b , and Γ varied between an upper and lower limit, the effect on this locus was studied. A similar study was performed for Γ held constant and b varied. The intention of the study was to ascertain whether a smooth variation in vortex strength or entrainment would produce a discontinuous change in vortex-sink

location.

Again U_c and s were set at 1.0 m/s and 1.0 m respectively. The solution of the Kutta condition was achieved by varying y_A between -0.5 and 0.0 in steps of 0.01 for each value of Γ and b , and using the NAG C05NBF algorithm to find the corresponding z_A for each y_A . The coefficient b was varied between -0.1 and -0.6 and the vortex strength Γ between -2.0 and -60.0 in a series of steps.

In general, the cases detailed in Table 4 can be summarised as showing that a decrease in Γ or an increase in b moves a vortex-sink location further away from the wing, as would be expected. Fig.3.30 highlights this behaviour for two particular cases. However, certain combinations of b and Γ resulted in erratic and discontinuous solutions. For $b \geq -0.3$, it was found that in an intermediate range of vortex strength the vortex-sink locations jumped from above to below the wing, as shown in the example of fig.3.31. In addition, for $b = -0.1$ a dramatic change in the trend of the locii can be seen at $\Gamma = -17.0$, fig.3.32, with the assumption of a positive, rather than negative, gradient, and locations for the vortex-sink lying only inboard of the leading edge. Also for $b = -0.1$, and $\Gamma \geq -10.0$, the normal solution behaviour with decreasing b was reversed, with the vortex-sink initially lying close to the wing, and moving away as b was decreased to -0.2. These last two types of behaviour were not found elsewhere.

From these results, and those of section 3.8.1, it was concluded that solution of the Kutta condition, and therefore the flow in the

crossflow plane, is highly dependent on the parameters b and Γ . As has been shown, small changes in these parameters can result in a dramatic change in the nature of the flow (of Catastrophe theory), and it was considered that such behaviour may well be related to vortex breakdown. In order to investigate this possibility more fully, it was necessary to extend the flow model into three dimensions. This was achieved through application of the non-conical force-free condition, as fully discussed in the following section.

3.9 Extension of the Model into Three Dimensions

It was required that the non-conical modified vortex-sink crossflow model be made the basis for a three-dimensional, or quasi-three-dimensional, model of the delta wing flow. This was to be achieved in such a way as to ensure that the variation of the parameter b could be easily studied, and any tendency to a critical flow condition identified. The approach adopted is summarised below.

At some point downwing of the apex, a location Z_{Ai} for the vortex-sink in the left half Z -plane was specified, along with an initial value b_i for the entrainment coefficient b . For a symmetric flow, the Kutta condition eqn.45 was invoked to provide the required value for Γ and thence Q . With the assumption that eqn.51 was valid at the initial location, the force-free condition eqn.50 gave the singularity strength gradients dQ/dx and $d\Gamma/dx$ for a specified value of C_i .

On the basis that

$$Q_{i+1} = Q_i + \frac{dQ_i}{dx} \Delta x \quad (60)$$

$$\Gamma_{i+1} = \Gamma_i + \frac{d\Gamma_i}{dx} \Delta x \quad (61)$$

the values of Q and Γ at the next downwing station $i+1$ could be obtained. Thus the only effect of an upwing station on its downwing

neighbour was to establish these sink and vortex strengths. There was no upwing effect from a downwing station, and therefore the trailing edge could not be modelled.

As shown in the previous section, the provision of Q and Γ for a crossflow plane provides a locus of solution points for the vortex-sink in the crossflow plane, and so an additional boundary condition was required to fix the vortex-sink at a definite location. Given this boundary condition it would then be possible to repeat the calculation procedure, and to step down the wing between successive crossflow planes to find a quasi-three-dimensional solution for the flow. However, only a semi-infinite delta wing can be considered as the trailing edge could not be modelled.

3.9.1 A Constraint on Vortex-Sink Motion

In the absence of any obvious additional boundary condition, and to facilitate development of the flow model, a simple constraint was placed on the spanwise variation of vortex-sink location. This required that

$$\frac{2y_{Ai}}{s_i} = \text{constant} \quad (65)$$

i.e. a conical variation was imposed. There was no solid physical basis for this condition. However, of the four variables y_A , z_A , Γ and b , it was considered that the variation of Γ and b would be of most importance in an investigation of vortex breakdown. In

addition, from section 3.8.2 it can be seen that, in most cases, for a variation in Γ or b the accompanying variation of the z coordinates of the locus is more marked than that of the y coordinates.

Therefore, it was judged that the constraint on y_A would have least impact on the results of the investigation, and the boundary condition of eqn.65 was imposed on the flow. This completed the quasi-three-dimensional model.

3.10 A Summary of the Flow Model

A complex potential based representation has been developed for the crossflow past a delta wing. The leading edge vortices are modelled by a pair of symmetrically placed point vortex and sink combinations, and the resulting lines of discontinuity in velocity potential are taken as indications of the presence of feeding sheets. It was found that the ratio b , of sink and vortex strengths, is a dominant control parameter in the crossflow, and at a critical value b_c the flow behaviour is similar to that at vortex breakdown. The existence of this critical ratio may well be related to the swirl-to-axial velocity ratio discussed in section 1.2 of Chapter 1. Thus it may be that the entrainment effect of a vortex plays a major role in the breakdown phenomenon.

A force-free condition for the vortex-sink-feeding sheet combination, coupled with a constraint on the spanwise vortex-sink motion, permits extension of the model to provide a quasi-three dimensional representation for the flow over a semi-infinite delta wing, in the region downwing of the apex and upwing of the trailing edge. Such a model permits the variation, and hence the importance, of the entrainment-related parameter to be fully investigated. However, it provides only a limited approximation to the real flow, as it allows no calculation of downwing effects and becomes progressively less accurate with increasing angle of attack. Consequently, the results obtained from any application of the model should be assessed qualitatively rather than quantitatively, as its level of approximation is such that numerically accurate results

cannot be obtained.

The application of this model to a vortex breakdown investigation is fully described in the following chapter.

Chapter 4

Application of the Flow Model to Vortex Breakdown Investigation

4.0 Introduction

In this chapter the quasi-three-dimensional flow model was initially assessed by its application to a single test case to ensure the proper functioning of its algorithm, as implemented in the FORTRAN program MODEL3D on the VAX 11/750 computer. An extensive range of starting solutions and wing parameters were then considered in turn to determine the effect of each on the development of the flow. Particular attention was directed to the parameter b , in order to ascertain whether its variation in three dimensions played a similar controlling role to that in the crossflow plane, and to determine whether the resulting behaviour was purely a numerical phenomenon or indicative of the physical process of vortex breakdown.

It was found that outwith a limited flow regime the parameter b again dominated the flow, as the calculation failed where b tended towards its critical value, thus providing further evidence of the role of the entrainment effect in vortex breakdown. The variations of the calculation failure, or breakdown location, with angle of attack and wing sweepback were in qualitative agreement with those found experimentally. It was concluded that the critical nature of the entrainment coefficient b does relate to vortex breakdown. Further results obtained indicate that it is possible to delay the

breakdown of the calculation, and hence the vortex flow, by suitable control of the initial entrainment coefficient, b_i .

4.1 The Test Case

The test case considered was that of a wing with a leading edge sweep $\Lambda = 70^\circ$, and at an angle of attack $\alpha = 20^\circ$. Both Λ and α were chosen to correspond approximately to the mid-range of wing parameters for which the flow was to be investigated, i.e. $60^\circ \leq \Lambda \leq 80^\circ$, $5^\circ \leq \alpha \leq 30^\circ$. The freestream velocity U_∞ and the wingspan s_i in the initial crossflow plane were set at 1.0 ms^{-1} and 1.0 m respectively.

For reasons to be explained in section 4.2, the initial vortex-sink location was expressed in polar coordinates as $r_i = 0.5 \text{ m}$, $\theta_i = 150^\circ$, based on the geometry of fig.4.1. In this case the plots of Γ and Q against b , for solution of the Kutta condition, are those of fig.4.2. It can be seen that $b_c = -0.56$, and so the value of b_i was set at -0.05 to ensure that it was far removed from this critical condition.

An additional coordinate x_d was defined, where x_d is the distance downwing of the starting location (where $s_i = 1.0 \text{ m}$), as opposed to x , which is the distance downwing of the apex.

The step-size, Δx , for the model was to be decided from the results of this test case, and therefore several runs of MODEL3D were performed for a range of step-sizes.

4.1.1 Test Results

It was initially intended to test MODEL3D over a run of 5000 steps in x , for various values of Δx . However, it was found that in every case the calculation failed before the run was completed. The actual value of x_d at which this failure occurred, is plotted against Δx in fig.4.3. Note that a limit exists above which no calculation is possible. For any value of Δx below the limit, the mechanism of solution failure was the same, and it was therefore decided that a step-size of 0.001 was best suited to provide sufficient detail of the flow without requiring excessive CPU time.

The solution behaviour which resulted in failure of the calculation is depicted in fig.4.4 (a-f). As can be seen, an increase in x_d initially produced an upward movement of the vortex-sink location, as a consequence of the growth in magnitudes of the vortex and sink strengths. However, the increase in z_A and the singularity strengths occurred more rapidly than might be expected. This can be explained by the high magnitudes of $d\Gamma/dx$ and dQ/dx shown in figs d and e. The rapid increase in vortex strength is a consequence of the employment of a concentrated vorticity representation, where the growth in point vortex strength over one step is far greater than it would be for individual elements of a distribution of vorticity. As a result the associated movement of the vortex-sink away from the surface is considerably amplified. It should be noted that at $x_d = 1.15$, z_A began to decrease, indicating the growing dominance of the sink as it "sucked" itself towards the wing. As x tended towards the calculation failure point at $x_d =$

1.53, the singularity strengths became very high, and it was the associated values of $d\Gamma/dx$ and dQ/dx that led to termination of the program run. (It had been found during the assessment of Δx that excessive values of the singularity strength gradients produced, in the majority of cases, numerical overflow errors. However, highly erratic solution behaviour was found in the remaining cases.

Therefore limits were imposed on the magnitudes of $d\Gamma/dx$ and dQ/dx which required that

$$\frac{d\Gamma}{dx} \geq -999 \quad (66)$$

$$\frac{dQ}{dx} \leq 999 \quad (67)$$

Violation of one or both of these conditions resulted in termination of the calculation, as in the test case. The conditions were sufficient to prevent any undesirable solution behaviour, whilst the essential character of the flow was unaffected. In any case, extremely high gradient values could almost certainly not be sustained in a real flow.)

Figure 4.4 f shows the reason for the appearance of the large gradients in vortex and sink strength as calculation failure was approached. The value of b in each crossflow plane is plotted, along with the critical value b_c for that plane, against the coordinate x_d . (The value for b_c was obtained by setting $\Gamma = -10000$ at the vortex-sink location in each downwing crossflow plane, and obtaining

the necessary value of b from eqn.45 of Chapter 3). As x_d tended to 1.53, there was an associated tendency of b to b_c , until at $x_d = 1.53$, the values of b and b_c were almost equal. From the results of Chapter 3, shown in fig.3.24, such a proximity of b to b_c must result in extremely high values of Q , Γ , dQ/dx and $d\Gamma/dx$, and the associated failure of the calculation.

The test case showed that the algorithm was functioning properly. It also indicated that the parameter b was dominant in the quasi-three-dimensional model. In addition, the behaviour of the singularity strengths and strength gradients as the critical value b_c was approached is similar to that reported in ref.19, where Hall attempted to identify the failure of the quasi-cylindrical approximation with the critical state. It was considered that the critical nature of b could be purely a numerical phenomenon, in the same way that Shi³² considered Hall's findings to simply be a result of the quasi-cylindrical approximation. However, as is shown in the investigations of this and the following chapter, if b is assumed to play a controlling role then it is possible to obtain fair qualitative agreement with experimental results.

4.2 The Investigative Procedure

From the Kutta condition of eqn.45, it was found that the only effect of varying the crossflow velocity and wingspan was to modify the required vortex and sink strengths without affecting the overall solution behaviour. It was therefore considered that holding both U_∞ and s_i constant would not seriously limit the investigation. Therefore, these were set at 1.0 m/s and 1.0 m respectively. However, a variation in Λ for a constant s_i will result in a change in x_i , since

$$x_i = s_i \cot \Lambda \quad (68)$$

To ensure a constant x datum, the location at which calculation failure occurred is always quoted as a distance, x_b , downwing of the apex. It should be obvious, however, that information on the variation of the flow parameters is only available downwing of x_i .

A relationship was sought between the initial vortex-sink location and the angle of attack α , in order that the experimentally observed variation of vortex core location with angle of attack could be represented. From the results of ref.5 reproduced in fig.4.5 (where c_o is the wing chord at the centreline), it can be seen that an increase in angle of attack produces an upward and inward movement of the core position, where the upward movement is more pronounced. To approximately model this behaviour, it was decided that the polar coordinate system of fig.4.1 should be employed, where

$$r_i = 0.5 \text{ m} \quad (69)$$

$$\theta_i = (170 - \alpha)^\circ, \quad 5^\circ \leq \alpha \leq 30^\circ \quad (70)$$

This models an inward, and more marked upward, movement of the initial vortex-sink location with increasing angle of attack, as shown in fig.4.6.

There remained four unspecified parameters: α , Λ , b_i and C_1 . Since C_1 is a constant of proportionality in the relationship between dQ/dx and $(d\Gamma/dx)_i$, a value was sought for it which would remain suitable over the full range of flows to be investigated. The determination of this value is discussed in the following subsection.

4.2.1 The Constant of Proportionality C_1

The effect of a variation in C_1 was determined for three test cases which encompassed the range of values of α and Λ to be considered. The results are listed in Table 5. From these, and the plots of fig.4.7, it can be seen that beyond a certain value of C_1 at higher angles of attack the solutions became oscillatory. However, as the value of C_1 was decreased the vortex-sink moved away from the wing surface increasingly quickly. To obtain a compromise between these types of behaviour, C_1 was set equal to 1.0. This was sufficient to ensure a smooth solution in every case while retaining a fair degree of physical realism.

Having thus set C_1 , it was then possible to proceed to the investigation proper, where the effects on the calculation of a

variation in α , Λ or b_i were to be assessed.

4.2.2 The Influence of α on x_b

For each case investigated, the values of Λ and b_i were held constant within the range $60^\circ \leq \Lambda \leq 80^\circ$, $-0.05 \geq b_i \geq -0.6$, as α was varied between 5° and 30° . The $r_i-\theta_i$ model of eqns.69 and 70 was assumed.

Two types of solution behaviour were identified. A typical result of the first type is shown in fig.4.8 (a-f). At lower values of α and $|b_i|$ the variation of z_A and Γ with x_d was almost linear over the entire x_d range, away from the region of high x gradients of z_A and Γ near the initial solution plane. However, the variation of Q was decidedly non-linear, with an initially abrupt increase followed by a more gradual fall to zero. The magnitude of Q remained small throughout. Away from the initial solution plane there was only a very slight tendency of b to b_c . It can be seen that the calculation was terminated at the point where b became equal to zero, i.e. at the point where the sink strength was required to change in sign and a solution of the proper sense was no longer possible.

The second type of behaviour is typified by the results shown in fig.4.9 (a-f). The calculation behaviour here was of the type described for the test case in section 4.1, i.e. the failure was a consequence of b tending very close to b_c .

The variation of x_b with α was the same for both types of

solution behaviour. As shown in fig.4.10 (a-c), for some limited range of α the values of x_b were considerably greater than for all other values of α . A variation in b_i served to alter the endpoints of this α range and modified the maximum value of x_b ; from fig.4.11 it can be seen that increasing (decreasing) b_i shifted the range to the right (left).

Figures 4.12 and 4.13 show that the effects on the x_b -vs- α solution of an increase (decrease) in the angle of wing sweepback, Λ , were to amplify (attenuate) the magnitude of the higher x_b range and to shift the associated α range to the left (right).

The influence of angle of attack on x_b could not be fully determined from this investigation. As can be seen in figs.4.10 - 4.13, from the regions of higher x_b onwards, an increase in α resulted in a decrease in x_b , as found experimentally with the upwing movement of vortex breakdown location with angle of attack. The regions of increasing x_b at lower values of α were unexpected. However, from the movement of the high x_b regions with b_i , it appeared that a relationship existed between α and b_i which would enable a solution to be obtained showing a smooth decrease in x_b with increasing α . It was hoped that the form of this relationship could be determined from a study of the direct influence of b_i on x_b (to be discussed in section 4.2.4).

4.2.3 The Influence of Λ on x_b

The values of α and b_i were held constant within the range

$5^\circ \leq \alpha \leq 30^\circ$, $-0.02 \geq b_i \geq -0.6$, as Λ was varied between 60° and 80° . Again r_i and θ_i were provided by eqns. 69 and 70.

At lower values of the angle of attack ($\alpha \leq 10^\circ$) for $b_i > -0.15$ the calculation was terminated when the required sink strength became negative, i.e. solution behaviour of the first type. However, outwith this limited region ($\alpha > 10^\circ$) the results obtained indicated solution behaviour of the second type. Numerical failure occurred as b tended to b_c , this failure being progressively delayed as Λ was increased, as shown in fig.4.14. This is in accordance with experimentally obtained variations of vortex breakdown location with the angle of wing sweepback, as can be seen from the results of Erickson reproduced in fig.1.8. Therefore it would appear that if the numerical failure of the calculation can be related to vortex breakdown, then MODEL3D provides some representation of the effect of sweepback.

4.2.4 The Influence of b_i on x_b

As has been discussed in the previous two subsections, it would appear that the initial entrainment coefficient b_i not only plays a considerable role in determining the value of x_b , but also controls the manner in which the failure of the calculation occurs. The variation of x_b with b_i was assessed for $5^\circ \leq \alpha \leq 30^\circ$ and $\Lambda = 60^\circ$, 65° , 70° , 75° and 80° .

It was found that for $\alpha = 5^\circ$ and 7.5° , no calculation failure occurred within 5000 steps, and the calculation was stopped at that point. This may suggest that the vortex flow does not break down at

these angles of attack. For $\alpha = 10^\circ$, 12.5° and 15° the variations of x_b with b_i were those of fig.4.15 (a-c). Considering the particular case of $\alpha = 10^\circ$ (which is typical of all three cases), for $0 > b_i \geq -0.12$, the calculation failed as the required sink strength became negative. For $b_i < -0.12$ the calculation failure occurred as b tended close to its critical value. As b_i was decreased below -0.12 , this failure was progressively delayed until at $b_i = -0.15$ a maximum of x_b existed. Further decreases in b_i resulted in a reduction x_b , and when b_i came close to the critical value for the initial crossflow plane (in this case for $b_i \leq -0.62$) the calculation failed immediately, i.e. at $x_d = 0.0$, $x_b = 1.374$ (the distance downwing of the apex at which the calculation started). For $\alpha = 12.5^\circ$ and 15° the solution behaviour was qualitatively the same, but with different limiting values for b_i .

It can be seen from fig.4.15 that as α was increased from 10° to 15° , the extent of the solution over which dx_b/db_i was positive was increased. For $\alpha > 15^\circ$, it is shown in figs.4.15 d,e and f that dx_b/db_i was always positive, and the maximum possible value of x_b existed at the highest value of b_i .

It was noticeable that as α was increased, the maximum attainable x_b was decreased, in accordance with experimental evidence on the movement of vortex breakdown location with angle of attack. The variation of maximum x_b with α for the five sweepback angles considered is shown in fig.4.16.

The required variation of b_i with α to produce the maximum x_b are

shown in fig.4.17. It can be seen that a smooth increase in b_i is required as α is increased. Beyond a limiting value of α , α_c , where the limit appears to be controlled by Λ , it is necessary for b_i to tend closely to zero whilst remaining negative.

On the basis of the results of this section, it was considered that if the mechanism for the numerical failure of the calculation is indeed of a similar nature to that responsible for the breakdown of a leading edge vortex, then the breakdown of the vortex could be delayed by a parameter related to b_i , the entrainment coefficient, as hypothesised in ref.68.

4.3 Summary of the Flow Investigation

It was found that two distinct forms of solution behaviour are possible using MODEL3D.

The first type of behaviour, which occurs only at low values of α and $|b_i|$, results in a failure of the calculation when the required sink strength becomes negative, i.e. the sink must become a source. However, the sense of the vortex is unaffected. No physical parallel for such behaviour exists, and it is considered that this first type of solution is simply an indication that the flow model is not representative of a real flow for the starting conditions chosen. This is evidenced by the decrease in sink strength that accompanies the later increases in vortex strength, when it would be expected that the entrainment effect of the vortex would increase. Such behaviour may be a consequence of the initial proximity of the vortex-sink to the wing.

The second type of behaviour is characterised by the calculation failure which occurs as b tends to its critical value, b_c , and by the resulting large values of vortex and sink strength. Numerical failure at these values of Γ and Q prevents b passing b_c , but it appears that the behaviour which results from the critical nature of b_c may well be related to vortex breakdown, and is not simply a numerical phenomenon. This statement can be justified not only for the reasons which have been set out in Chapter 3, but also on the basis of the qualitative agreement of solutions from MODEL3D with experimental results. In particular, further evidence for the

validity of MODEL3D as a representation of the breakdown of a leading edge vortex is provided by the fact that the variation of x_D with α and Λ is comparable to the dependence of the breakdown location in a real flow on the angle of attack and wing sweepback.

The results obtained from MODEL3D indicate that the initial entrainment coefficient, b_i , plays a dominant role in establishing the type and location of the numerical failure, or "breakdown", of the calculation, and hence the vortex flow. It would appear that control of some parameter relating to the entrainment effect of a leading edge vortex may well permit the breakdown of that vortex to be delayed. The prospects for such control are discussed in the following chapter.

Chapter 5

Prospects for the Control of Vortex Breakdown

5.0 Introduction

It was shown in Chapter 4 that the numerical failure of calculations employing MODEL3D could be delayed by selection of a suitable initial value b_i for the entrainment coefficient. On the basis that this numerical failure could be related to the breakdown of a leading edge vortex, boundary curves were derived for the variation of b_i with angle of attack which would ensure the persistence of a well ordered vortex over the order of one initial wingspan, i.e. 1.0 m, downwing of the calculation starting point.

Earlier investigations of possible methods of vortical flow control were then considered, as evidence was sought to provide verification of the role of entrainment in vortex breakdown. These investigations indicated that concepts such as the tangential blowing of air from the leading edge of a highly swept wing can offer considerable benefits in terms of high angle of attack performance. The application of these concepts is discussed in the light of the findings of the MODEL3D investigation. It would appear that the enhancement of vortex flow possible through the application of spanwise blowing may well be related to the control effect of the blowing on the entrainment level of the vortex.

5.1 Determination of the b_i - vs - α Boundary Curves

It was shown in the preceding chapter that an optimum value of b_i existed for each angle of attack, at which the maximum delay could be obtained of the numerical breakdown of the calculation. Although the assumption was made that similar optimisation of a real three-dimensional flow would be possible, and that a practical means of entrainment control could be found, it was considered unlikely that precise optimisation could be obtained in the presence of, for example, unsteady and viscous effects. Therefore, suitable boundary curves were sought for a b_i - vs - α variation which would ensure that, for a b_i - α combination lying on or within the curves, breakdown would be delayed to beyond a defined distance downwing of the initial solution plane. The range of the available flow control could then be assessed.

As stated in the introduction, it was stipulated that the breakdown should not occur within 1.0 m downwing of the initial crossflow plane. It was considered that in a real flow a delay of vortex breakdown of at least this order of magnitude would be required before the development of a suitable control system would be considered worthwhile.

The results of this investigation are shown in figs.5.1-5.5. It should be noted that a pairing of b_i and α lying above the upper curve b_u will result in a failure within 1000 steps as b tends to its critical value. A pairing lying beneath the lower curve b_l will result in a failure either of this critical type or as the sink

strength becomes negative. Although this latter type of failure would appear to be unrelated to vortex breakdown, its inclusion was necessary as it provided a limit to the calculation.

It can be seen that at lower angles of attack there exists considerable scope for the variation of b_i within the boundary curves of figs.5.1-5.5, i.e. precise control of entrainment is not necessary. As the angle of attack increases, the boundary curves move closer together, and their proximity to each other becomes such that only a very narrow range of b_i enables breakdown to be delayed to the required extent. Therefore it is obvious that there is an increasing demand for control precision associated with an increasing angle of attack. For all cases, beyond $\alpha \cong 25^\circ$ the required delay cannot be achieved, and control of b_i can provide only very limited benefits.

It should be remembered that MODEL3D is based on an approximate quasi-three-dimensional model of the high angle of attack flow past a delta wing. It was therefore very necessary to seek evidence from other sources on the possibility, or otherwise, of delaying or preventing the breakdown of a leading edge vortex by directly controlling flow entrainment into the vortex core.

5.2 Applications of Leading Edge and Spanwise Blowing

The possibility of leading edge vortex enhancement by the application of blowing has been the subject of considerable research in recent years, with the goal of improved manoeuvrability for fighter aircraft at high angles of attack. A variety of blowing concepts have been studied, and these are summarised below.

5.2.1 Leading Edge Blowing

Two types of leading edge blowing have been investigated:

(i) blowing a jet of air outwards from the leading edge in the wing plane.

(ii) blowing a jet of air tangential to a rounded leading edge, as shown in fig.5.6.

Method (i) would intuitively be expected to increase the strength of the leading edge vortices and thereby the lift acting on the wing. An experimental investigation by Trebble⁶⁹ has shown that this is indeed the case, and the theoretical investigation of Barsby⁷⁰ has further indicated the importance of parameters such as the rate of blowing and the angle of the jet to the wing centre line. The possible effect of the blowing on vortex breakdown was not investigated experimentally, as can be seen from fig.5.7, where the highest angle of attack tested was $\alpha = 20^\circ$. It may be considered that the effect of the jet in strengthening the vortex will provide

added resistance to vortex breakdown. However, it can be noted that fig.5.7 shows that for a blowing coefficient C_{μ} of 0.025, the increase in C_L is only of the order of 4% at $\alpha = 20^\circ$, and any delaying effect on breakdown would be expected to be of a similar magnitude. This value of C_{μ} corresponds approximately to the maximum attainable blowing for a current fighter aircraft (where the blowing is driven by bleed air from the engine compressors), and so it would appear that the benefits available from this form of leading edge blowing are not sufficient to justify the development of a complex control system to enable its practical application.

Tangential leading edge blowing (TLEB), method (ii), has only recently been postulated as a means of controlling the delta wing vortical flowfield. By injecting small amounts of momentum into the crossflow near separation, Wood et al^{71,72} found that it was possible to re-energise the flow and delay separation. This modification of the separation point obviously alters the Kutta condition and leads to a change in both primary and secondary vortex locations and strengths.

The results reported by Wood indicate that this method of blowing has a considerable effect on the flowfield. At subcritical angles of attack TLEB shifts the primary vortex inboard and weakens it, whilst increasing the leading edge suction (as shown in fig.5.8) such that the overall normal force acting on the wing is unaffected. At higher angles of attack, where vortex breakdown would occur in an unblown flow, the effect of TLEB is to re-establish the vortical flow structure up to $\alpha = 60^\circ$, as indicated by the pressure distributions

of fig.5.8 for $\alpha = 45^\circ$, thereby removing flow unsteadiness and increasing the normal force. Only small amounts of blowing are required to produce these marked changes in flow behaviour. It has also been found that tangential blowing only from a limited region of the leading edge at the apex produces similar results to those obtained from TLEB across the full wingspan.

As stated earlier, tangential leading edge blowing is a new concept, and as such requires further investigation. Nevertheless, the initial results indicate that it may well be a practical means of vortex breakdown control.

5.2.2 Spanwise Blowing

It has been widely shown, for example in refs.73-75, that it is possible to obtain enhancement of a leading edge vortex by direct control of the flow within the vortex core. Such control can be obtained by the spanwise blowing of a jet, or jets, of air over the upper surface of a slender wing just aft of the leading edge. A test blowing arrangement for a F4-C aircraft is shown in fig.5.9.

Various blowing configurations have been considered in attempts not only to optimise the effects of blowing on the aerodynamic performance of the wing, but also to gain an understanding of the underlying beneficial flow mechanism. In general it has been found that the application of spanwise blowing results in increased manoeuvrability and improved handling qualities. The increases in lift obtained are an order of magnitude greater than that obtained

through conventional leading edge blowing, for example in the case shown in fig.5.10 an increase in C_L of 25% at $\alpha = 20^\circ$ for $C_\mu = 0.02$ in the spanwise direction, as opposed to an increase of 4% at $C_\mu = 0.025$ from the leading edge. Most importantly for the purposes of this investigation, vortex breakdown can be delayed by the order of 10° .

The reason that spanwise blowing results in a delay of vortex breakdown has not yet been fully established. A widely held belief is that the momentum or momentum gradient of the jet stabilises the vortex when it is entrained into the vortex core. An alternative explanation is that the vortex is stabilised as a consequence of the additional entrainment effect of the entrained jet. Gersten³⁵ investigated this possibility experimentally by pulsing the spanwise jet of air and thereby increasing its entrainment. Although Gersten concluded that this additional entrainment had no noticeable effect on the breakdown of the vortex, no careful variation of the entrainment was attempted; as the results of MODEL3D have indicated that such a variation (rather than a simple increase in entrainment) may be necessary to delay vortex breakdown, such a result is not surprising.

However, Gersten went on to investigate the effects of blowing on vortex breakdown in a transonic flow. By reference to Catastrophe theory (as discussed in Appendix 2) it was found that a bimodal flow existed, fig.5.11, indicating the hysteresis of the breakdown location with C_μ . As can be seen in fig.5.12, the value of C_μ required for the flow state to move to the higher level of x_b is

approximately fourteen times higher than that required for it to remain there. (The catastrophe surface is shown in fig.5.13). Although there has been no further evidence from other sources of such flow behaviour, Gersten's work at the very least indicates the applicability of Catastrophe theory in the investigation of vortex breakdown.

It can be concluded that the application of spanwise blowing to a slender wing will considerably delay vortex breakdown. However, further research is necessary to uncover the underlying flow mechanism which is responsible for the success of this method of vortex control.

5.3 Interpretation of Blowing and MODEL3D Results

As the method of tangential leading edge blowing is based on the ability to modify the position of crossflow separation on a wing of rounded leading edge, it is not possible to obtain any representation of its effect with MODEL3D, where the separation point is fixed at a sharp leading edge. However, some interpretation can be attempted of the degree of success achieved by conventional leading edge and spanwise blowing by comparison with the results of MODEL3D.

It was noted that conventional leading edge blowing directly strengthened the primary vortex, but could provide only a very limited delay of vortex breakdown at practical blowing rates. At these same blowing rates, a more marked delay of breakdown could be obtained by blowing in the spanwise direction, where the blowing jet interacted directly with the vortex core. Some explanation can be offered for the greater success of spanwise blowing, by reference to eqn.71, derived in ref.76 by Verhaagen for a slender conical vortex core, where entrainment was modelled by a distribution of sink strength along the vortex core.

$$\frac{Q(x_c)}{U_{ce} x_c} = \pi c^2 \left[-1 + \sqrt{1 + 2 \left[\frac{V_\theta}{U_{ce}} \right]^2} \right] \quad (71)$$

where x_c = coordinate along vortex axis

r_c = radius of rotational core

c = r_c / x

U_{ce} = axial velocity at edge of core

V_θ = circumferential velocity at edge of core

Leading edge blowing provides an increase in V_θ , and thence Γ , with little effect on the axial velocity at the edge of the vortex core. The increase in V_θ is accompanied by an almost linear growth in Q , which for a constant U_{ce} will result in a limited variation of the ratio $Q/\Gamma = b$, as shown in the example below.

$$\text{Assume } V_\theta = 5.0 \text{ m s}^{-1}, U_{ce} = 2.5 \text{ m s}^{-1}$$

$$\rightarrow Q = 5.0 x_c \pi c^2, \Gamma = -10.0 \pi r_c$$

$$\rightarrow Q/\Gamma = b = -0.5 \frac{x_c c^2}{r_c}$$

If V_θ is increased to 10.0 m s^{-1} for a constant U_{ce}

$$\rightarrow Q = 11.862 x_c \pi c^2, \Gamma = -20.0 \pi r_c$$

$$\rightarrow b = -0.593 \frac{x_c c^2}{r_c}$$

A 100% increase in V_θ gives an 18.6% decrease in b .

From the results of MODEL3D it can be seen that control of the ratio b determined the calculation failure location. If it is accepted that this failure is related to vortex breakdown, then the limited control of vortex breakdown possible with leading edge blowing may be a consequence of this blowing method's limited authority over b .

Spanwise blowing results in a jet interacting with the vortex core, with considerably greater influence on U_{ce} than on V_θ . Therefore, by variation of the blowing rate, considerable control could be obtained of the sink strength Q , and thence b . This is

highlighted in the following example.

$$\text{Assume } V_{\theta} = 5.0 \text{ m s}^{-1}, U_{ce} = 5.0 \text{ m s}^{-1}$$

$$\rightarrow Q = 3.660 x_c \pi c^2, \Gamma = 10.0 \pi r_c$$

$$\rightarrow b = -0.366 \frac{x_c c^2}{r_c}$$

By comparison with the earlier example, a 100% increase in U_{ce} has resulted in a 26.8% increase in b .

From the example for leading edge blowing, it was noted that an increase in V_{θ} resulted in a decrease in b . By the application of MODEL3D, it was earlier found that in most cases an increase in b , i.e. an decrease in its magnitude, was required to delay the calculation failure. As can be seen from the examples above, such a variation of b was only possible through the application of spanwise blowing. This provides a possible explanation for the greater control effect of spanwise blowing, as compared to leading edge blowing, on vortex breakdown.

5.4 Summary of Control Prospects

From the results of MODEL3D it was found that at high angles of attack precise control of the ratio b was required in order that the numerical failure of the calculation should be delayed beyond 1.0 m downwing. An associated review of practical methods of vortical flow control indicated that both tangential leading edge blowing and spanwise blowing offer considerable benefits in terms of aerodynamic performance. It was deduced that the greater delay of vortex breakdown through the application of spanwise blowing, as compared to conventional leading edge blowing, may well be a result of the beneficial control effect of the former on the entrainment effect of the vortex, as measured in MODEL3D by the ratio b of sink-to-vortex strength. If this is the case, then it would provide further evidence on the role of the entrainment of flow into a vortex on the subsequent breakdown of that vortex.

Chapter 6

Conclusions

From a survey of previous theoretical and experimental investigations of the breakdown of slender wing leading edge vortices, it was concluded that a simple computer-based analytical investigation of the phenomenon would require the development of a new model for the flowfield.

A quasi-three-dimensional representation was determined for the high angle of attack flow over a delta wing, and implemented as the program MODEL3D on the VAX11/750 computer. The major conclusions that can be drawn from the development of MODEL3D, and its application to an investigation of vortex breakdown, are summarised below.

(1) Experimental evidence indicates that the mechanism of vortex breakdown is largely an inviscid process. If, in addition, the rotationality of a leading edge vortex and its feeding sheet are considered to be concentrated at the vortex core location, then an inviscid, irrotational, complex-potential-based representation of a slender wing flowfield is acceptable for use in an investigation of the breakdown phenomenon.

(2) The simplest possible model for the crossflow past a delta wing is that of two point vortices in the presence of a flat plate. As

reported by Smith and Clark⁶³ and verified here, the necessary boundary conditions requiring smooth outflow at the leading edges and stationary singularity locations cannot be satisfied simultaneously. Therefore, such a model is unrealistic.

(3) By the addition of a sink to both point vortices, it is possible to model the entrainment of flow into the leading edge vortices. Such an approach has been attempted previously by Coe⁶⁵ and Verhaagen⁷⁶; however, it is believed that the work reported in this thesis is the first to consider a purely analytical vortex-sink model for the crossflow. For the same boundary conditions as in the point vortex model, the solution behaviour is unrealistic, with apparent dependence on the parameter b , the ratio of sink-to-vortex strength.

(4) Modification of the boundary conditions for the vortex-sink model, by replacement of the stationary singularity requirement with a force-free condition, had not been attempted previously, and provides more realism by consideration of a feeding-sheet effect and allows extension of the model into three dimensions. Conical solutions are possible in certain cases, but are unrealistic. The non-conical model, necessary for an investigation of vortex breakdown, requires one further boundary condition.

(5) The parameter b plays the dominant role in determining the solution for the crossflow plane in a non-conical flow. At a certain critical value b_c , the discontinuous change in solution behaviour is such that it may well be related to vortex breakdown in three dimensions. It has been shown that the existence of b_c could be

indicative of a critical swirl-to-axial velocity ratio, which experiment has shown to be of importance in vortex breakdown. Therefore, the entrainment of flow into a vortex may play a role in its subsequent breakdown.

(6) Extension of the non-conical vortex-sink model into three dimensions is possible with the assumption of a conical variation of the spanwise coordinate of vortex-sink location. Only upwing influences can be considered, and as a result MODEL3D is effectively three-dimensional.

(7) Below an angle of attack of ten degrees, calculations using MODEL3D are terminated as the required sink strength becomes negative. The reason for this behaviour cannot be fully established, but is believed to be a consequence of the initial proximity of the vortex-sink to the wing.

(8) Above ten degrees angle of attack, calculations fail as b tends towards its critical value at some downwing location. The variation of the location of x_b with angle of attack and angle of wing sweepback is in qualitative agreement with that found experimentally. However, quantitative agreement cannot be expected from such an approximate model. The detailed behaviour of individual solutions is, in general good, although the variation of the vertical coordinate of vortex-sink location is excessive as the calculation steps downwing. It is believed that this is a consequence of MODEL3D employing concentrated, rather than distributed, vorticity; the increase in point vortex strength over one step is far greater

than it would be for individual elements of a distribution of vorticity, and therefore the associated movement of the vortex-sink away from the surface is amplified. The behaviour of the singularity strengths and strength gradients as b_c is approached is in accordance with that found by Hall¹⁹, where the appearance of large axial gradients terminated a quasi-cylindrical calculation of vortex flow. Hall's identification of calculation failure with the critical state for vortex breakdown is also in agreement with the solution behaviour found for MODEL3D.

(9) By careful control of the initial value specified for b , it is possible to achieve a marked delay of the failure of the calculation. In the light of this result, it is considered that control of the entrainment levels in a real vortex flow may provide a means of delaying its breakdown. A study of practical methods of vortex flow control indicates that the considerable flow enhancement and delay of vortex breakdown possible through the application of spanwise blowing over the upper surface of a slender wing, may well be related to such an effect on the entrainment level of the leading edge vortex.

(10) The results of this study strongly indicate that the entrainment of flow into a leading edge vortex plays a major role in the breakdown of that vortex. However, it is very necessary to emphasise that MODEL3D provides only a very approximate representation of the high angle of attack flow past a delta wing: it is only possible to calculate the flow over a middle section of the wing, no downwing effects can be considered, the concentration

of vorticity at one point is highly restrictive and the model becomes progressively less accurate with increasing angle of attack.

(11) Despite the restrictions of MODEL3D, the results obtained from its application justify further investigation of the importance of entrainment effects in vortex breakdown. It is recommended that three synergistic approaches be employed in such an investigation.

(i) A catastrophe theory analysis of the phenomenon should be undertaken, with particular attention directed to the possibility that the dominant control parameter is related to the entrainment effect of the vortex.

(ii) The results from C.F.D. studies should be examined for any controlling role of the entrainment level.

(iii) Most importantly, an extensive and detailed programme of experimental research is required. This should be based on laser doppler velocimetry surveys of the vortical flowfield above a delta wing at high angles of attack, with close examination of all three velocity components as breakdown is approached. Also, the wing should be subject to a variety of blowing methods to establish the mechanism of vortex enhancement and breakdown delay. Associated flow visualisation studies would assist in the interpretation of the L.D.V. data.

It is believed that such an investigative procedure would provide an important step towards establishing the cause of vortex breakdown.

Appendix 1

Laser Doppler Velocimetry

Laser Doppler Velocimetry (LDV) provides a non-intrusive means of flow measurement on the basis of the Doppler effect on a beam of light incident upon a moving particle, i.e. the light scattered from the particle is of a different frequency from that of the incident beam, and this change in frequency can be directly related to the velocity of the particles through the equation

$$f_D = \frac{1}{\lambda} \bar{U} \cdot \left[\bar{e}_s - \bar{e}_i \right] \quad (\text{A1.1})$$

where \bar{e}_s = unit vector in scattering direction

\bar{e}_i = unit vector in incident direction

\bar{U} = velocity vector

λ = wavelength of incident light

The basic requirements for an LDV system are:

(1) a means of producing a coherent beam of light i.e. a laser

(2) focussing and detecting optics

- (3) a photomultiplier to convert the received optical signal to an electrical signal
- (4) a processing system to reduce the electrical signals to the Doppler frequency or flow velocity
- (5) light reflecting particles within the flow - this may necessitate seeding if the flow medium is air.

It should be obvious that as the complexity of the flowfield to be investigated increases, far greater performance and flexibility is required of the LDV system. The application of such systems to two and three-dimensional studies of vortex breakdown is well discussed in refs.13-17. The remainder of this Appendix considers only the LDV equipment available in the Department of Aeronautics and Fluid Mechanics at the University of Glasgow.

The coherent light source is provided by a 15 mW monochromatic (red) Helium-Neon laser. This in itself imposes considerable limits on the possible uses of the LDV system:

- (1) in certain flows it may be necessary to detect the light scattered backwards from the particles in the flow, i.e. to use the system in backscatter mode. The low level of light scattered in this direction, as compared to the forward direction, may require a more powerful light source, such as a 5 W Argon-Ion laser, if sufficient scattered light is to be received by the detecting optics.

(2) if the distance from the light scattering particle to the detecting optics is greater than the order of 1.0 m, then it is doubtful whether the He-Ne laser will provide a sufficient intensity of scattered light, particularly in the backscatter mode, and again an Argon-Ion laser may be required. Therefore it would not be possible to use the present LDV system in the University's 5 ft x 7 ft Handley-Page wind tunnel.

(3) in vortical flows the number of light-scattering particles is low in areas of high vorticity. Use of a powerful laser would enable more measurements to be taken within these areas.

(4) with the focussing and beam-splitting optics available at present, the He-Ne laser based system can only measure one velocity component at any one time. However, this restriction could be removed by the purchase of suitable polarising and detecting optics. It would then be possible to simultaneously measure two velocity components by detecting the light scattered from horizontally and vertically polarised beams that are incident upon the flow from different directions. (With the two colour blue-green Argon-Ion laser, such polarisation is unnecessary as colour separation in the detecting optics can achieve the same result).

From the above restrictions it can be seen that, using the 15 mW

He-Ne laser, only one-dimensional measurements of flows with relatively low vorticity and small scale can be attempted. Suitable polarisation optics would enable two-dimensional measurements of similar flows.

The processing electronics available at present consist of a counter processor, which simply provides a readout of the Doppler frequency of the incoming signal. This is adequate for a steady, laminar flow. However, for an unsteady and turbulent flow, further connection of the counter processor to a mini-computer would be required to provide information on, for example, velocity fluctuations and turbulence levels. Development of the processing software for the mini-computer would be a lengthy and involved task.

Despite the limits of the present LDV system, it could be successfully applied to the measurement of, for example, fully developed pipe flows. (It would first be necessary to commission the system; a simple water channel with a glass-walled section is available and suitable for use in such a task). It should, however, be obvious from the above summary of the system's capabilities that an application of the system to study of the highly-three-dimensional and unsteady vortex breakdown flowfield would be completely impractical.

Appendix 2

Catastrophe Theory

Consider a system that is subject to a discontinuous phenomenon, the occurrence of which is governed by the form of potential function depicted on the left of fig.A2.1. A stable state of the system exists at point A where the function has a minimum; it is assumed that the system lies initially at this point. Subsequent variation of a parameter controlling the system may modify the form of the governing potential such that an additional minimum is created at point B, as shown to the right in fig.A2.1. However, the system remains in the first minimum, until it is completely removed by further variation of this control parameter, and the system must then jump to minimum B. Thus a smooth variation of the control parameter produces a discontinuous change in the system behaviour. Such a change of state is called a "catastrophe".

The study of this type of discontinuous behaviour in potential systems was revolutionised by Thom, who set out the principles of Catastrophe theory. From its basis in multi-dimensional geometry, the theory has indicated that seven elementary catastrophes exist in a control space of four or less dimensions. Study of these catastrophes has been undertaken in connection with many areas of the physical, life and social sciences.

It is the three-dimensional cusp catastrophe, shown in fig.A2.2,

that is of particular interest in this study of vortex breakdown. It is hypothesised that the surface of the plot could be considered to represent the vortex behaviour, whether well-ordered or "burst", where this behaviour is measured on the vertical axis. The curve on the surface where the upper and lower sheets fold over into the middle sheet is projected downwards into the plane of CP1 and CP2, the two control parameters, where its trace is called the bifurcation set. (It can be seen that this bifurcation set has a sharp point, forming a cusp, hence the name cusp catastrophe). If the variation of the control parameters is such that the path P1 is followed across the cusp, then the vortex behaviour will remain well-ordered on the lower sheet, until the point Q1 is reached, where a sudden jump to the upper sheet occurs and the vortex will break down. If the vortex has already undergone breakdown, then if path P2 is followed, it will have no regular structure until point Q2 is reached, where a catastrophic jump to the lower sheet will result in the formation of a vortex. (There is no jump to the middle sheet, as marked by the point (4)*, as it is considered to represent inaccessible behaviour. This sheet could be removed from the plot, but is retained for the purpose of clarity.)

It can be noted that a hysteresis effect exists, in that the jumps from the upper to lower sheet and vice-versa, occur on opposite sides of the cusp. This can be explained by reference to the variation of potential shown in fig.A2.1; if the path P1 in fig.A2.2 was considered to produce this variation, then simply reversing the direction of P1 would not produce a jump from B to A at the same point as from A to B in the original case. The system would remain

at point B until this point disappeared and then jump to point A. Within the confines of the cusp, bimodal behaviour is possible, i.e. the vortex could be either formed or burst, depending on the path followed.

As discussed in Chapter 5, an experimental investigation of vortex breakdown has revealed such a hysteresis effect, where control parameters were identified relating to the angle of attack of the wing, and the entrainment of flow into the vortex. Further confirmation of this result has not been provided but this, combined with the discontinuous nature of vortex breakdown, justifies a rigorous mathematical application of Catastrophe theory in an investigation of vortex breakdown. However, the difficulties in determining a suitable governing potential function are such that qualitative applications may be all that are possible in the near future.

Appendix 3

The Transformation From the Wing (Z) Plane to the Cylinder (Z₂) Plane

Consider an intermediate transformation between the cylinder and wing plane, such that $Z_2 = iZ_1$.

The transformation from the Z₂-plane to the Z-plane is then simply of the Kutta-Joukowski form,

$$Z = Z_2 + \frac{a^2}{Z_2} \quad (3.1)$$

and so

$$Z_2^2 - Z_2Z + a^2 = 0 \quad (3.2)$$

$$\Rightarrow Z_2 = \frac{Z \pm \sqrt{Z^2 - 4a^2}}{2} \quad (3.3)$$

It must be determined whether the + or - case is correct.

From the consideration that the flows at infinity in the Z and Z₂-planes should be equivalent, it can be deduced that the + case should be selected. Since $Z_1 = -iZ_2$, it can be written as in eqn.24 that

$$Z_1 = \frac{-i (Z + \sqrt{Z^2 - 4a^2})}{2} \quad (3.4)$$

Appendix 4

Determination of the Governing Complex Potential in the Z₁ Plane for the Point Vortex Model

The relevant flow geometry is shown in fig.3.2. It is considered that the governing complex potential W has two components,

$$W = W_1 + W_2 \quad (4.1)$$

where W_1 is the complex potential for a cylinder in a uniform flow without vortices and W_2 is the complex potential for vortices in the presence of a cylinder. Therefore, for vortices located at Z_{A1} and Z_{B1}

$$W_1 = U_c \left(Z_1 + \frac{a^2}{Z_1} \right) \quad (4.2)$$

$$W_2 = -\frac{i\Gamma_1}{2\pi} \left[\ln(Z_1 - Z_{A1}) - \ln(a^2 - Z_1 \overline{Z_{A1}}) + \ln Z_1 \right] \\ - \frac{i\Gamma_2}{2\pi} \left[\ln(Z_1 - Z_{B1}) - \ln(a^2 - Z_1 \overline{Z_{B1}}) + \ln Z_1 \right] \quad (4.3)$$

and so the expression for W reduces to that given in eqn.25.

Appendix 5

Determination of the Stationary Vortex Boundary Condition

It is known that a point vortex can induce no velocity at its own centre, and therefore an additional complex potential W' is defined, where

$$W' = W + \frac{i\Gamma}{2\pi} \ln (Z - Z_A) \quad (5.1)$$

such that the following equality

$$\lim_{Z \rightarrow Z_A} \left[\frac{dW'}{dZ} \right] = 0 \quad (5.2)$$

is the necessary condition for the vortex to be stationary.

This requires that

$$\lim_{Z \rightarrow Z_A} \left[\frac{dW'}{dZ_1} \frac{dZ_1}{dZ} \right] = 0 \quad (5.3)$$

which leads to

$$\left[U_c \left[1 - \frac{a^2}{z_1^2} \right] - \frac{i\Gamma}{2\pi} \left[\frac{-z_{A1}}{a^2 - z_1 z_{A1}} - \frac{1}{z_1 - z_{B1}} + \frac{-z_{B1}}{a^2 - z_1 z_{B1}} \right] \right] \frac{dz_1}{dz} \Big|_{z=z_A}$$

$$- \frac{i\Gamma}{2\pi} \lim_{z \rightarrow z_A} \left[\left[\frac{1}{z_1 - z_{A1}} - \frac{1}{z - z_A} \frac{dz}{dz_1} \right] \frac{dz_1}{dz} \right] = 0 \quad (5.4)$$

Evaluating only the limit term,

$$L = \lim_{z \rightarrow z_A} \left[\frac{\frac{dz_1}{dz}}{\frac{z_1 - z_{A1}}{z - z_A}} - \frac{1}{z - z_A} \right] \quad (5.5)$$

This can be expressed as

$$L = \lim_{z \rightarrow z_A} \left[\frac{\frac{dz_1}{dz}}{\frac{z_1 - z_{A1}}{z - z_A}} - 1 \right] / (z - z_A) \quad (5.6)$$

By applying l'Hopital's rule, it can be deduced that this is equivalent to

$$L = \lim_{z \rightarrow z_A} \frac{d}{dz} \left[\frac{\frac{dz_1}{dz}}{\frac{z_1 - z_{A1}}{z - z_A}} \right] \quad (5.7)$$

which, by the product rule, is given by

$$\lim_{Z \rightarrow Z_A} \frac{\frac{Z_1 - Z_{A1}}{Z - Z_A} \frac{d^2 Z_1}{dZ^2} - \frac{dZ_1}{dZ} \left[\frac{(Z - Z_A) \frac{dZ_1}{dZ} - (Z_1 - Z_{A1})}{(Z - Z_A)^2} \right]}{\left[\frac{Z_1 - Z_{A1}}{Z - Z_A} \right]^2} \quad (5.8)$$

which can be further reduced to

$$\lim_{Z \rightarrow Z_A} \frac{\frac{d^2 Z_1}{dZ^2} - \frac{dZ_1}{dZ} \left[\frac{\frac{\frac{dZ_1}{dZ}}{Z_1 - Z_{A1}} - 1}{Z - Z_A} \right]}{\frac{Z_1 - Z_{A1}}{Z - Z_A}} \quad (5.9)$$

which is equivalent to

$$L = \frac{\frac{d^2 Z_1}{dZ^2} - \frac{dZ_1}{dZ} L}{\frac{dZ_1}{dZ}} \Bigg|_{Z=Z_A} \quad (5.10)$$

This expression can be manipulated to give

$$L = \frac{1}{2} \frac{\frac{d^2 z_1}{dz^2}}{\frac{dz_1}{dz}} \Big|_{z=z_A} \quad (5.11)$$

Substitution of this expression in eqn.5.4 then permits the determination of those flow states, if any, where the stationary vortex boundary condition is satisfied.

Appendix 6

Reduction of the Kutta Condition for the Point Vortex Model to One

Real Equation

As shown in eqn.34 of Chapter 3, the Kutta condition for the point vortex model can be written as

$$2 U_C - \frac{i\Gamma_1}{2\pi} W_3 = 0 \quad (6.1)$$

where for a solution at $Z_1 = ai$ (corresponding to the transformation of the left-hand leading edge to the Z_1 -plane)

$$W_3 = \frac{1}{ai - Z_{A1}} - \frac{Z_{A1}}{a^2 - aiZ_{A1}} - \frac{1}{ai - Z_{B1}} + \frac{Z_{B1}}{a^2 - aiZ_{B1}} \quad (6.2)$$

Z_{A1} and Z_{B1} are complex and as such can be expressed in terms of their real and imaginary parts,

$$Z_{A1} = y_{A1} + iz_{A1} \quad (6.3)$$

$$Z_{B1} = y_{A1} - iz_{A1} \quad (6.4)$$

which leads to the expression for W_3 given overleaf.

$$W_3 = \frac{1}{ai - y_{A1} - iz_{A1}} - \frac{y_{A1} + iz_{A1}}{a^2 - ai (y_{A1} + iz_{A1})}$$

$$- \frac{1}{ai - y_{A1} + iz_{A1}} + \frac{y_{A1} - iz_{A1}}{a^2 - ai (y_{A1} - iz_{A1})} \quad (6.5)$$

$$\Rightarrow W_3 = \frac{-ai}{a^2 - az_{A1} + iay_{A1}} + \frac{y_{A1} - iz_{A1}}{a^2 - az_{A1} - iay_{A1}}$$

$$+ \frac{ai}{a^2 + az_{A1} + iay_{A1}} - \frac{y_{A1} + iz_{A1}}{a^2 + az_{A1} - iay_{A1}} \quad (6.6)$$

$$\Rightarrow W_3 = \frac{-a^3i + iaz_{A1}^2 + iay_{A1}^2}{(a^2 - az_{A1} + iay_{A1})(a^2 - az_{A1} - iay_{A1})}$$

$$+ \frac{a^3i - iaz_{A1}^2 - iay_{A1}^2}{(a^2 + az_{A1} + iay_{A1})(a^2 + az_{A1} - iay_{A1})} \quad (6.7)$$

$$\Rightarrow W_3 = i \left[\frac{-a^3 + az_{A1}^2 + ay_{A1}^2}{(a^2 - az_{A1})^2 + a^2y_{A1}^2} + \frac{a^3 - az_{A1}^2 - ay_{A1}^2}{(a^2 + az_{A1})^2 + a^2y_{A1}^2} \right] \quad (6.8)$$

Substitution of this wholly imaginary expression for W_3 in eqn.6.1 shows that the Kutta condition reduces to one real equation.

Appendix 7

Determination of the Stationary Vortex-Sink Boundary Condition

The modified complex potential W' is defined as in Appendix 5

$$W' = W + \frac{i\Gamma}{2\pi} \ln (Z - Z_A) \quad (7.1)$$

and so the velocity at the vortex-sink centre is given by

$$\frac{dW'}{dZ} = \left[\frac{dW}{dZ_1} + \frac{i\Gamma}{2\pi} \left[\frac{1}{Z - Z_A} \right] \frac{dZ}{dZ_1} \right] \frac{dZ_1}{dZ} \quad (7.2)$$

i.e. the vortex component induces no velocity at its own centre.

For a stationary vortex-sink it is required that

$$\lim_{Z \rightarrow Z_A} \left[\frac{dW'}{dZ} \right] = 0 \quad (7.3)$$

$$\lim_{Z \rightarrow Z_A} \left[\frac{dW'}{dZ_1} \frac{dZ_1}{dZ} \right] = 0 \quad (7.4)$$

which leads to the condition (7.5) given overleaf.

$$\begin{aligned}
& \left[U_c \left[1 - \frac{a^2}{z_1^2} \right] - \frac{i\Gamma}{2\pi} \left[\frac{-z_{A1}}{a^2 - z_1 z_{A1}} - \frac{1}{z_1 - z_{B1}} + \frac{z_{B1}}{a^2 - z_1 z_{A1}} \right] \right. \\
& - \frac{b\Gamma}{2\pi} \left[\frac{-z_{A1}}{a^2 - z_1 z_{A1}} + \frac{1}{z_1 - z_{B1}} - \frac{-z_{B1}}{a^2 - z_1 z_{A1}} - \frac{2}{z_1} \right] \left. \right] \frac{dz_1}{dz} \Big|_{z=z_A} \\
& - \frac{i\Gamma}{2\pi} \lim_{z \rightarrow z_A} \left[\left[\frac{1}{z_1 - z_{A1}} - \frac{ib}{z_1 - z_{A1}} - \frac{1}{z - z_A} \frac{dz}{dz_1} \right] \frac{dz_1}{dz} \right] = 0 \quad (7.5)
\end{aligned}$$

Evaluating only the limit term, it is found that this can be expressed as in eqn.7.6, given below.

$$L1 = \lim_{z \rightarrow z_A} \left[\frac{(1 - ib) \frac{dz_1}{dz}}{\frac{z_1 - z_{A1}}{z - z_A}} - 1 \right] / (z - z_A) \quad (7.6)$$

By applying l'Hopital's rule, it can be deduced that this is equivalent to

$$L1 = \lim_{z \rightarrow z_A} \frac{d}{dz} \left[\frac{(1 - ib) \frac{dz_1}{dz}}{\frac{z_1 - z_{A1}}{z - z_A}} \right] \quad (7.7)$$

which, by comparison with eqn.5.7 of Appendix 5, can be reduced to

$$L1 = (1 - ib) L \quad (7.8)$$

$$\Rightarrow L1 = \frac{1}{2} (1 - ib) \frac{\frac{d^2 z_1}{dz_1^2}}{dz_1} \quad (7.9)$$

Substitution of this expression in eqn.7.5 then permits the determination of those flow states, if any, where the stationary vortex-sink boundary condition is satisfied.

Appendix 8

Reduction of the Kutta Condition for the Vortex-Sink Model to One

Real Equation

As shown in eqn.43 of Chapter 3, the Kutta condition for the vortex-sink model can be written as

$$iW_2 + bW_5 = \frac{4\pi U_C}{\Gamma} \quad (8.1)$$

At $Z_1 = ai$ (corresponding to a solution at the left hand leading edge in the Z-plane) W_2 reduces to the wholly imaginary function W_3 , as derived in Appendix 6.

The function W_5 is expressed as

$$W_5 = \frac{1}{ai - Z_{A1}} - \frac{Z_{A1}}{a^2 - aiZ_{A1}} + \frac{1}{ai - Z_{B1}} - \frac{Z_{B1}}{a^2 - aiZ_{B1}} - \frac{2}{ai} \quad (8.2)$$

As in Appendix 6, Z_{A1} and Z_{B1} are expressed in terms of their real and imaginary parts to give eqn.(8.3) overleaf.

$$W_5 = \frac{1}{ai - y_{A1} - iz_{A1}} - \frac{y_{A1} + iz_{A1}}{a^2 - ai(y_{A1} + iz_{A1})} + \frac{1}{ai - y_{A1} + iz_{A1}} - \frac{y_{A1} - iz_{A1}}{a^2 - ai(y_{A1} - iz_{A1})} + \frac{2i}{a} \quad (8.3)$$

$$\Rightarrow W_5 = \frac{-a^3i + 2ia^2z_{A1} - 2a^2y_{A1} - iaz_{A1}^2 - iay_{A1}^2}{a(a^3 - 2a^2z_{A1} + az_{A1}^2 + ay_{A1}^2)} - \frac{a^3i + 2ia^2z_{A1} + 2a^2y_{A1} + iay_{A1}^2 + iaz_{A1}^2}{a(a^3 + 2a^2z_{A1} + ay_{A1}^2 + az_{A1}^2)} + \frac{2i}{a} \quad (8.4)$$

$$\Rightarrow W_5 = -\frac{i}{a} - \frac{2ay_{A1}}{a^3 - 2a^2z_{A1} + az_{A1}^2 + ay_{A1}^2} - \frac{i}{a} - \frac{2ay_{A1}}{a^3 + 2a^2z_{A1} + ay_{A1}^2 + az_{A1}^2} + \frac{2i}{a} \quad (8.5)$$

$$\Rightarrow W_5 = \frac{-2y_{A1}}{a^2 - 2az_{A1} + z_{A1}^2 + y_{A1}^2} + \frac{-2y_{A1}}{a^2 + 2az_{A1} + z_{A1}^2 + y_{A1}^2} \quad (8.6)$$

Substitution of this wholly real expression for W_5 in eqn.8.1 shows that the Kutta condition for this vortex-sink model reduces to one real equation.

Appendix 9

The Non-Dimensional Form of the Kutta Condition for the Vortex-Sink

Model

Expressing the Kutta condition of eqn.8.1 of Appendix 8 in terms of y_{A1} and z_{A1} , it is found that

$$\frac{a^3 - az_{A1}^2 - ay_{A1}^2}{(a^2 - az_{A1})^2 + a^2y_{A1}^2} - \frac{a^3 - az_{A1}^2 - ay_{A1}^2}{(a^2 + az_{A1})^2 + a^2y_{A1}^2} - \frac{2by_{A1}}{a^2 - 2az_{A1} + z_{A1}^2 + y_{A1}^2} - \frac{2by_{A1}}{a^2 + 2az_{A1} + z_{A1}^2 + y_{A1}^2} = \frac{4\pi U_C}{\Gamma} \quad (9.1)$$

Given that

$$(a^2 - az_{A1})^2 + a^2y_{A1}^2 = a^2 (a^2 - 2az_{A1} + z_{A1}^2 + y_{A1}^2) \quad (9.2)$$

$$(a^2 + az_{A1})^2 + a^2y_{A1}^2 = a^2 (a^2 + 2az_{A1} + z_{A1}^2 + y_{A1}^2) \quad (9.3)$$

eqn.9.1 can be simplified to

$$\frac{a^2 - z_{A1}^2 - y_{A1}^2 - 2aby_{A1}}{a^2 - 2az_{A1} + z_{A1}^2 + y_{A1}^2} - \frac{a^2 - z_{A1}^2 - y_{A1}^2 + 2aby_{A1}}{a^2 + 2az_{A1} + z_{A1}^2 + y_{A1}^2} = \frac{4\pi U_C a}{\Gamma} \quad (9.4)$$

After obtaining a common denominator, eqn.9.4 reduces to eqn.9.5 given overleaf.

$$\frac{a^3 z_{A1} - a z_{A1}^3 - a y_{A1}^2 z_{A1} - a^3 b y_{A1} - a b y_{A1} z_{A1}^2 - a b y_{A1}^3}{a^4 - 2a^2 z_{A1}^2 + 2a^2 y_{A1}^2 + z_{A1}^4 + 2y_{A1}^2 z_{A1}^2 + y_{A1}^4} = \frac{\pi U_c a}{\Gamma} \quad (9.5)$$

Dividing top and bottom by a^4 , it is found that by defining the non-dimensional parameters y_n and z_n as

$$y_n = \frac{y_{A1}}{a}, \quad z_n = \frac{z_{A1}}{a} \quad (9.6)$$

eqn.9.5 can be expressed as

$$\frac{z_n - z_n^3 - y_n^2 z_n - b y_n - b y_n z_n^2 - b y_n^3}{1 - 2z_n^2 + 2y_n^2 + z_n^4 + 2y_n^2 z_n^2 + y_n^4} = \frac{\pi U_c a}{\Gamma} \quad (9.7)$$

which is the non-dimensional form of the Kutta condition given in eqn.46 of Chapter 3.

Appendix 10

Force Balance on the Vortex-Sink-Feeding Sheet Element

It was required that the total force acting on the vortex-sink-feeding sheet combination, shown in fig.3.21 should be equal to zero.

From Blasius theorem, it can be found that the force on a combined vortex-sink in a flowfield of velocity V_0 is given by

$$F_{v-s} = -\rho V_0 (Q + i\Gamma) \quad (10.1)$$

In this model there are two components of the velocity V_0 - one component V_f from the freestream velocity and one component V_* from the crossflow velocity. It is found that (assuming the angle of attack, α , and the angle of vortex inclination to the wing, dZ_A/dx , to be similar) the freestream component can be approximately calculated from

$$V_f = U_\infty \frac{\overline{dZ_A}}{dx} - iU_\infty\alpha \quad (10.2)$$

The crossflow component V_* is given by the complex velocity in the limit as the vortex-sink centre is approached.

By defining the parameter V_{ns} as

$$V_{ns} = V_* - iU_\infty\alpha \quad (10.3)$$

the force on the vortex-sink is given by

$$F_{v-s} = -\rho \left[U_\infty \frac{\overline{dz_A}}{dx} + V_{ns} \right] (Q + i\Gamma) \Delta x \quad (10.4)$$

As stated in section 3.6 of Chapter 3, it is considered that two orthogonal components of feeding sheet circulation are present. The component of the freestream velocity normal to the feeding sheet is equal to $U_\infty \cos\alpha$, and the extent of the feeding sheet in the crossflow plane is assumed to be equal to the distance from the leading edge to the vortex-sink, i.e. $(Z_A + s/2)$. From consideration of the force calculation in ref.44, it was concluded that this would result in a force F_{fs} on the feeding sheet given by

$$F_{fs} = -\rho U_\infty \cos\alpha \left[\left[\frac{d\Gamma}{dx} \right]_1 + i \frac{d\Gamma}{dx} \right] \left[Z_A + \frac{s}{2} \right] \Delta x \quad (10.5)$$

As stated in eqn.49 of Chapter 3, it is considered that

$$\frac{dQ}{dx} = C_1 \frac{d\Gamma}{dx} \quad (10.6)$$

and so, given that

$$F_{v-s} + F_{fs} = 0 \quad (10.7)$$

the force-free condition can be expressed as

$$\frac{1}{C_1} \frac{dQ}{dx} + i \frac{d\Gamma}{dx} = \frac{- \left[U_\infty \frac{dZ_A}{dx} + V_{ns} \right] (Q + i\Gamma)}{U_\infty \cos \alpha \left[Z_A + \frac{s}{2} \right]} \quad (10.8)$$

It should be obvious that this provides only an approximate force balance, the accuracy of which decreases with increasing angle of attack.

Appendix 11

A Conical Simplification of the Vortex-Sink-Feeding Sheet Force

Balance

Making the simplifying assumptions of conical flow as detailed in eqns.51-53 of Chapter 3, and setting $C_1 = 1$, the force balance of eqn.10.8 in Appendix 10 reduces to

$$\frac{Q}{x} + i \frac{\Gamma}{x} = \frac{- \left[U_{\infty} \frac{\overline{z_A}}{x} + v_{ns} \right] (Q + i\Gamma)}{U_{\infty} \cos \alpha \left[z_A + \frac{s}{2} \right]} \quad (11.1)$$

$$\Rightarrow U_{\infty} \cos \alpha \left[\frac{z_A}{x} + \frac{s}{2x} \right] = - U_{\infty} \frac{\overline{z_A}}{x} - v_{ns} \quad (11.2)$$

Since

$$\frac{s}{2} = x \tan (90 - \Lambda) \quad (11.3)$$

the force balance reduces to

$$v_{ns} + U_{\infty} \left[\left[\frac{z_A}{x} + \cot \Lambda \right] \cos \alpha + \frac{\overline{z_A}}{x} \right] = 0 \quad (11.4)$$

References

- (1) Peckham, D.H. and Atkinson, S.A., 'Preliminary Results of Low Speed Wind Tunnel Tests on a Gothic Wing of Aspect Ratio 1.0', R.A.E. TN. No. Aero 2504, 1957.
- (2) Earnshaw, P.B., 'An Experimental Investigation of the Structure of a Leading-Edge Vortex', A.R.C. R&M 3281, 1962.
- (3) Earnshaw, P.B. and Lawford, J.A., 'Low-Speed Wind-Tunnel Experiments on a Series of Sharp Edged Delta Wings', A.R.C. R&M 3424, 1966.
- (4) Stahl, W.H., 'Aerodynamics of Low Aspect Ratio Wings', AGARD LS-98 Missile Aerodynamics, 1979.
- (5) Verhaagen, N.G., 'An Experimental Investigation of the Vortex Flow Over Delta and Double-Delta Wings at Low Speed', Delft University of Technology, Department of Aerospace Engineering, Report LR-372, 1983.
- (6) Lambourne, N.C. and Bryer, D.W., 'The Bursting of Leading-Edge Vortices - Some Observations and Discussion of the Phenomenon', A.R.C. R&M 3282, 1962.
- (7) Sarpkaya, T., 'Vortex Breakdown in Swirling Conical Flows', A.I.A.A. Journal, Vol.9, No.9, 1971.

- (8) Leibovich, S., 'Vortex Stability and Breakdown', AGARD CP 342 Aerodynamics of Vortical Type Flows in Three Dimensions, 1983.
- (9) Kuchemann, D., 'The Aerodynamic Design of Aircraft', Pergamon Press, 1978.
- (10) Sarpkaya, T., 'Effect of the Adverse Pressure Gradient on Vortex Breakdown', A.I.A.A. Journal, Vol.12, No.5, 1974.
- (11) Erickson, G.E., 'Water Tunnel Flow Visualisation: Insight into Complex Three-Dimensional Flow Fields', A.I.A.A. Paper No. 79-1530, 1979.
- (12) Erickson, G.E., 'Flow Studies of Slender Wing Vortices', A.I.A.A. Paper No. 80-1423, 1980.
- (13) Chigier, N.A., 'Measurement of Vortex Breakdown Over a Delta Wing Using a Laser Anemometer', N.E.A.R. TR 62, 1974.
- (14) Anders, K.A., 'LDV Measurements of the Velocity Field of a Leading Edge Vortex Over a Delta Wing Before and After Vortex Breakdown', V.K.I. Technical Note 142, 1982.
- (15) Payne, F.M. and Nelson, R.C., 'An Experimental Investigation of Vortex Breakdown on a Delta Wing', NASA CP 2416 Vortex Flow Aerodynamics, 1986.

- (16) Owen, F.K. and Peake, D.J., 'Vortex Breakdown and Control Experiments in the Ames-Dryden Water Tunnel', NASA TM 89410, 1986.
- (17) Delery, J., Pagan, D. and Solignac, J-L., 'On the Breakdown of the Vortex Induced by a Delta Wing', Second International Colloquium on Vortical Flows, B.B.C. Baden, 1987.
- (18) Pickering, C.J.D. and Halliwell, N.A., 'Particle Image Velocimetry: A New Field Measurement Technique', Optical Measurements in Fluid Mechanics, 1985.
- (19) Hall, M.G., 'Vortex Breakdown', Annual Review of Fluid Mechanics, No.4, 1972.
- (20) Hall, M.G., 'A Numerical Method for Solving the Equations for a Vortex Core', A.R.C. R&M 3467, 1967.
- (21) Ludwig, H., 'Vortex Breakdown', D.L.V.R. Report 70-40, 1970.
- (22) Harvey, J.K., 'Some Observations of the Vortex Breakdown Phenomenon', Journal of Fluid Mechanics, Vol.14, 1962.
- (23) Bossel, H.H.K., 'Vortex Breakdown Flowfield', The Physics of Fluids, Vol.12, No.3, 1969.
- (24) Squire, H.B., 'Analysis of the Vortex Breakdown Phenomenon', Imperial College Department of Aeronautics Report No.102, 1960.

- (25) Benjamin, T.B., 'Theory of the Vortex Breakdown Phenomenon', Journal of Fluid Mechanics, Vol.14, 1962.
- (26) Benjamin, T.B., 'Some Developments in the Theory of Vortex Breakdown', Journal of Fluid Mechanics, Vol.28, 1967.
- (27) Escudier, M.P. and Keller, J.J., 'Vortex Breakdown: A Two-Stage Transition', AGARD CP 342, 1983.
- (28) Escudier, M.P. and Keller, J.J., 'Essential Aspects of Vortex Breakdown', Colloquium on Vortex Breakdown, R.W.T.H. Aachen, 1985.
- (29) Leibovich, S., 'The Structure of Vortex Breakdown', Annual Review of Fluid Mechanics, No.10, 1978.
- (30) Leibovich, S., 'Attempts to Assess the Effects of Azimuthal Asymmetries on Vortex Breakdown', Colloquium on Vortex Breakdown, R.W.T.H. Aachen, 1985.
- (31) Leibovich, S., 'On a Synthetic Theoretical Scenario for Vortex Breakdown', Second International Colloquium on Vortical Flows, B.B.C. Baden, 1987.
- (32) Shi, X., 'Relation Between the Quasi-Cylindrical Approximation and Critical Theory for Swirling Flow', Second International Colloquium on Vortical Flows, B.B.C. Baden, 1987.

- (33) Zeeman, E.C., 'Catastrophe Theory', Addison-Wesley Publishing Company, 1977.
- (34) Lu, Y-C., 'Singularity Theory and an Introduction to Catastrophe Theory', Springer-Verlag, 1976.
- (35) Gersten, K., Kiske, S., Pagendarm, H-G., Schmitz, O. and Schmucker, A., 'Vortex Breakdown Control by Jet Injection', Colloquium on Vortex Breakdown, R.W.T.H. Aachen, 1985.
- (36) Liu, C.H., 'Review of Vortex Interaction, Stability and Breakdown Research at NASA', Second International Colloquium on Vortical Flows, B.B.C. Baden, 1987.
- (37) Grabowski, W.J. and Berger, S.A., 'Solutions of the Navier-Stokes Equations for Vortex Breakdown', Journal of Fluid Mechanics, Vol.75, 1976.
- (38) Shi, X., 'Numerical Simulation of Vortex Breakdown', Colloquium on Vortex Breakdown, R.W.T.H. Aachen, 1985.
- (39) Pagan, D. and Benay, R., 'Vortex Breakdown Induced by an Adverse Pressure Gradient: Experimental and Numerical Approaches', A.I.A.A. Paper No. 87-2487, 1987.
- (40) Hitzel, S., 'Vortex Breakdown of Leading Edge Vortices Above Swept Wings - Its Governing Terms in the Describing Equations', Dornier Report BF30-2576/84, 1984.

- (41) Hitzel, S. and Wagner, B., 'Euler-Rechnungen zum Multinationalen Transonic Vortex-Flow-Experiment', Dornier Report BF18/86B, 1987.
- (42) Rizzi, A., 'Modelling Vortex Flowfields by Supercomputers with Super-Size Memory', Aeronautical Journal, April 1985.
- (43) Legendre, R., 'Ecoulement au Voisinage de la Pointe avant d'une Aile a Forte Fleche aux Incidences Moyennes', La Recherche Aerospatiale (O.N.E.R.A.) No.30, 1952 and No.31, 1953.
- (44) Smith, J.H.B., 'Modelling Three-Dimensional Vortex Flows in Aerodynamics', V.K.I. Lecture Series 1986-08, Introduction to Vortex Dynamics, 1986.
- (45) Brown, C.E. and Michael, W.H., 'On Slender Delta Wings with Leading-Edge Separation', NACA TN 3430, 1955.
- (46) Mangler, K.W. and Smith, J.H.B., 'A Theory of Slender Delta Wings with Leading Edge Separation', R.A.E. TN No. Aero 2442, 1956.
- (47) Mangler, K.W. and Smith, J.H.B., 'Calculation of the Flow Past Slender Delta Wings with Leading Edge Separation', R.A.E. Report No. Aero 2593, 1957.
- (48) Smith, J.H.B., 'Improved Calculations of Leading Edge Separation from Slender Delta Wings', R.A.E. TR No. 66070, 1966.

- (49) Peace, A.J., 'A Multi-Vortex Model of Leading-Edge Vortex Flows', International Journal for Numerical Methods in Fluids, Vol.3, 1983.
- (50) Johnson, F.T., Lu, P., Tinoco, F.N. and Epton, M.A., 'An Improved Panel Method for the Solution of Three-Dimensional Leading-Edge Vortex Flows', NASA CR 3278, 1980.
- (51) Nangia, R.K. and Hancock, G.J., 'A Theoretical Investigation for Delta Wings with Leading-Edge Separation at Low Speeds', A.R.C. CP 1086, 1970.
- (52) Hoeijmakers, H.W.M., 'Vortex-Fitted Potential Solution Compared with Vortex-Captured Euler Solution for Delta Wing with Leading-Edge Vortex Separation', A.I.A.A. Paper No. 84-2144.
- (53) Hall, M.G., 'On the Vortex Associated with Flow Separation from a Leading Edge of a Slender Wing', R.A.E. TN No. Aero 2629, 1959.
- (54) Hall, M.G., 'A Theory for the Core of a Leading Edge Vortex', R.A.E. Report No. Aero 2644, 1960.
- (55) Stewartson, K. and Hall, M.G., 'The Inner Viscous Solution for the Core of a Leading -Edge Vortex', Journal of Fluid Mechanics', Vol.15, 1963.

- (56) Mangler, K.W. and Weber, J., 'The Flow Field Near the Centre of a Rolled-Up Vortex Sheet', Journal of Fluid Mechanics, Vol.30, 1967.
- (57) Leonard, A., 'Vortex Methods for Flow Simulation', Journal of Computational Physics, Vol.37, 1980.
- (58) Nakamura, Y., Leonard, A. and Spalart, P.R., 'Numerical Simulation of Vortex Breakdown by the Vortex-Filament Method', AGARD CP 342, 1983.
- (59) Luckring, J.M., 'A Theory for the Core of a Three-Dimensional Leading-Edge Vortex', A.I.A.A. Paper No. 85-0105, 1985.
- (60) Pullin, D., 'Calculation of the Steady Conical Flow past a Yawed Slender Delta Wing with Leading Edge Separation', A.R.C. R&M 3767, 1975.
- (61) Milne-Thomson, L.M., 'Theoretical Hydrodynamics', Macmillan and Co., 1949.
- (62) Coe, P.L., 'Stationary Vortices Behind a Flat Plate Normal to the Freestream in an Incompressible Flow', A.I.A.A. Journal, December 1972.
- (63) Smith, J.H.B. and Clark, R.W., 'Nonexistence of Stationary Vortices Behind a Two-Dimensional Normal Plate', A.I.A.A. Journal, August 1975.

- (64) The Numerical Algorithms Group, FORTRAN Library Manual Mark 12, 1987.
- (65) Coe, P.L., 'A Vortex Entrainment Model Applied to Slender Delta Wings', A.I.A.A. Journal, January 1974.
- (66) Mourtos, N.J., 'Flow Past a Flat Plate with a Vortex-Sink Combination', Joint Institute for Aeronautics and Acoustics Report JIAA-TR58, Stanford University, 1984.
- (67) Drazin, P.G. and Reid, W.H., 'Hydrodynamic Stability', Cambridge University Press, 1981.
- (68) Bryce, S.G., 'A New Analytical Approach to Vortex Breakdown Investigation', A.I.A.A. Paper No. 87-2495, 1987.
- (69) Trebble, W.J.G., 'Exploratory Investigation of the Effects of Blowing From the Leading Edge of a Delta Wing', A.R.C. R&M 3518, 1968.
- (70) Barsby, J.E., 'Calculations of the Effect of Blowing from the Leading Edges of a Slender Delta Wing', A.R.C. R&M 3692, 1972.
- (71) Wood, N.J. and Roberts, L., 'The Control of Vortical Lift on Delta Wings by Tangential Leading Edge Blowing', A.I.A.A. Paper No. 87-0158, 1987.

(72) Wood, N.J., Roberts, L. and Lee, K.T., 'The Control of Vortical Flow on a Delta Wing at High Angles of Attack', A.I.A.A. Paper No. 87-2278, 1987.

(73) Seginer, A. and Salomon, M., 'Augmentation of Fighter-Aircraft Performance by Spanwise Blowing over the Wing Leading Edge', AGARD CP 342, 1983.

(74) Huffman, J.K., Hahne, D.E. and Johnson, T.D., 'Experimental Investigation of the Aerodynamic Effects of Distributed Spanwise Blowing on a Fighter Configuration', A.I.A.A. Paper No. 84-2195, 1984.

(75) Shi, Z., Wu, J.M. and Vakili, A.D., 'An Investigation of Leading-Edge Vortices on Delta Wings with Jet Blowing', A.I.A.A. Paper No. 87-0330, 1987.

(76) Verhaagen, N. and Kruisbrink, A.C.H., 'The Entrainment Effect of a Leading-Edge Vortex', A.I.A.A. Paper No. 85-1584, 1985.

Table 1

Estimated Solutions for the Point Vortex Model

At each location the initial estimated value for vortex strength was set at -1.0, -5.0 and -10.0.

A converged / non-converged final solution is indicated by the entry C / NC.

		Spanwise vortex coordinate					
		-0.6	-0.5	-0.4	-0.3	-0.2	-0.1
Vertical vortex coordinate	0.6	NC	NC	NC	NC	NC	NC
	0.5	NC	NC	NC	NC	NC	NC
	0.4	NC	NC	NC	NC	NC	NC
	0.3	NC	NC	NC	NC	NC	NC
	0.2	NC	NC	NC	NC	NC	NC
	0.1	NC	NC	NC	NC	NC	NC

Table 2

Solution Behaviour for the Unmodified Vortex-Sink Model

The behaviour types 1, 2, 3 and 4 listed in the table below correspond to the four types of solution behaviour discussed in section 3.5, i.e.

1 = solutions possible within the range $-0.72 \leq b \leq -0.15$

2 = z +ve solutions possible for $-1.0 \leq b \leq -0.02$

3 = z -ve solutions possible for $-1.0 \leq b \leq -0.02$

4 = no solutions possible.

In each case the initial estimated solution was set at

$y_A = -s/2$, $z_A = s/2$ and $\Gamma = -5.0$.

		Velocity U_c (m/s)					
		1.0	2.0	3.0	4.0	5.0	6.0
Wingspan s (m)	1.0	1	2	4	3	1	2
	2.0	2	2	1	1	1	4
	3.0	4	1	4	1	1	3
	4.0	2	4	1	2	1	3
	5.0	4	1	1	1	1	3
	6.0	4	2	4	4	2	4

Table 3

Conical Solutions for the Modified Vortex-Sink Model

The entries in the table below indicate whether convergence (C), or non-convergence (NC), was found in conical solutions of the modified vortex-sink model at the values specified for Λ and α .

		Wing Sweepback Angle Λ				
		60.0	65.0	70.0	75.0	80.0
Angle of Attack α	5.0	C	NC	NC	NC	C
	10.0	NC	C	C	C	C
	15.0	C	C	NC	C	C
	20.0	C	C	C	C	C
	25.0	C	C	C	C	C
	30.0	C	C	C	C	NC

Table 4

Effect of a Variation in Γ and b on Solution of the Kutta Condition

The entries in the table below indicate the smooth (S) or erratic (E) behaviour of solutions to the Kutta condition for the values of Γ and b shown.

		b					
		-0.1	-0.2	-0.3	-0.4	-0.5	-0.6
vortex strength Γ	-2.0	S	S	S	S	S	S
	-3.0	S	S	S	S	S	S
	-4.0	S	S	S	S	S	S
	-5.0	S	S	S	S	S	S
	-6.0	S	S	S	S	S	S
	-7.0	S	S	S	S	S	S
	-8.0	S	S	S	S	S	S
	-9.0	E	S	S	S	S	S
	-10.0	E	S	S	S	S	S
	-11.0	S	S	S	S	S	S
	-12.0	S	E	S	S	S	S
	-13.0	S	E	S	S	S	S
	-14.0	E	S	S	S	S	S
	-15.0	E	S	S	S	S	S
	-16.0	S	S	E	S	S	S
	-17.0	S	S	E	S	S	S
	-18.0	S	S	E	S	S	S
	-19.0	S	S	S	S	S	S
	-20.0	S	S	S	S	S	S
	-40.0	S	S	S	S	S	S
-60.0	S	S	S	S	S	S	

Table 5

Solution Behaviour with C_1

The three test cases for which the effect of C_1 was assessed are detailed below. In each case $U = 1.0$ m/s, $s = 1.0$ m and $\Delta x = 0.001$. In the table, the solution behaviour is given as S (smooth) or O (oscillatory).

Case 1: $\alpha = 5^\circ$, $\Lambda = 60^\circ$ and $b_i = -0.05$.

Case 2: $\alpha = 20^\circ$, $\Lambda = 70^\circ$ and $b_i = -0.3$.

Case 3: $\alpha = 30^\circ$, $\Lambda = 80^\circ$ and $b_i = -0.15$.

Constant of proportionality C_1	Case 1	Case 2	Case 3
	1.0	S	S
1.1	S	S	S
1.2	S	S	O
1.3	S	S	O
1.4	S	O	O
1.5	S	O	O
2.0	S	O	O
2.5	S	O	O

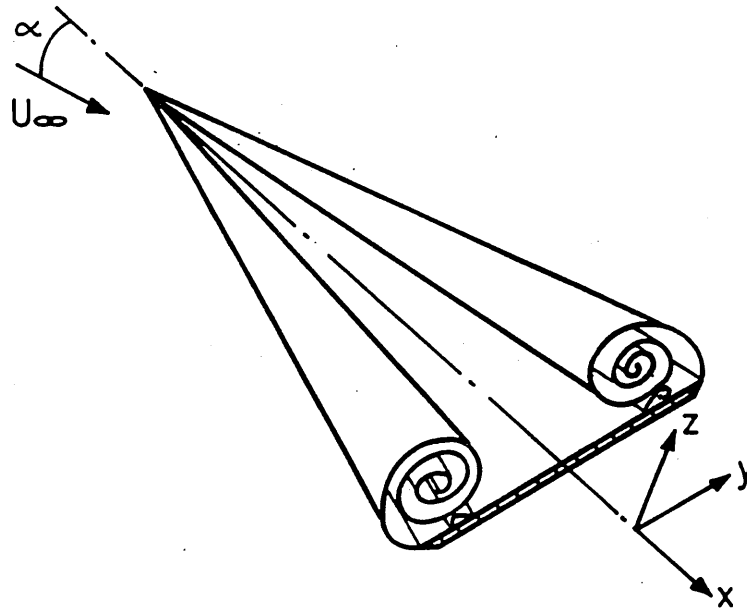


Fig.1.1 The High Angle of Attack Flow Over a Delta Wing

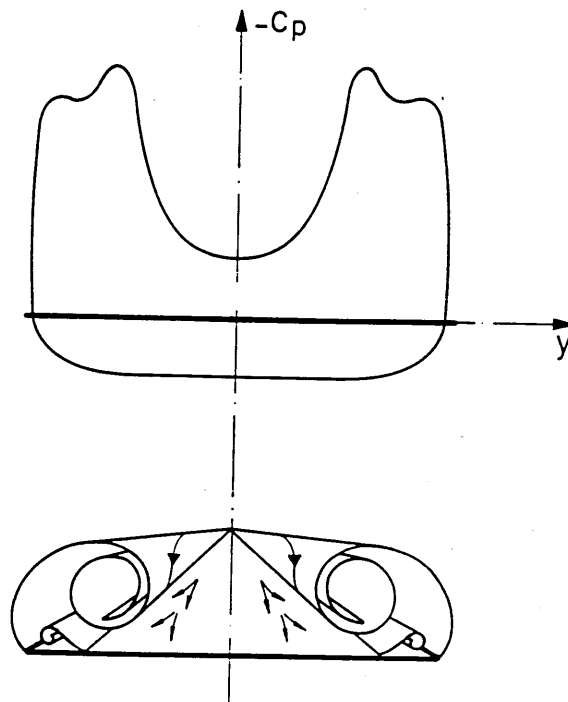


Fig.1.2 Pressure Distribution in the Crossflow Plane⁴

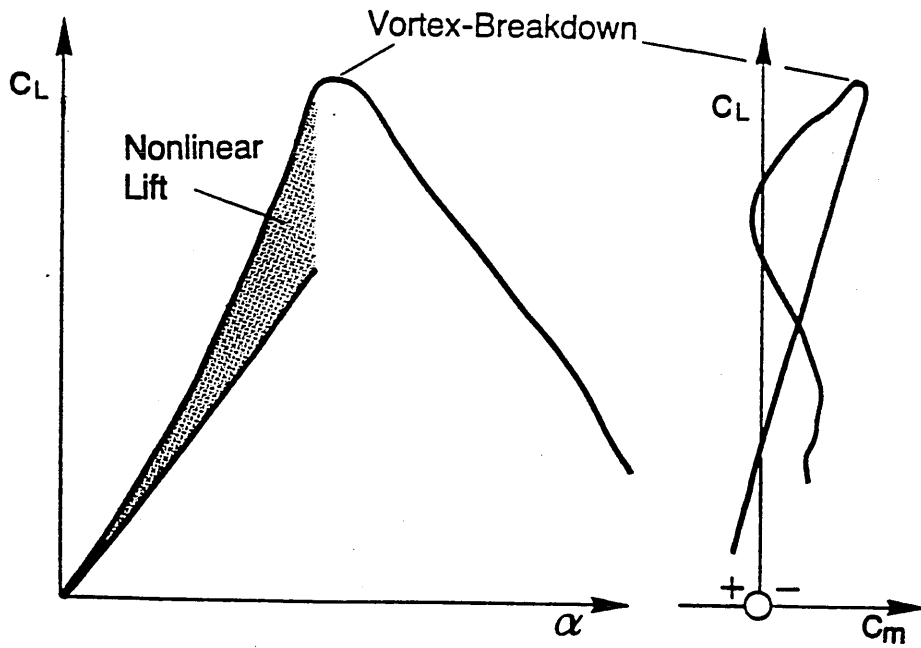


Fig.1.3 Lift and Pitching Moment Variations with α 40

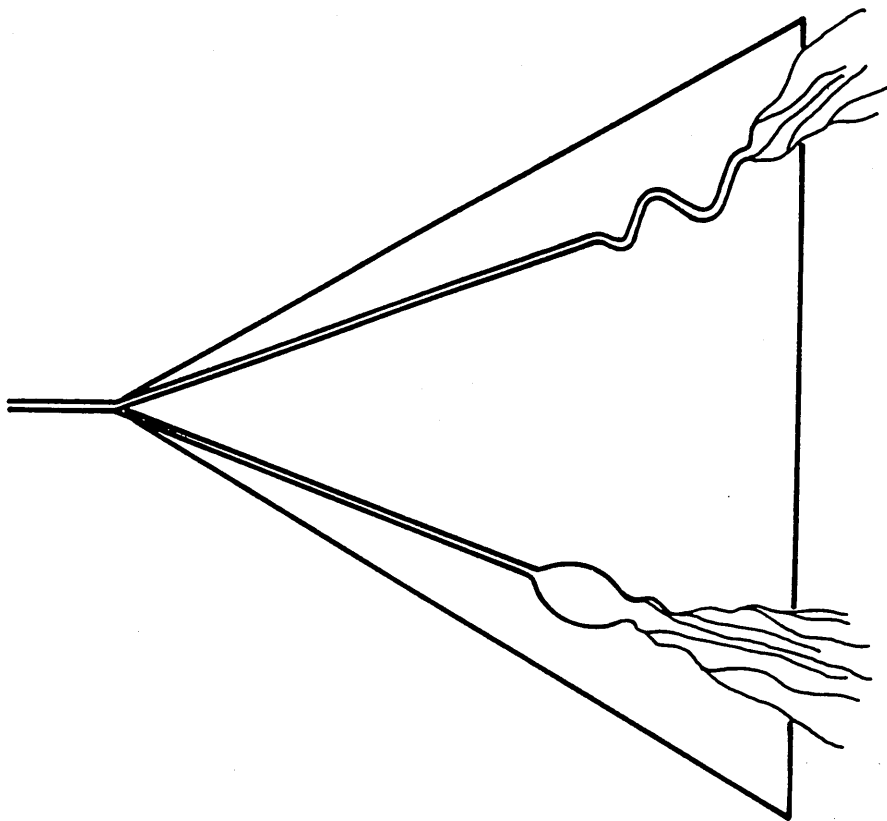


Fig.1.4 Two Possible Types of Vortex Breakdown

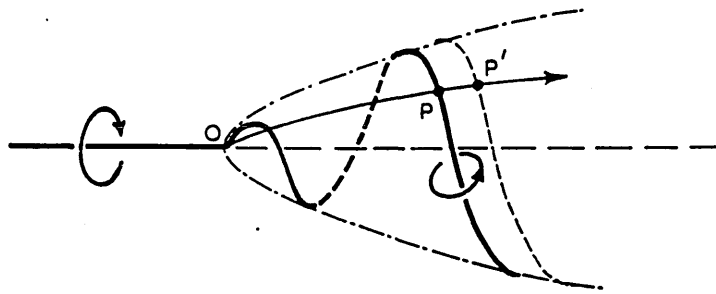


Fig.1.5 Path Taken by Particle P Through Breakdown Region ⁶

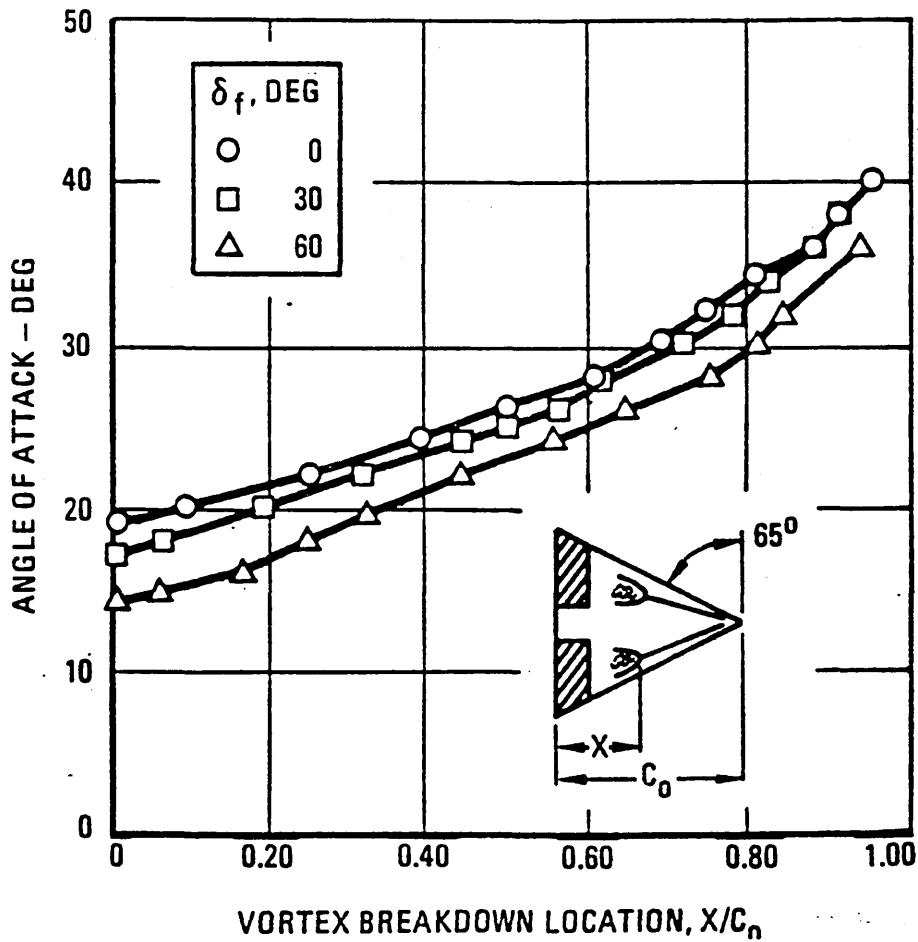


Fig.1.6 Effect of Trailing Edge Flap Deflection ¹¹

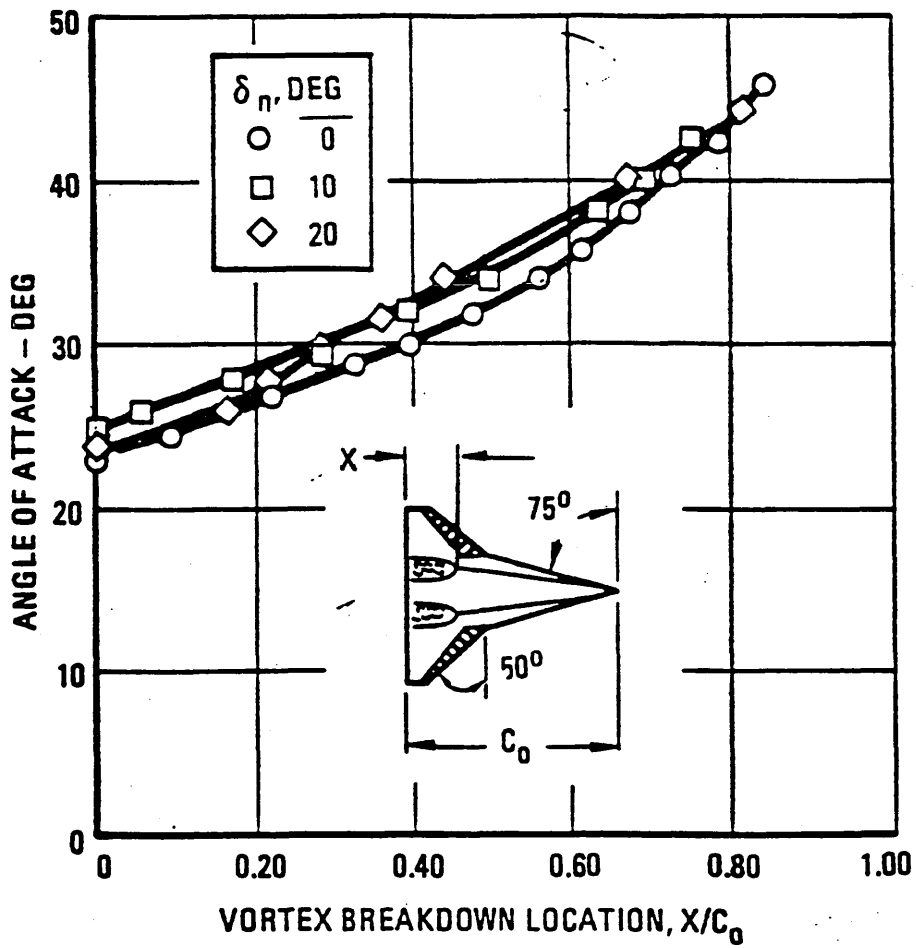


Fig.1.7 Effect of Leading Edge Flap Deflection ¹²

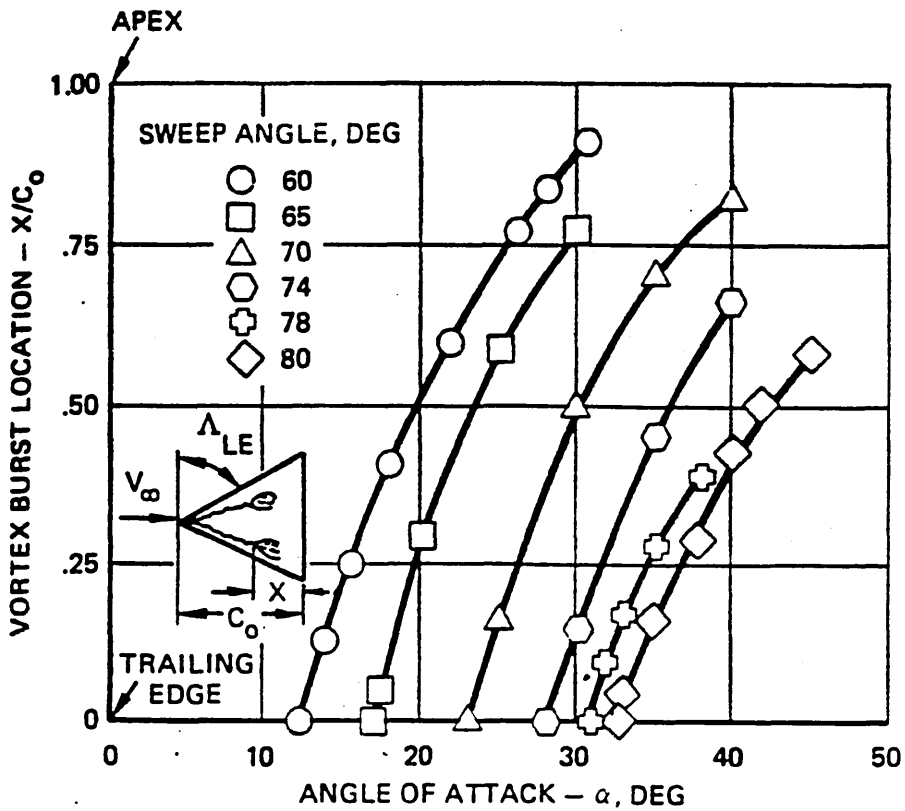


Fig.1.8 Effect of Wing Sweepback ¹²

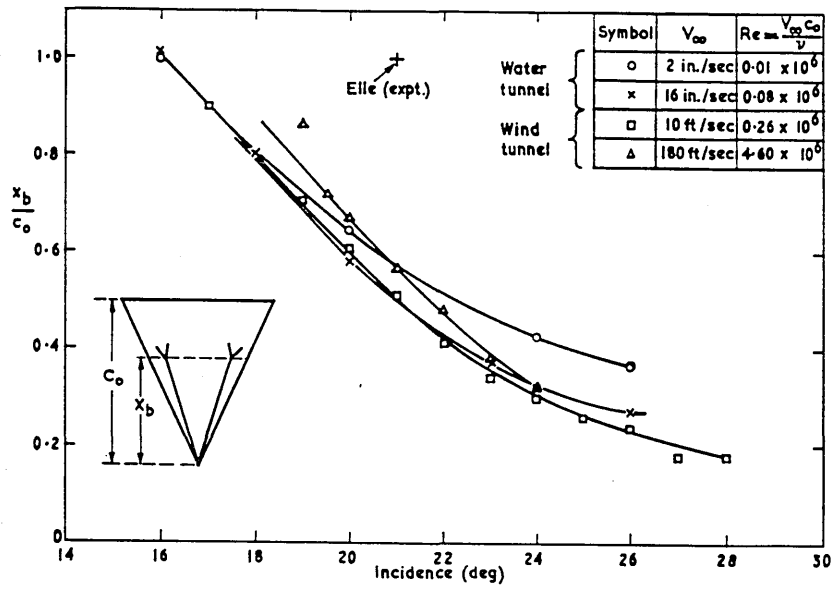


Fig.1.9 Effect of Reynolds' Number ⁶

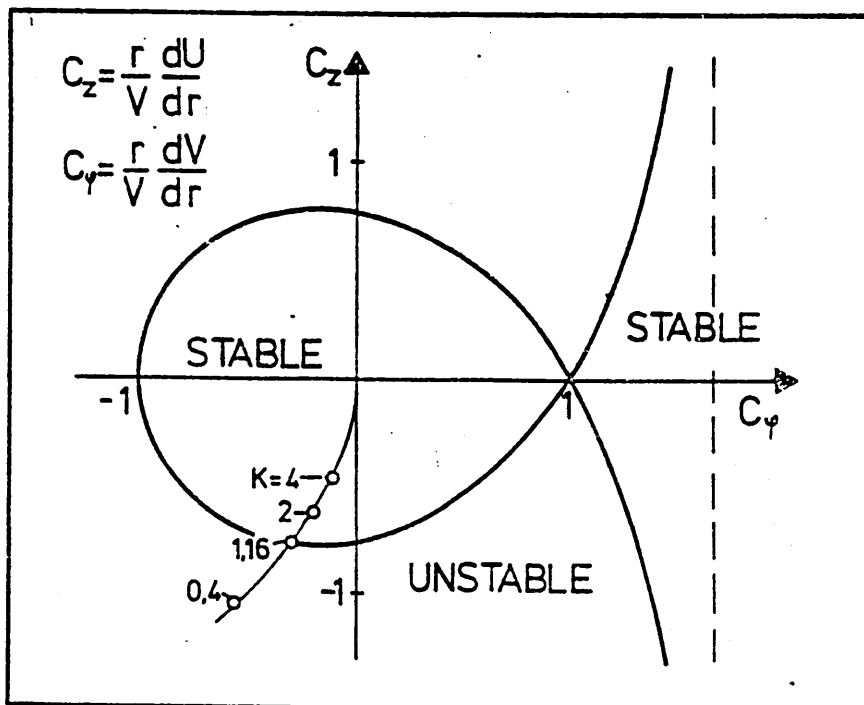


Fig.1.10 Ludwig's Stability Diagram ¹⁴

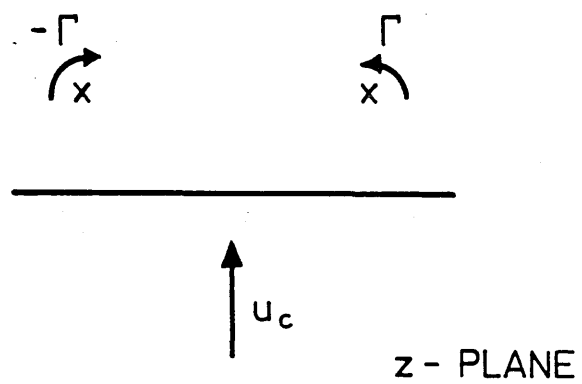


Fig.2.1 Legendre's Crossflow Model

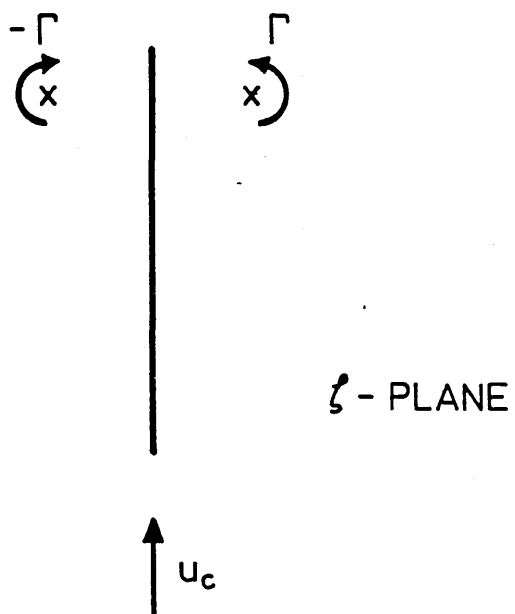


Fig.2.2 Transformation to the ζ -Plane

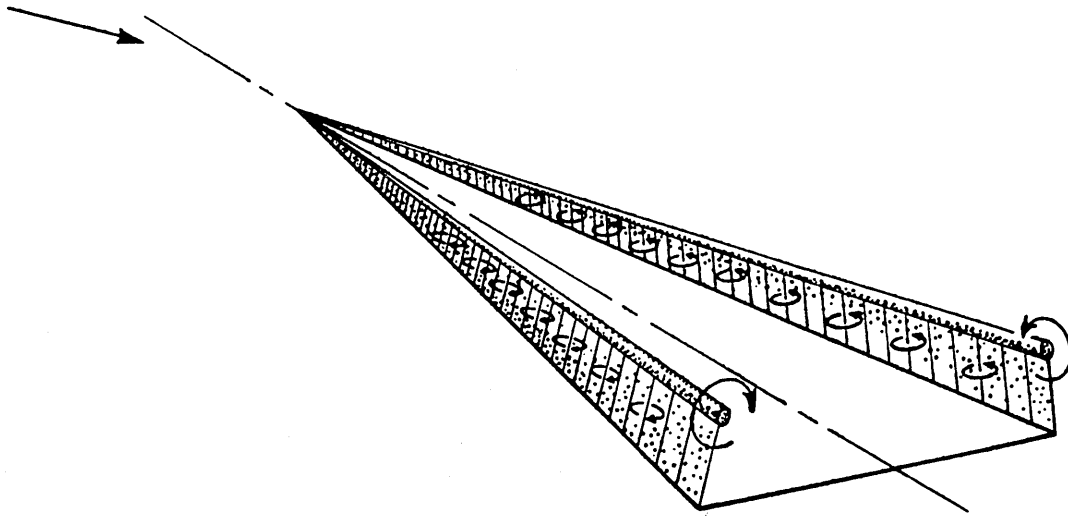


Fig.2.3 Brown and Michael's Model for the Delta Wing Flow ⁴⁵

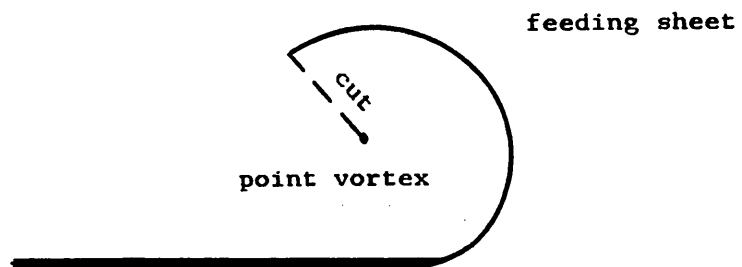


Fig.2.4 Mangler and Smith's Model for the Crossflow

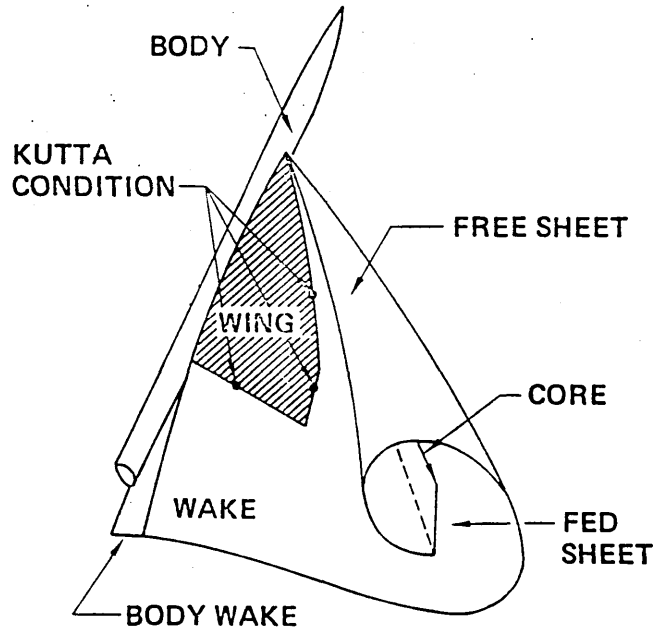


Fig.2.5 Johnson et al Model for the Delta Wing Flow ⁵⁰

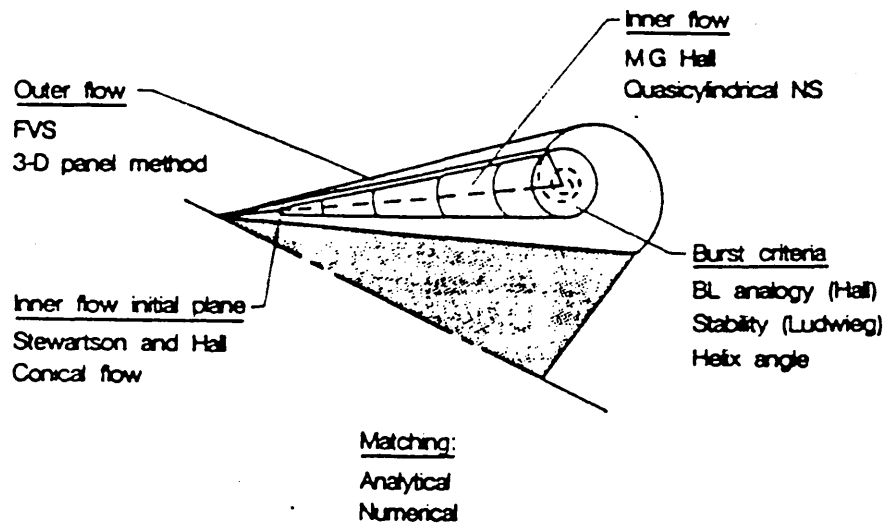


Fig.2.6 Luckring's Comprehensive Model for the Leading Edge Vortex ⁶⁰

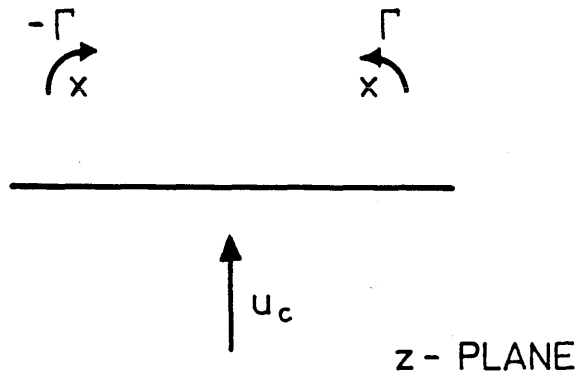


Fig.3.1 The Point Vortex Model

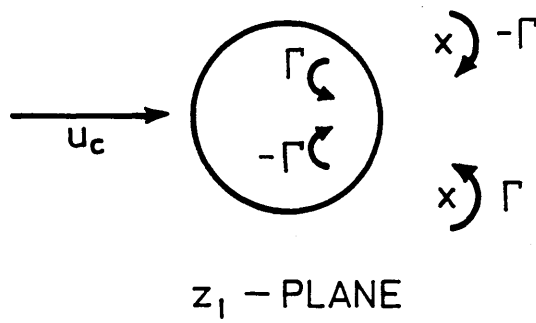


Fig.3.2 Transformation to the z_1 -Plane

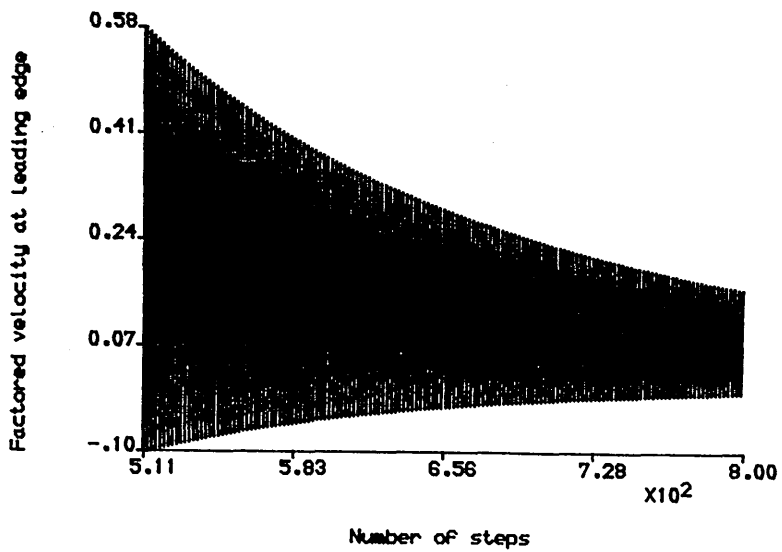
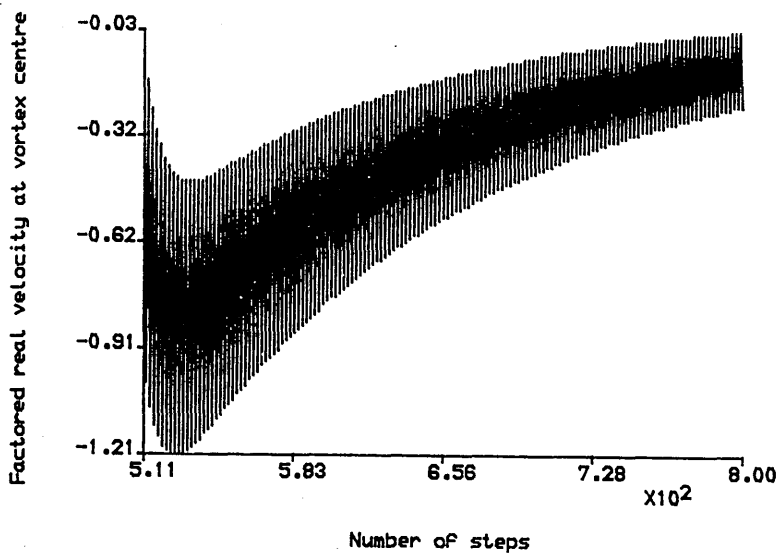
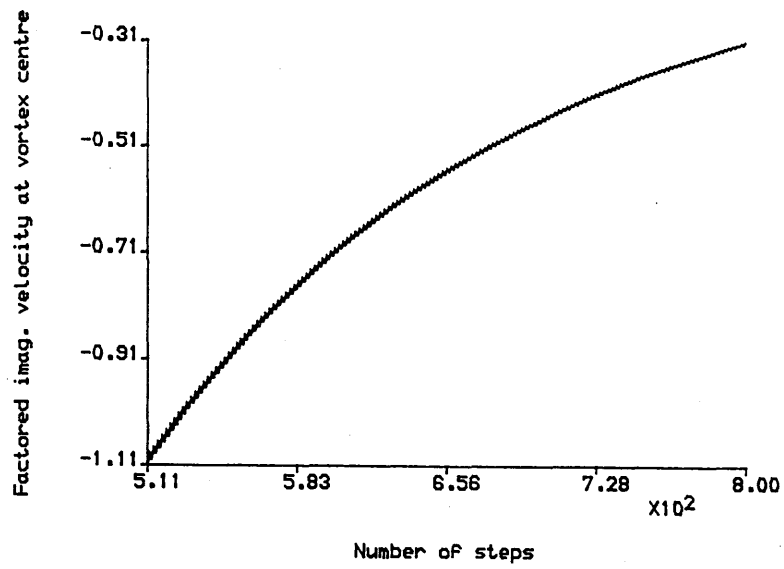


Fig.3.3 Non-Convergence of Point Vortex Solution

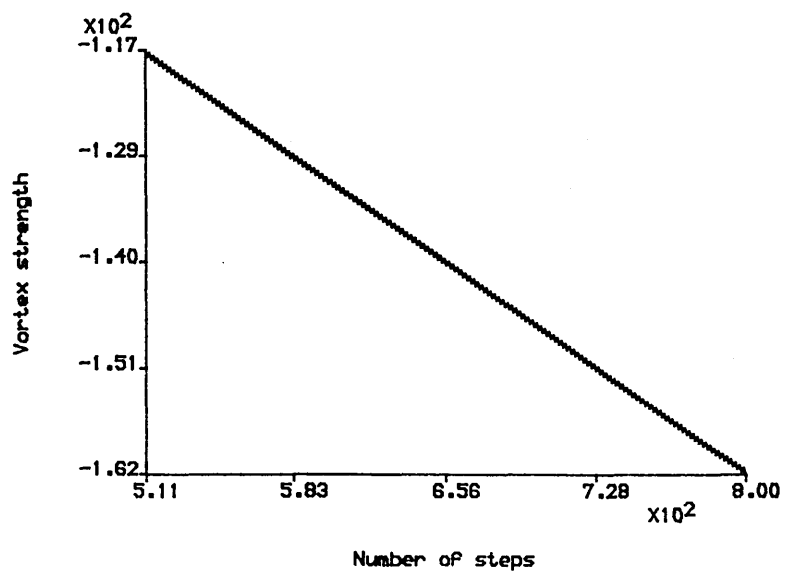
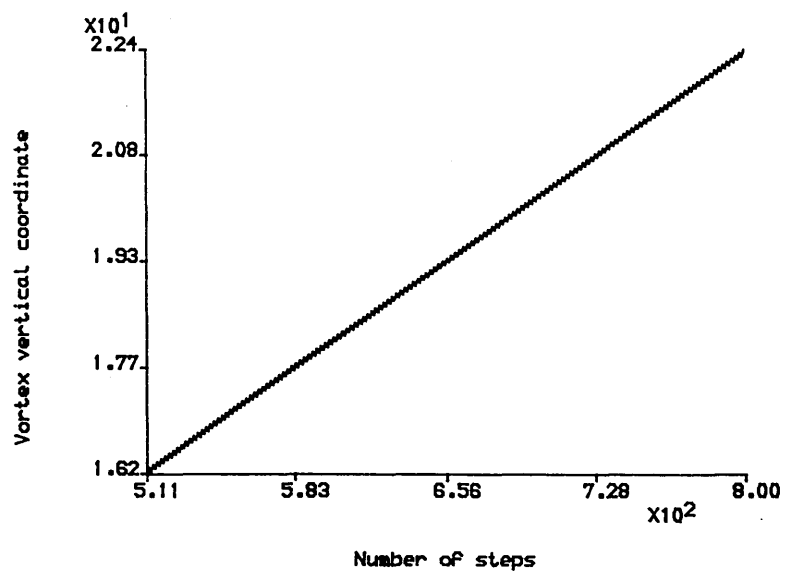
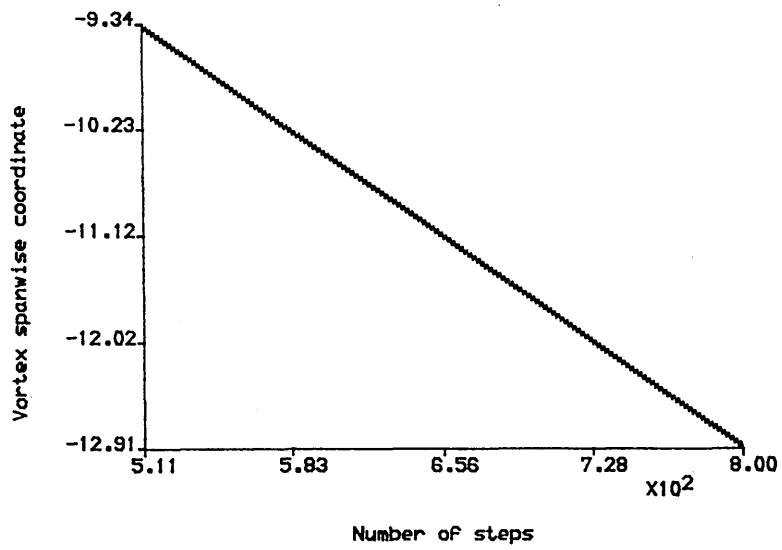


Fig.3.4 Non-Convergence of Point Vortex Solution

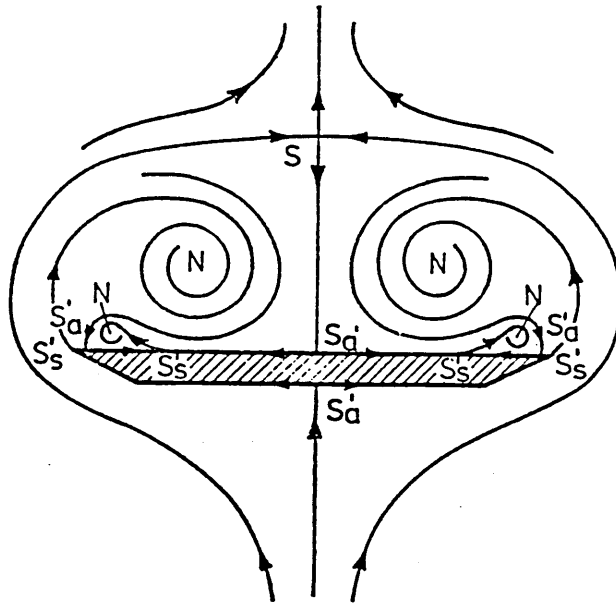


Fig.3.5 Crossflow Streamlines of Verhaagen ⁵

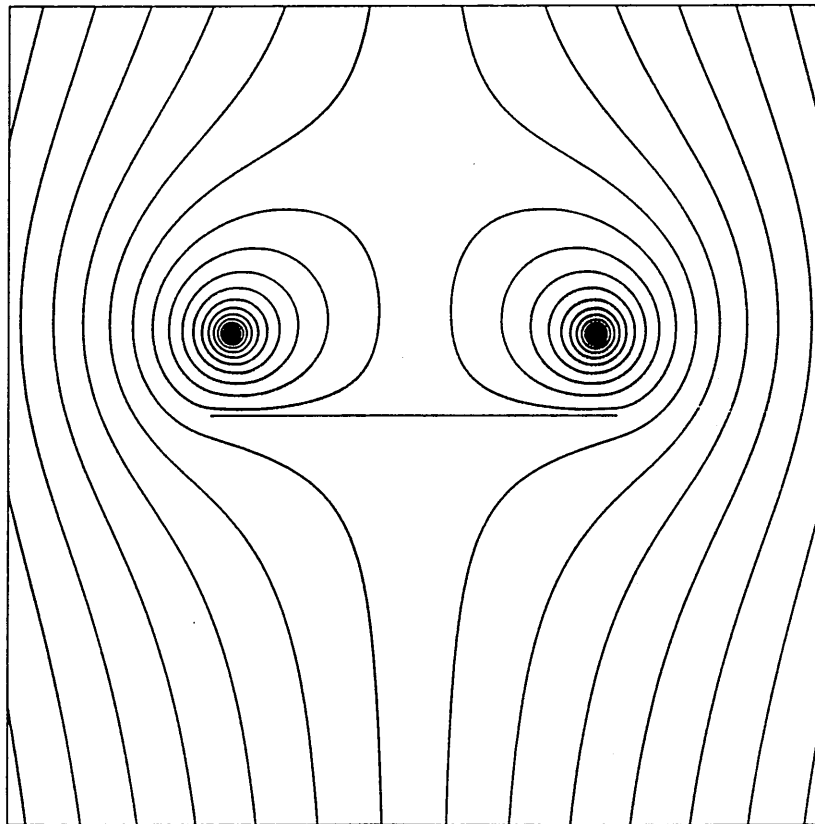


Fig.3.6 Crossflow Streamlines from Point Vortex Model

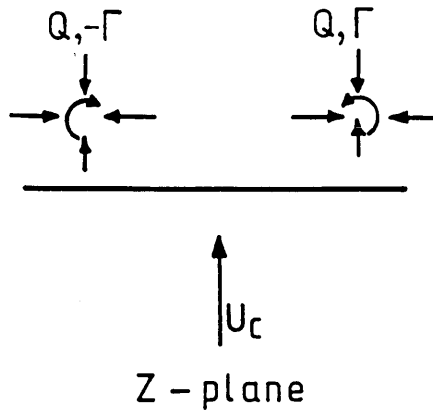


Fig.3.7 The Vortex-Sink Model

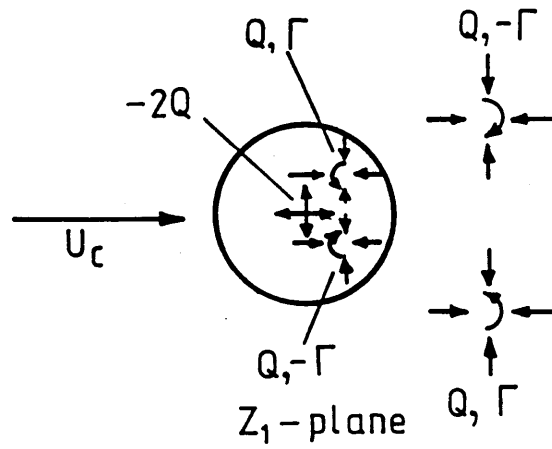


Fig.3.8 Transformation to the Z_1 -Plane

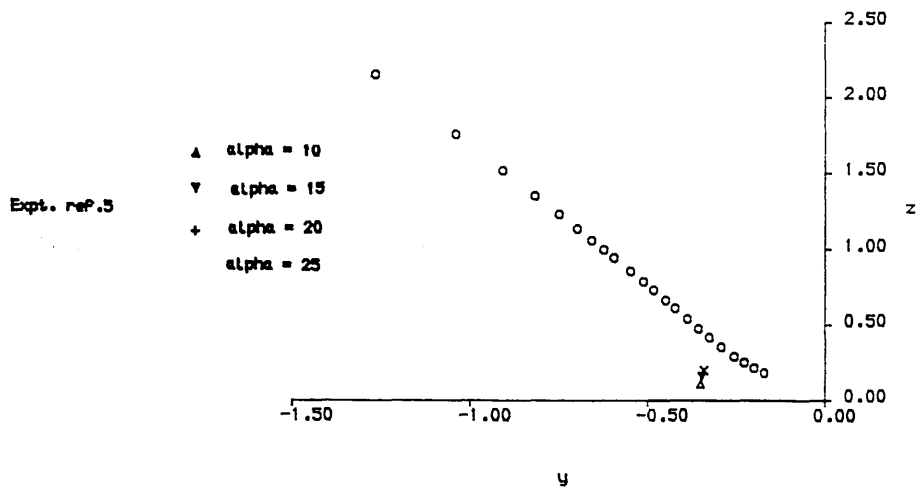


Fig.3.9 Vortex-Sink Solution Locations (type 1)

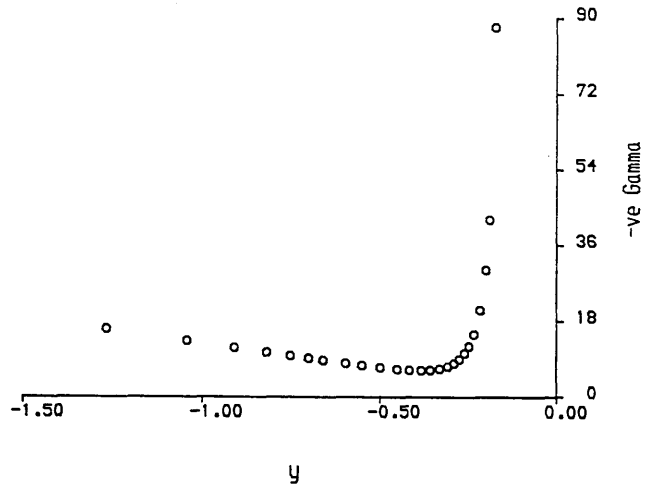


Fig.3.10 Vortex Strength - vs - y (type 1)

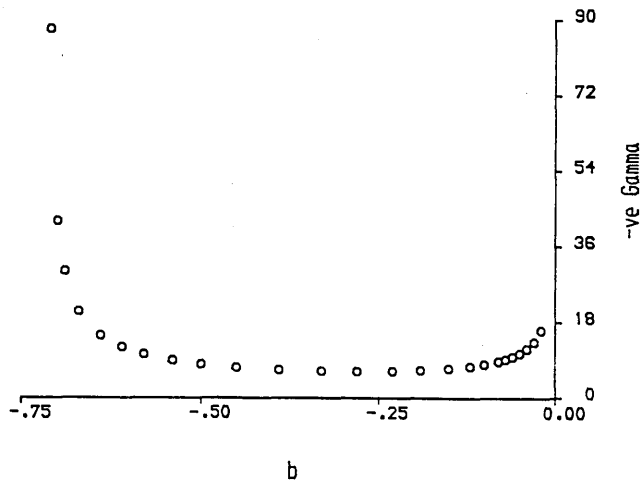


Fig.3.11 Vortex Strength - vs - b (type 1)

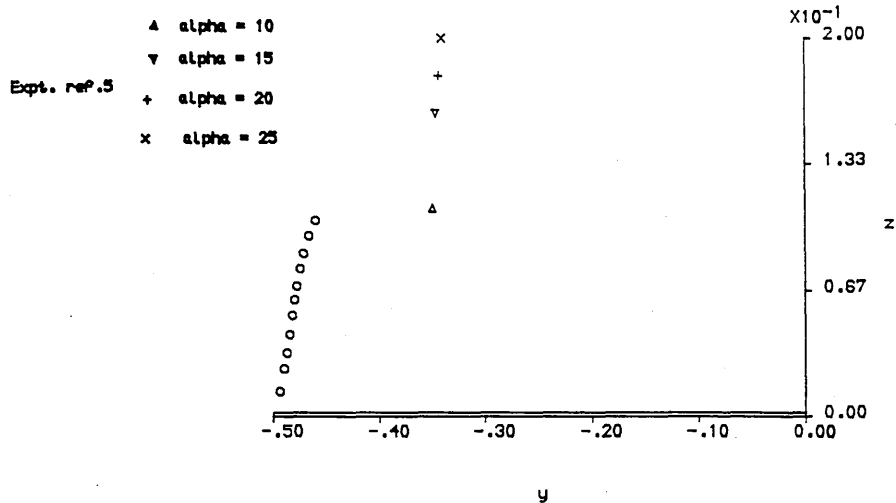


Fig.3.12 Vortex-Sink Solution Locations (type 2)

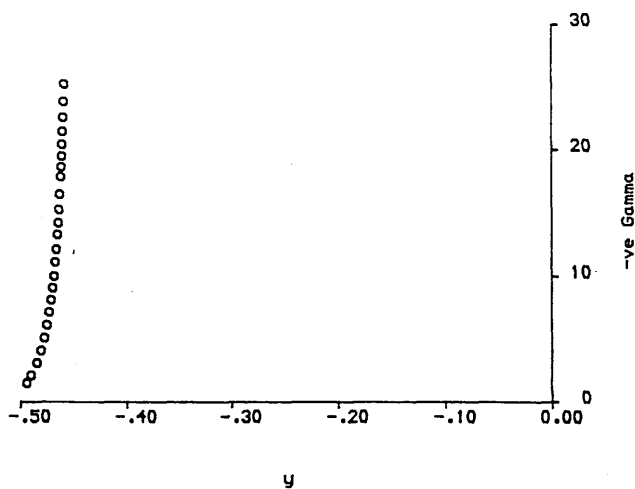


Fig.3.13 Vortex Strength - vs - y (type 2)

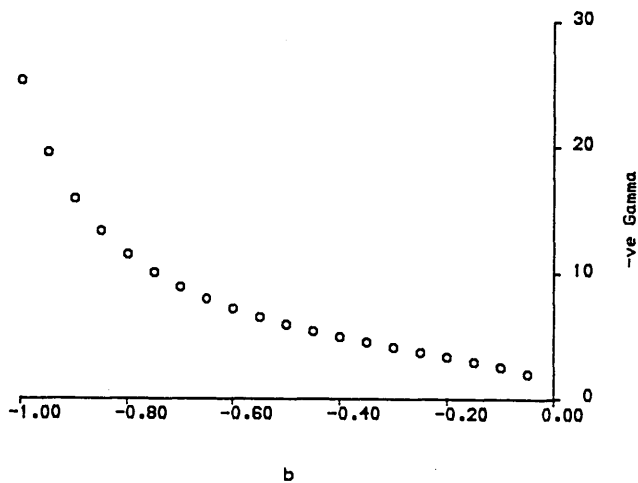


Fig.3.14 Vortex Strength - vs - b (type 2)

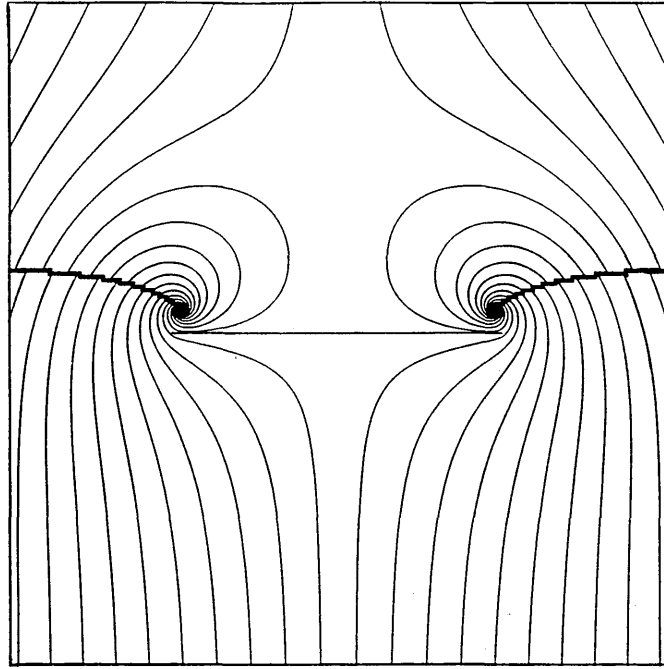


Fig.3.15 Crossflow Streamlines for Typical Solution of Type 2

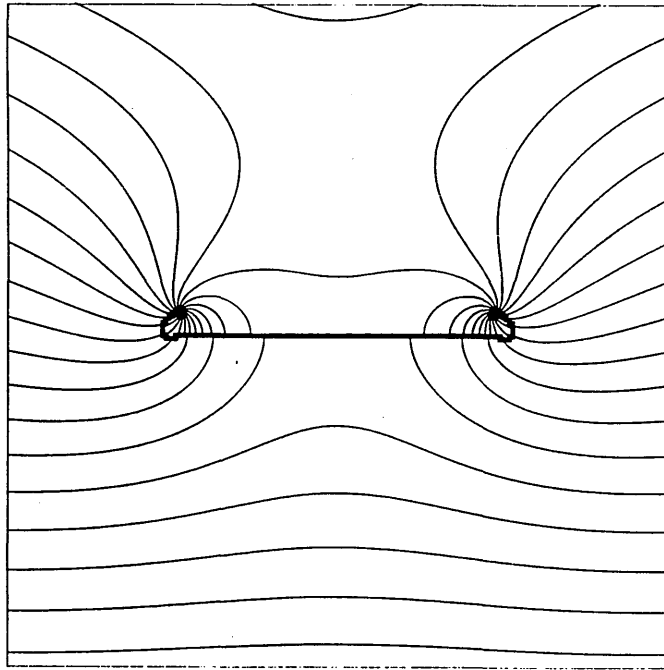


Fig.3.16 Crossflow Equipotentials For Typical Solution of Type 2

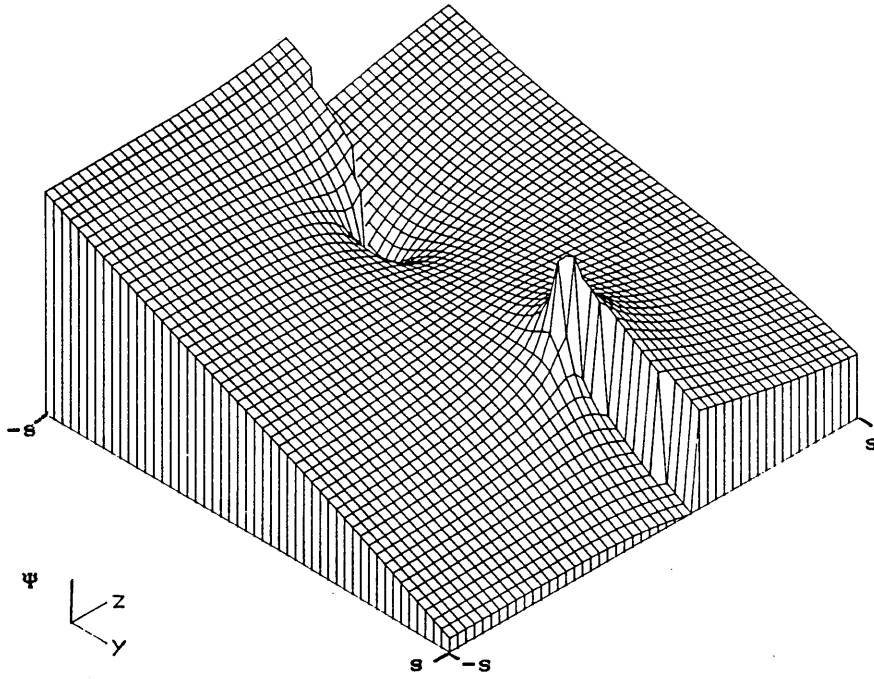


Fig.3.17 Three-Dimensional Plot of Ψ - vs - y and z

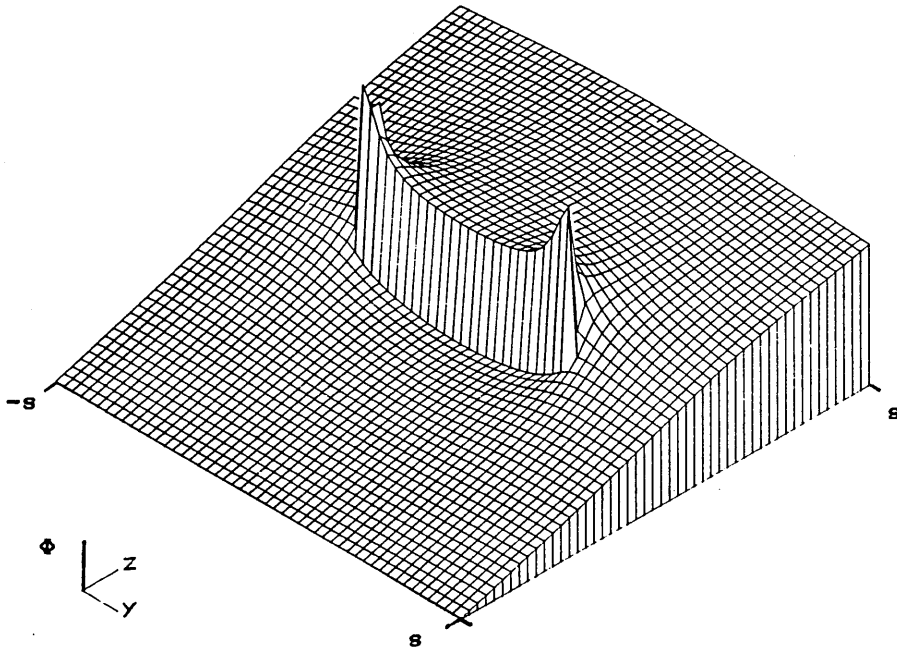


Fig.3.18 Three-Dimensional Plot of Φ - vs - y and z

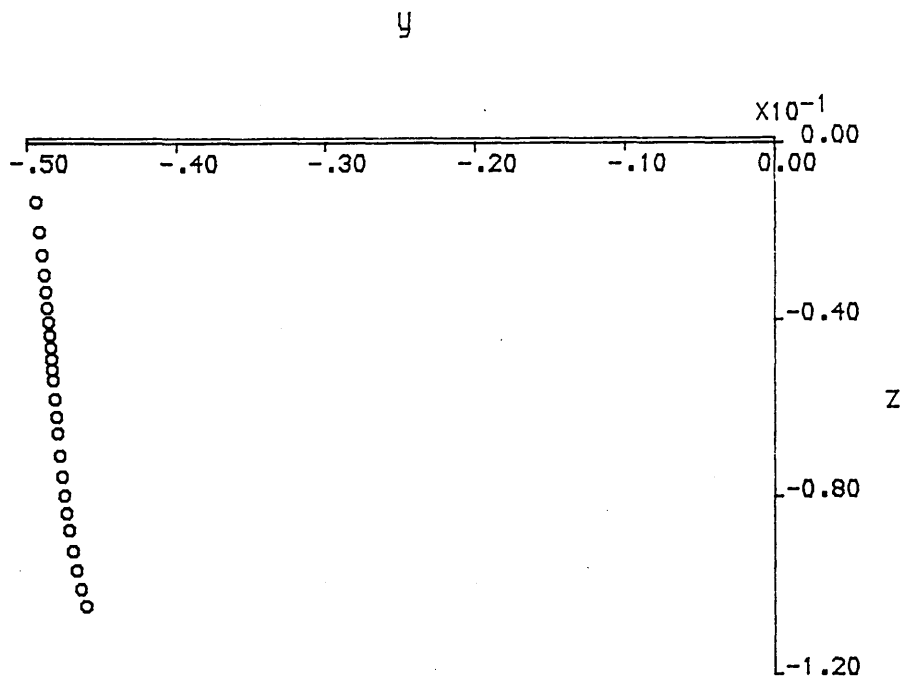


Fig.3.19 Vortex-Sink Solution Locations (type 3)

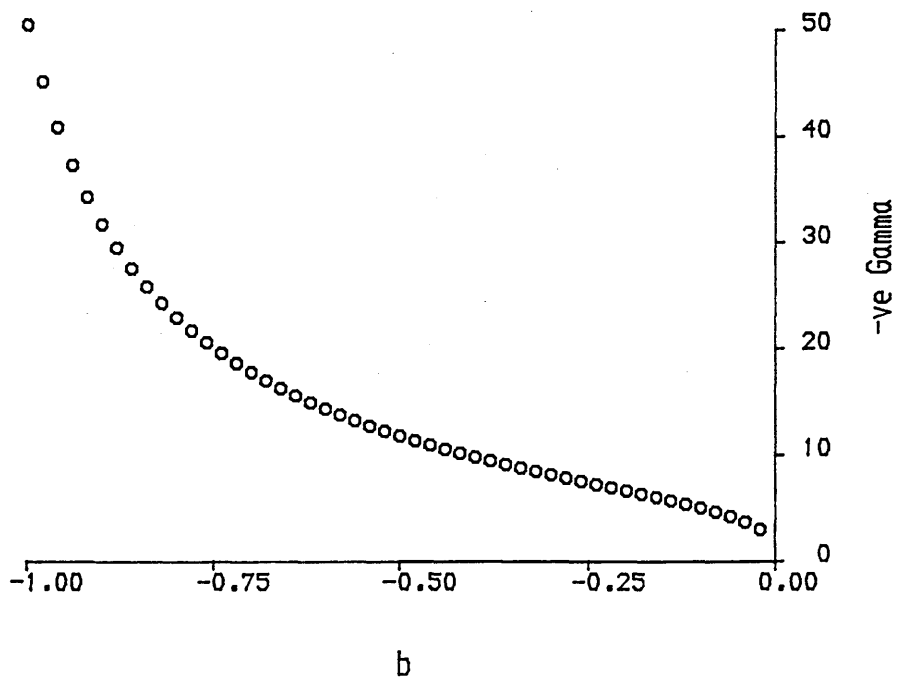


Fig.3.20 Vortex Strength - vs - b (type 3)

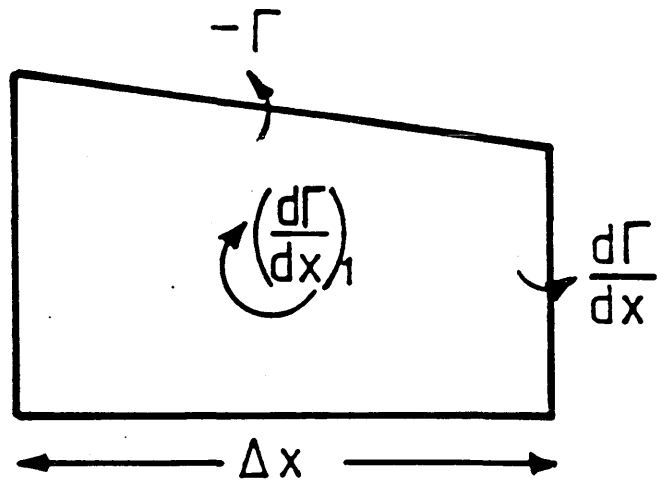


Fig.3.21 Element of Vortex-Sink-Feeding Sheet Combination

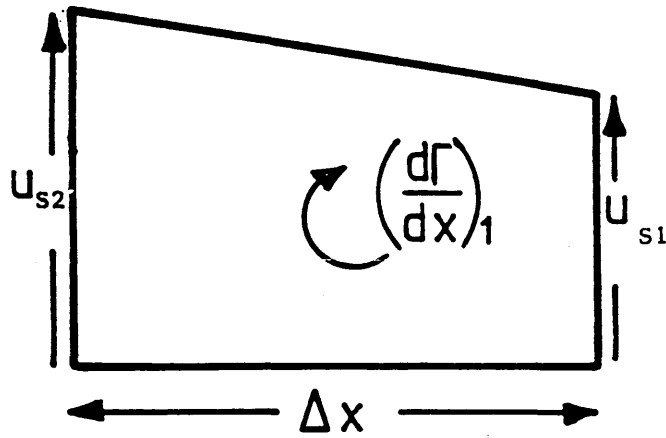


Fig.3.22 Velocity Difference Across Element of Feeding Sheet

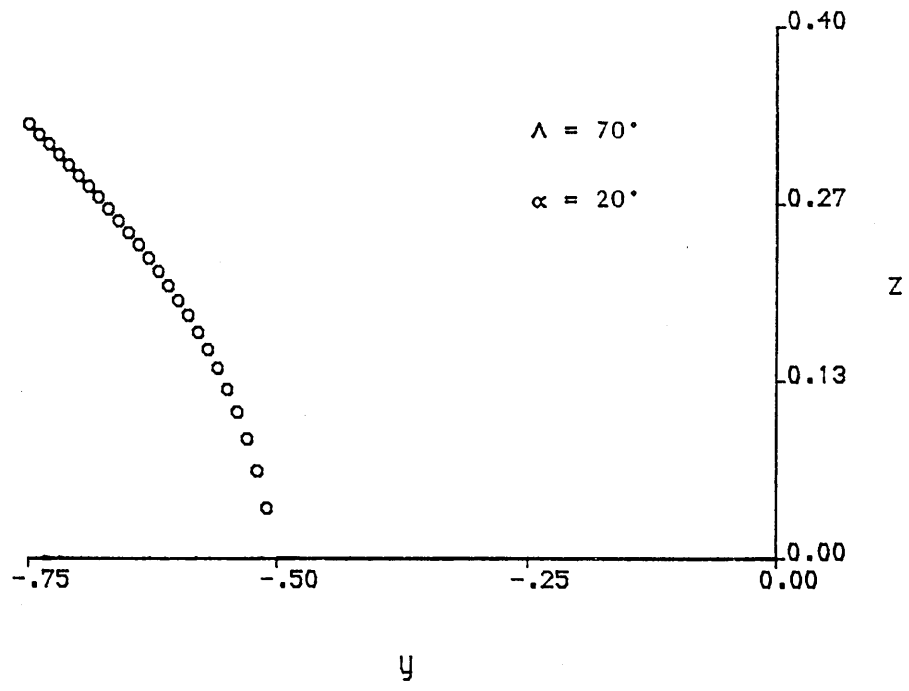


Fig.3.23(a) Conical Solution Locations for Modified Vortex-Sink Model

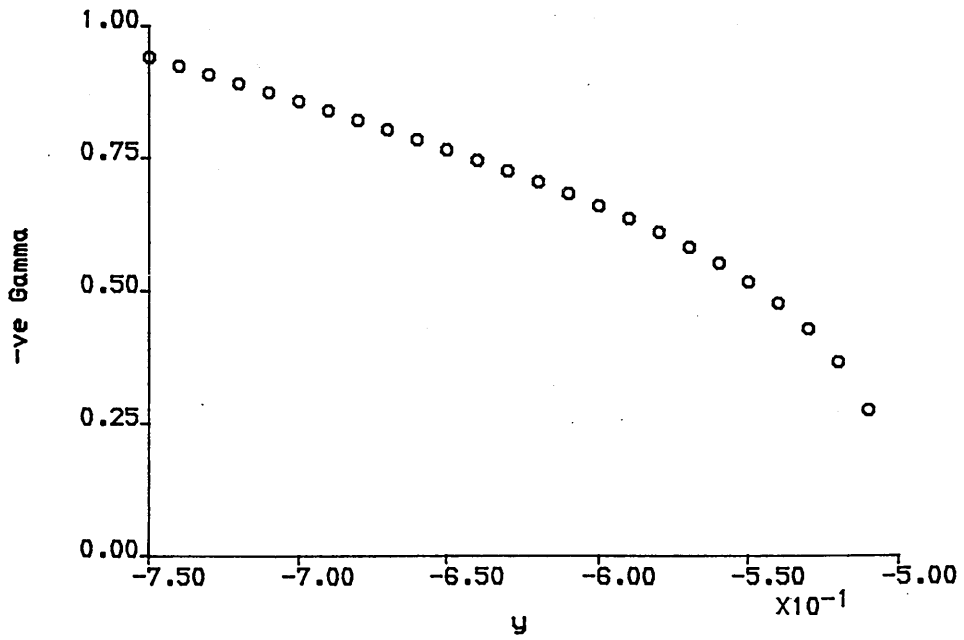


Fig.3.23(b) Associated Variation of Vortex Strength with y

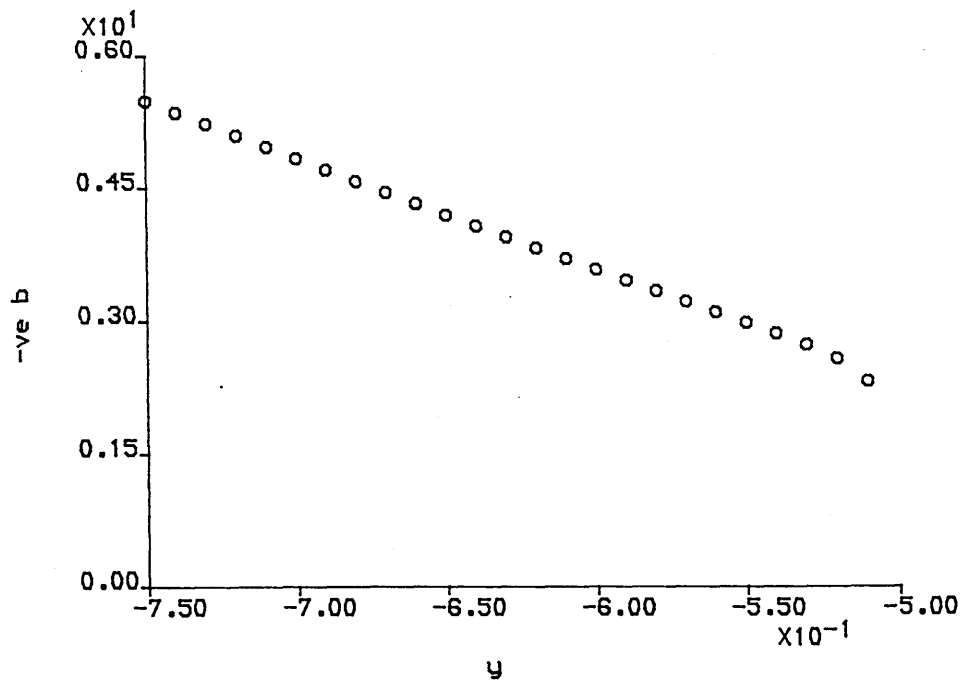


Fig.3.23(c) Associated Variation of b with y

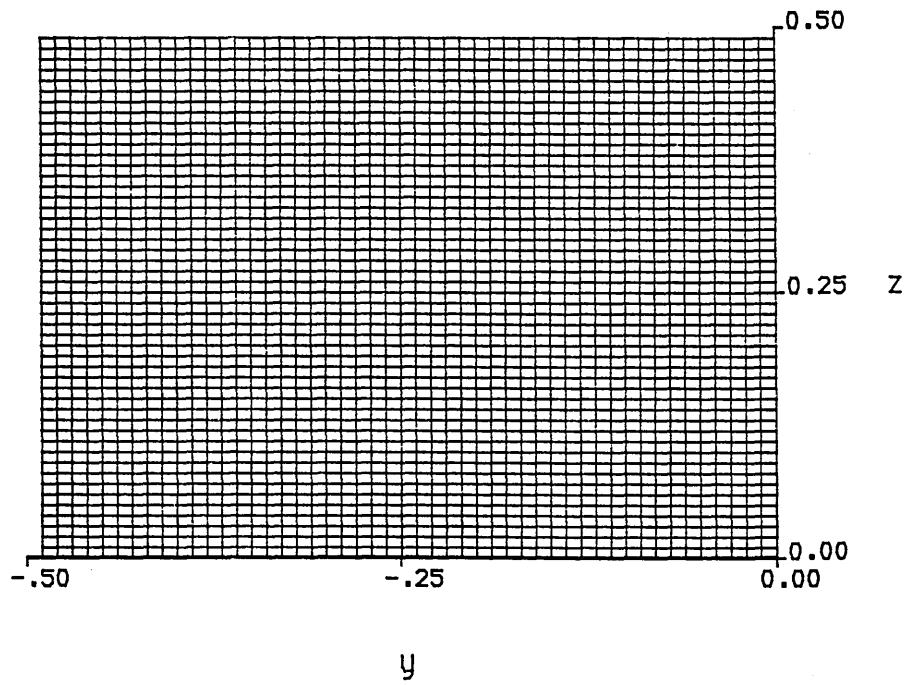


Fig.3.24 Mesh for Non-Conical Investigation

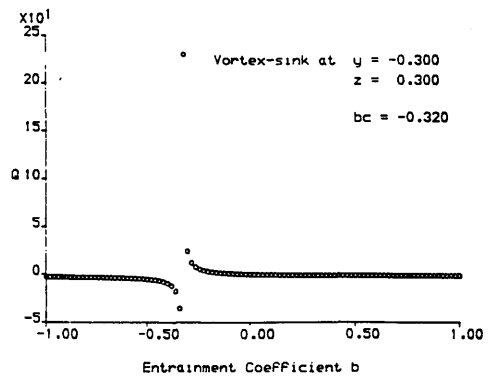
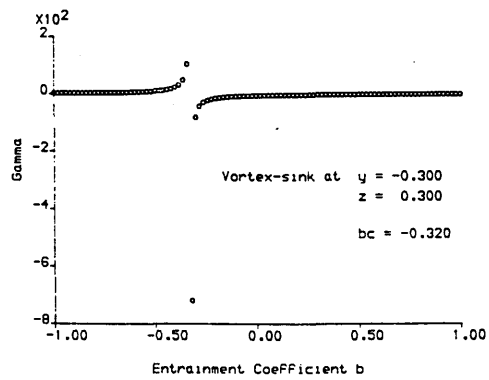
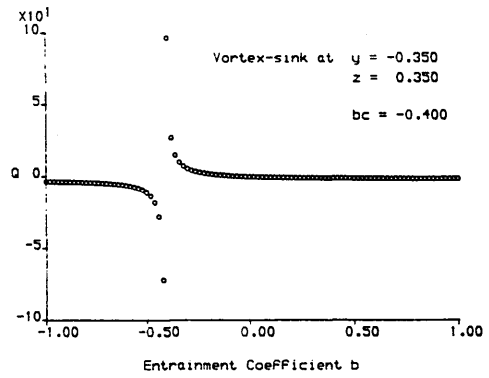
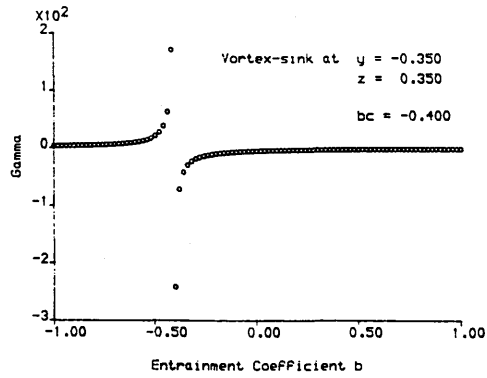
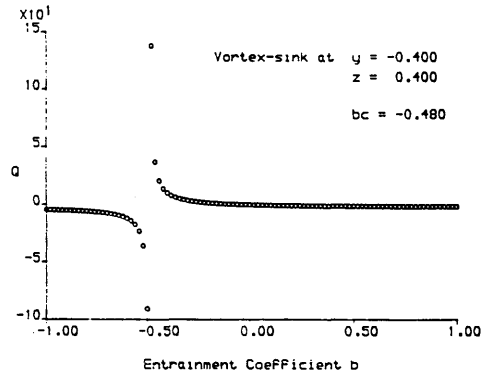
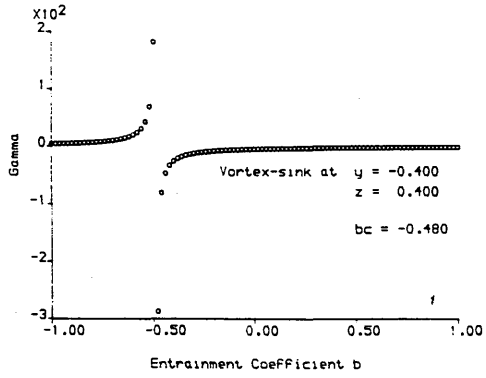
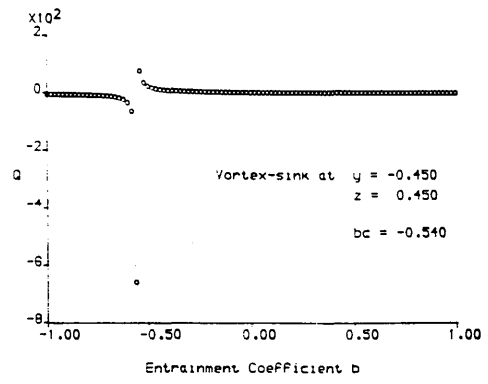
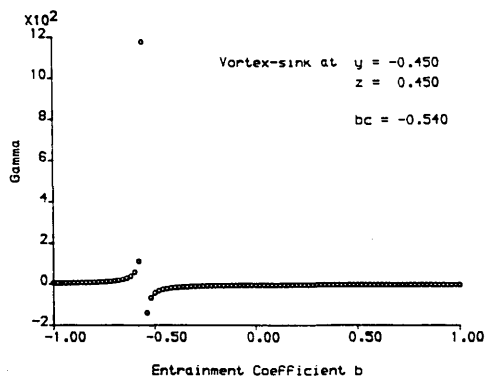


Fig.3.25 Four Typical Cases Showing Critical Nature of b in Q and Γ Solutions

Artificial surface

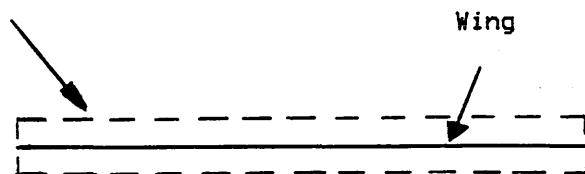


Fig.3.26 Artificial Surface Required for Pressure Calculation

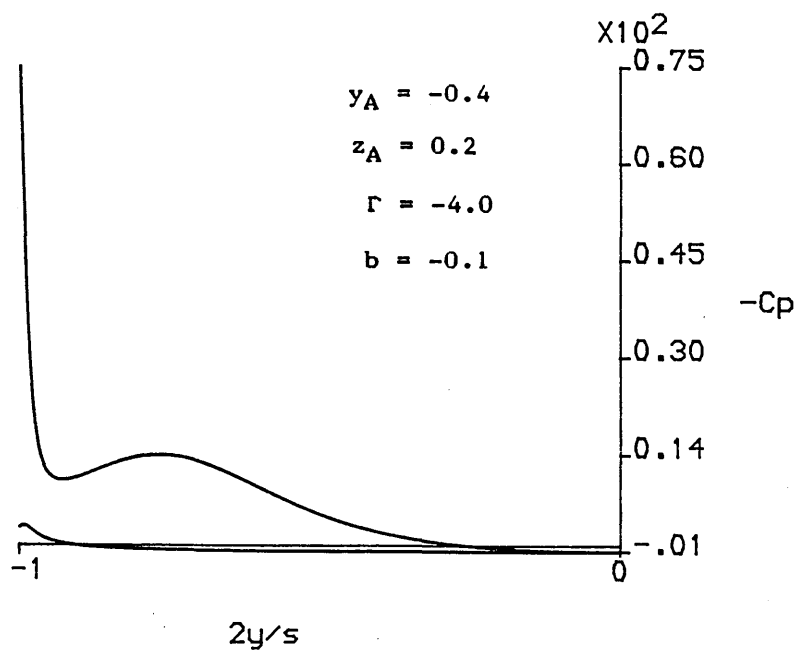


Fig.3.27 Typical Pressure Distribution

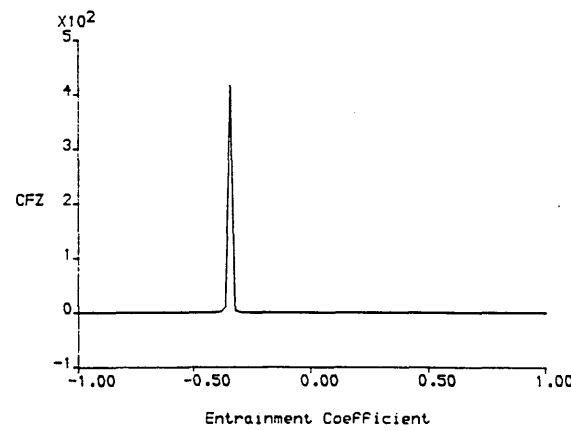
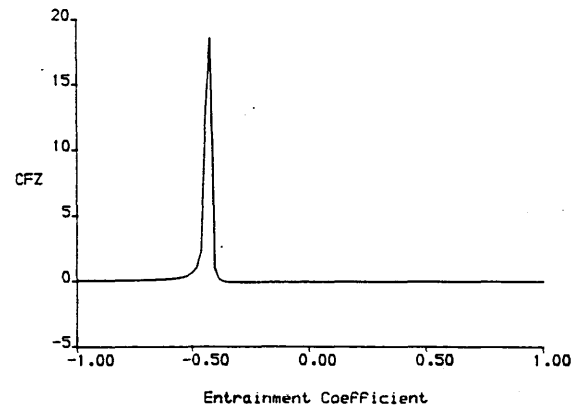
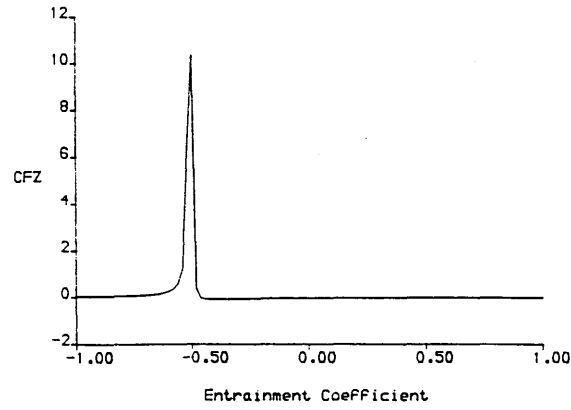
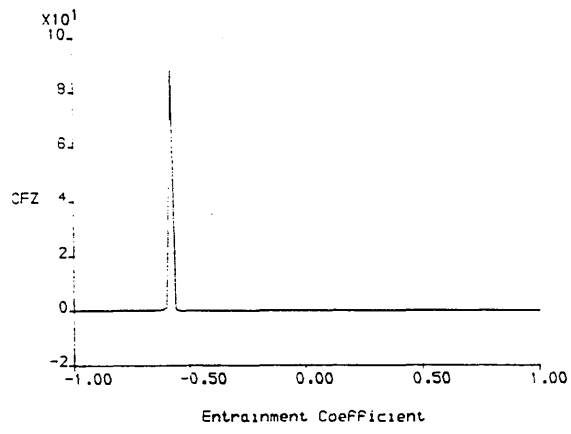


Fig.3.28 Variation of C_{FZ} with b for Four Cases of Fig.3.25

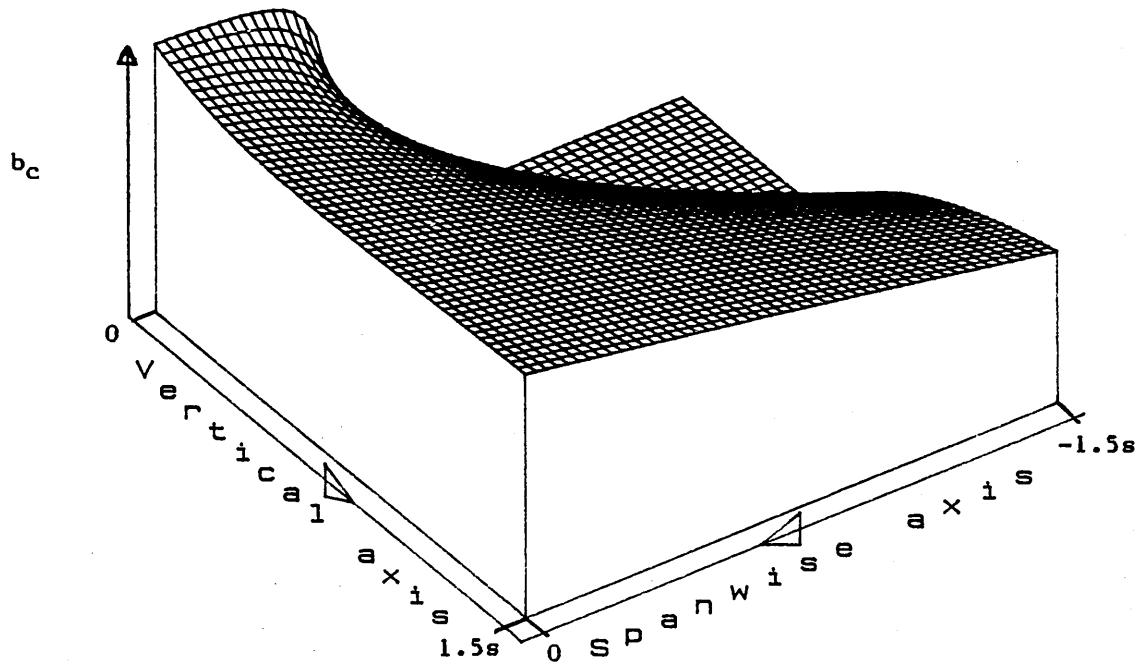
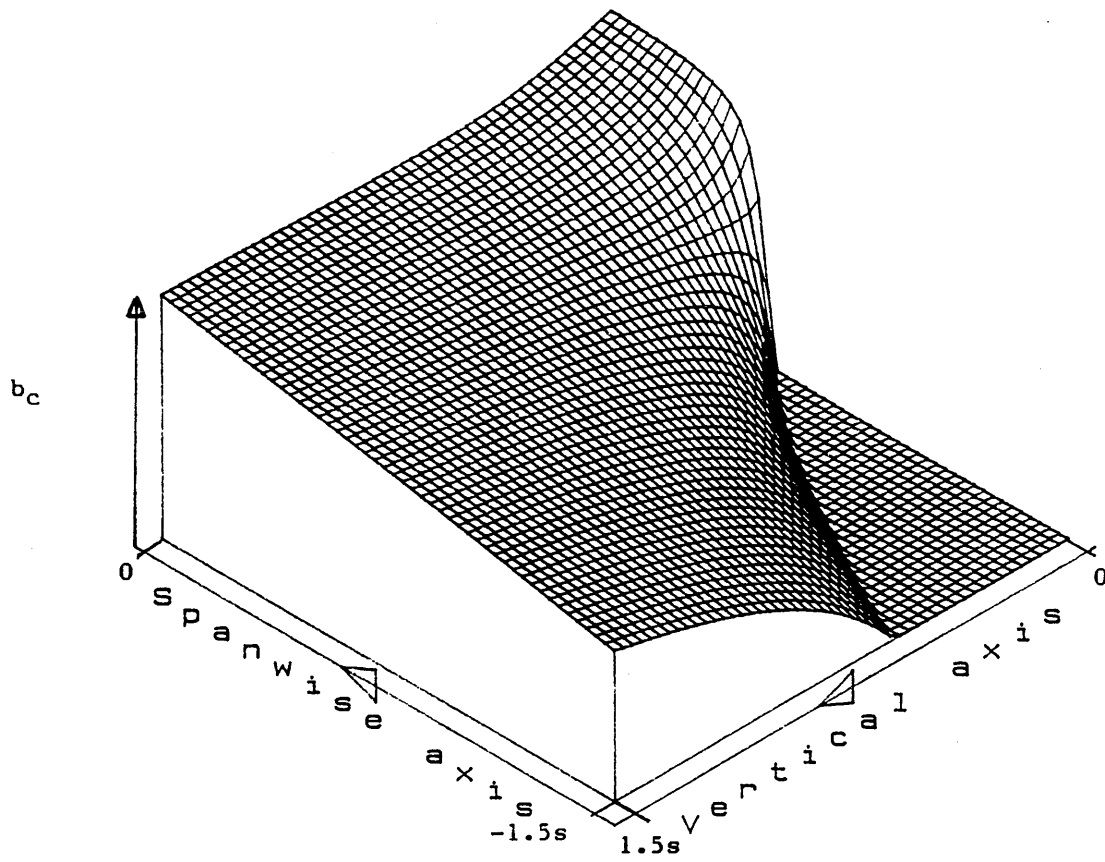


Fig.3.29 Two Views of Three-Dimensional Plot of b_c - vs - y_A and z_A

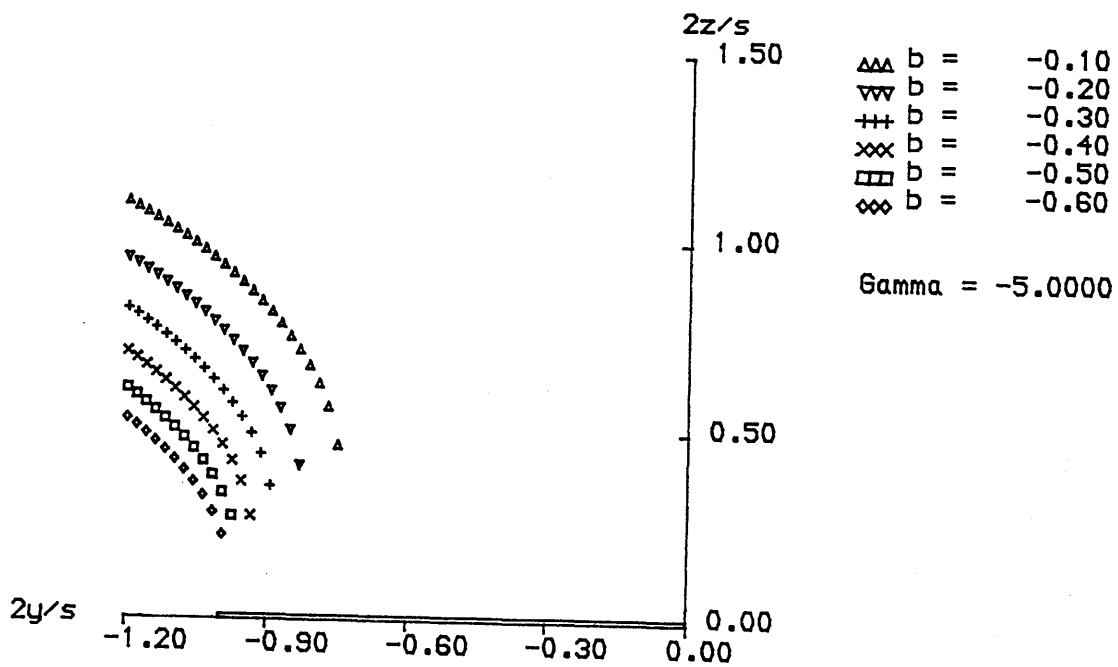
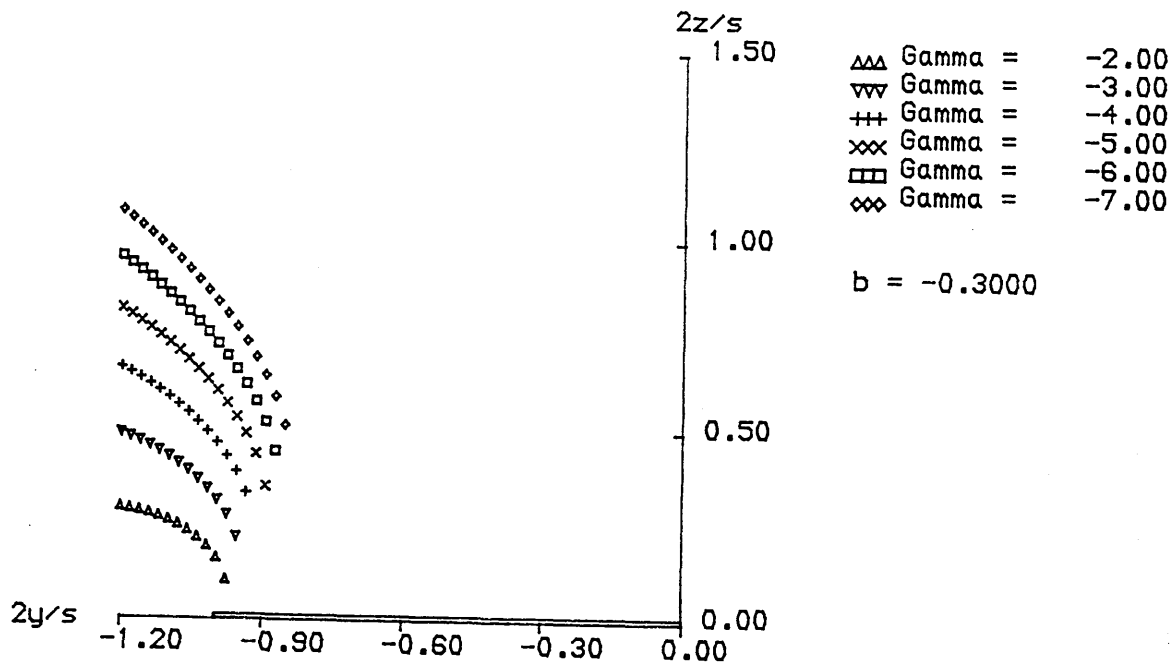


Fig.3.30 Typical Variations of Vortex-Sink Location with b and Γ

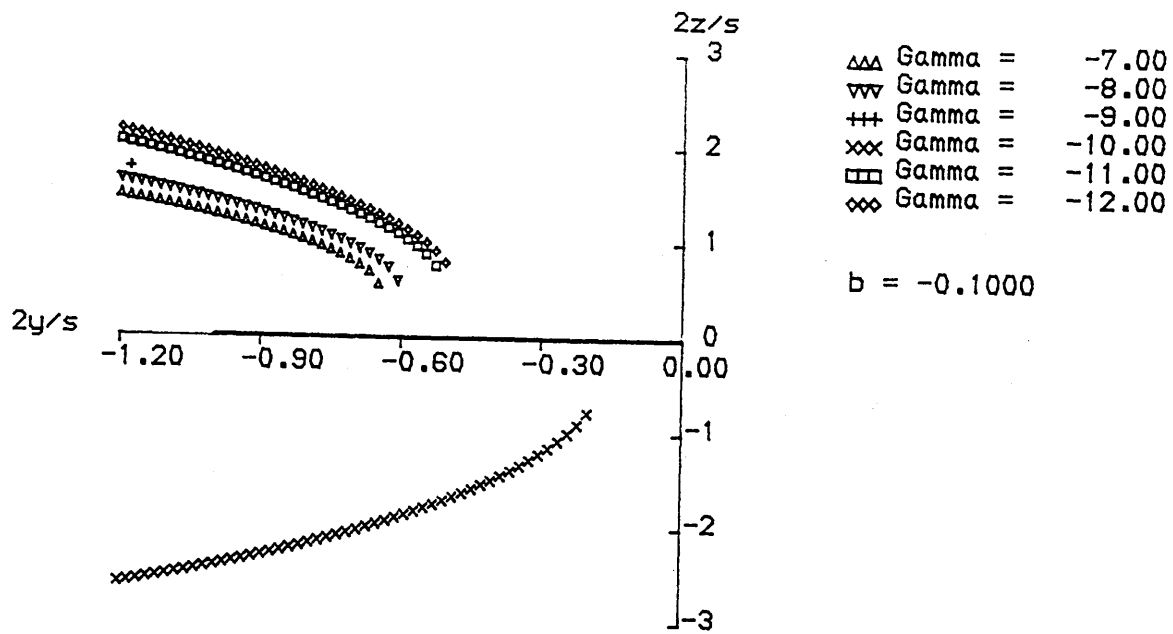


Fig.3.31 Discontinuous Solution Behaviour

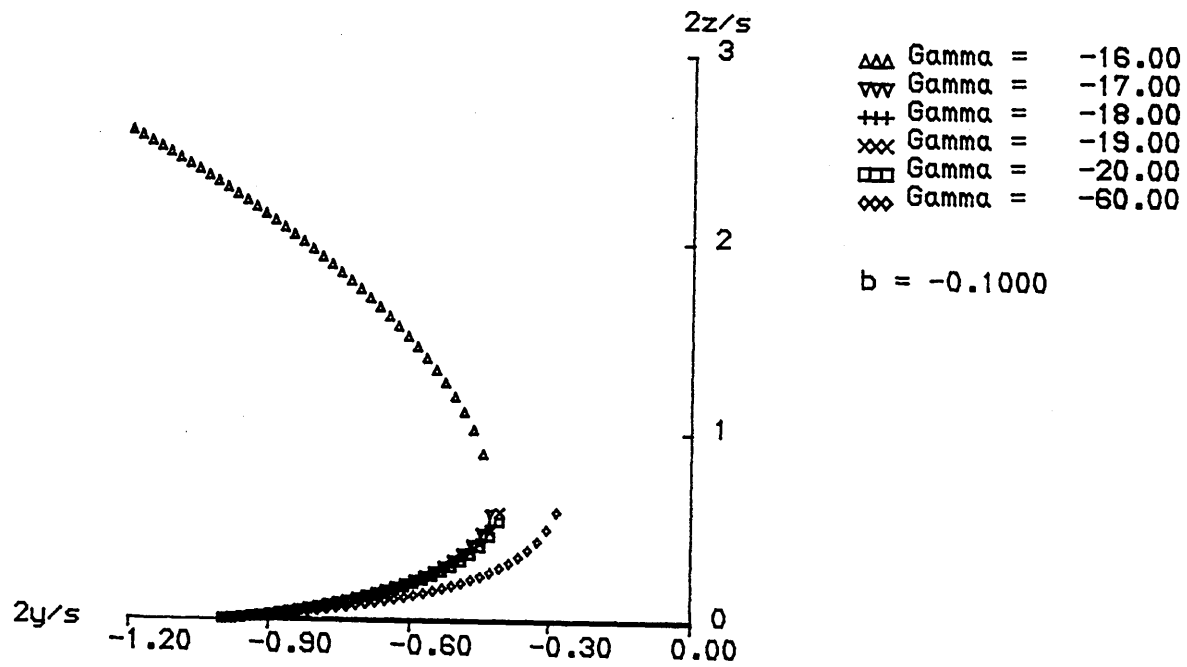


Fig.3.32 Reversal of Solution Trend

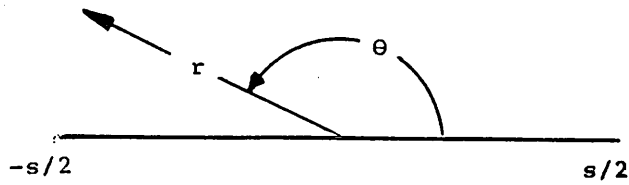


Fig.4.1 Polar Coordinate Geometry for Z-Plane

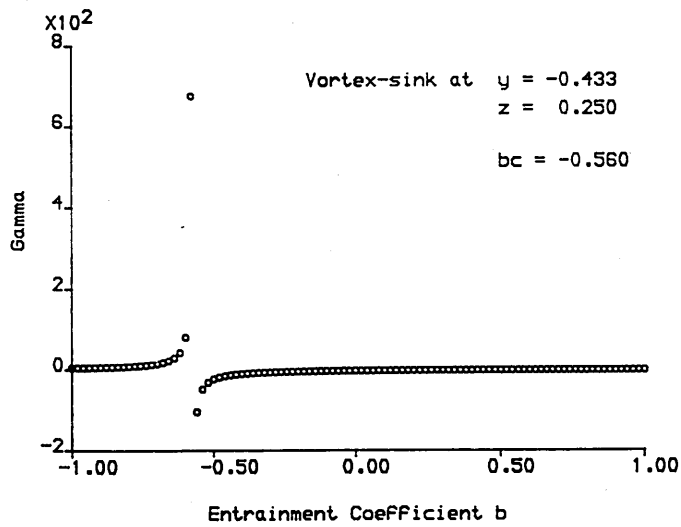


Fig.4.2(a) Variation of Γ with b for $r_A = 0.5$, $\theta_A = 150^\circ$

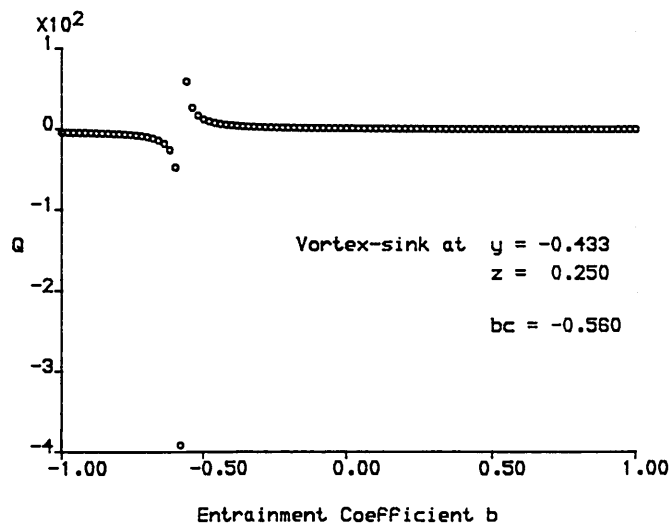


Fig.4.2(b) Variation of Q with b for $r_A = 0.5$, $\theta_A = 150^\circ$

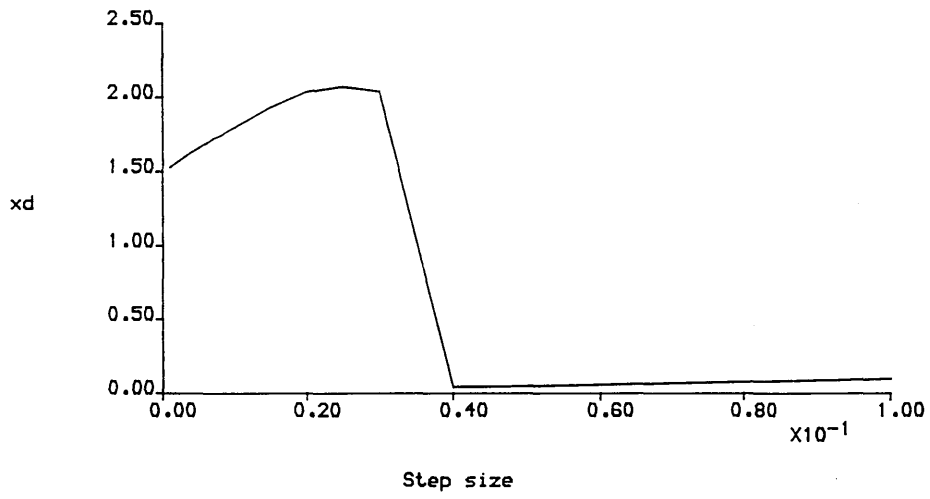


Fig.4.3 Variation of Calculation Failure Location with Step-Size

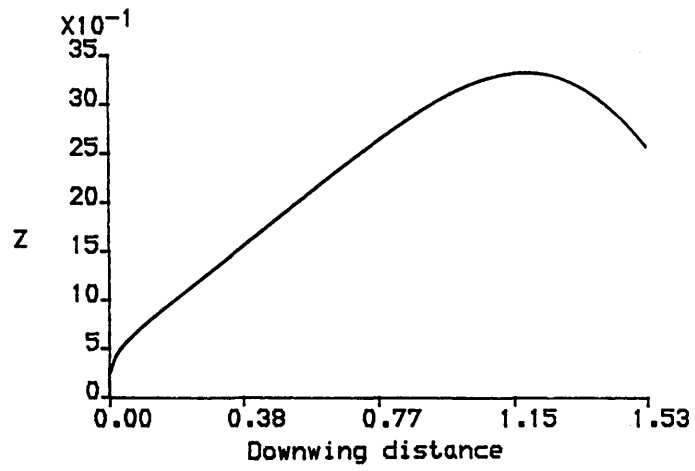


Fig.4.4(a)

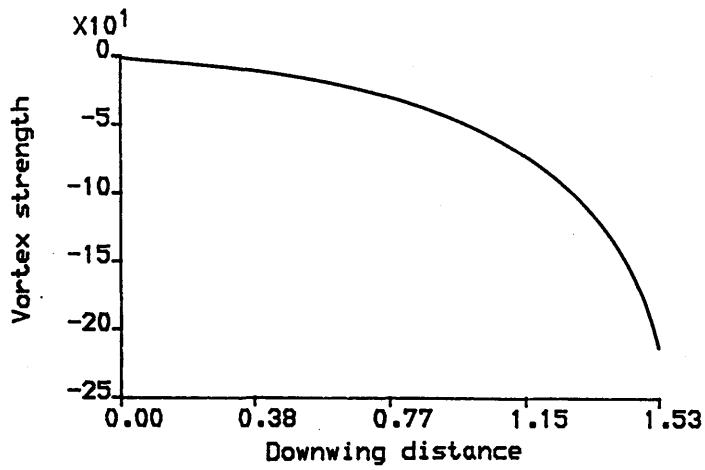


Fig.4.4(b)

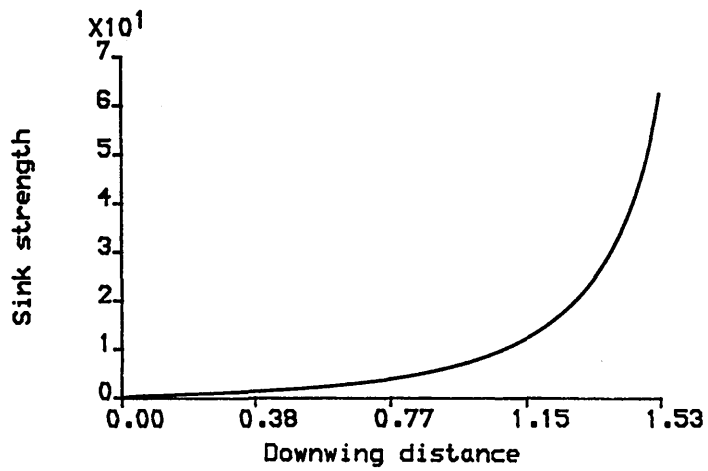


Fig.4.4(c)

Figs.4.4 (a-c) Solution Behaviour for $U = 1.0 \text{ m/s}$ $s_i = 1.0 \text{ m}$
 $\alpha = 20^\circ$ $\Lambda = 70^\circ$ $b_i = -0.05$ $C_1 = 1.0$

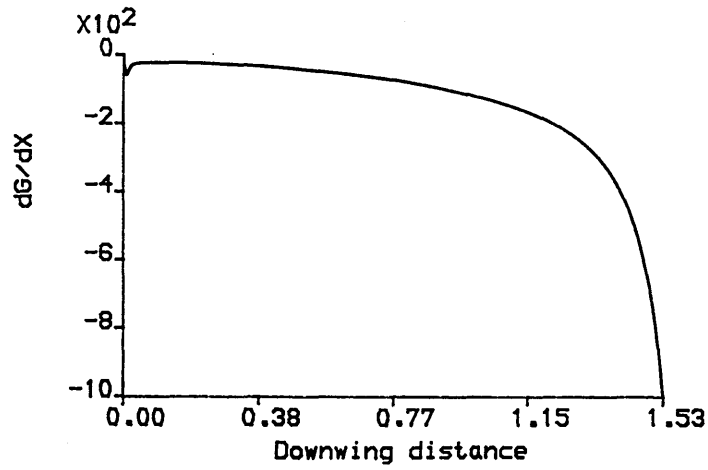


Fig.4.4(d)

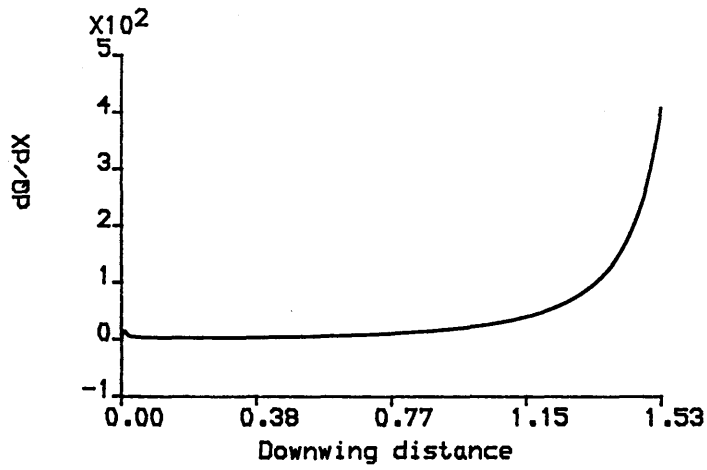


Fig.4.4(e)

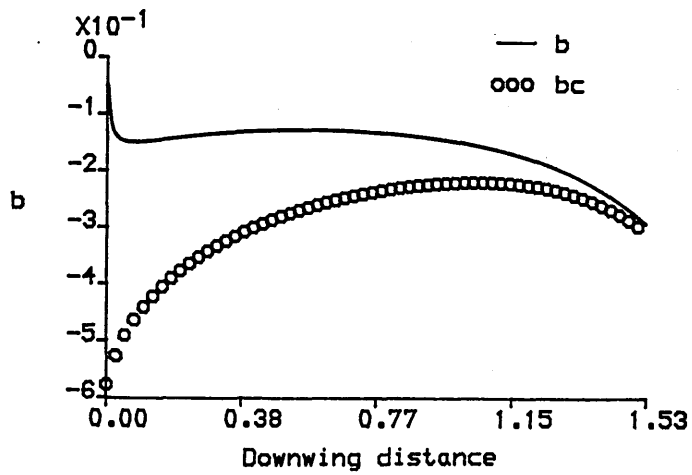


Fig.4.4(f)

Figs.4.4(d-f) Solution Behaviour for $U = 1.0 \text{ m/s}$ $s_i = 1.0 \text{ m}$
 $\alpha = 20^\circ$ $\Lambda = 70^\circ$ $b_i = -0.05$ $C_1 = 1.0$

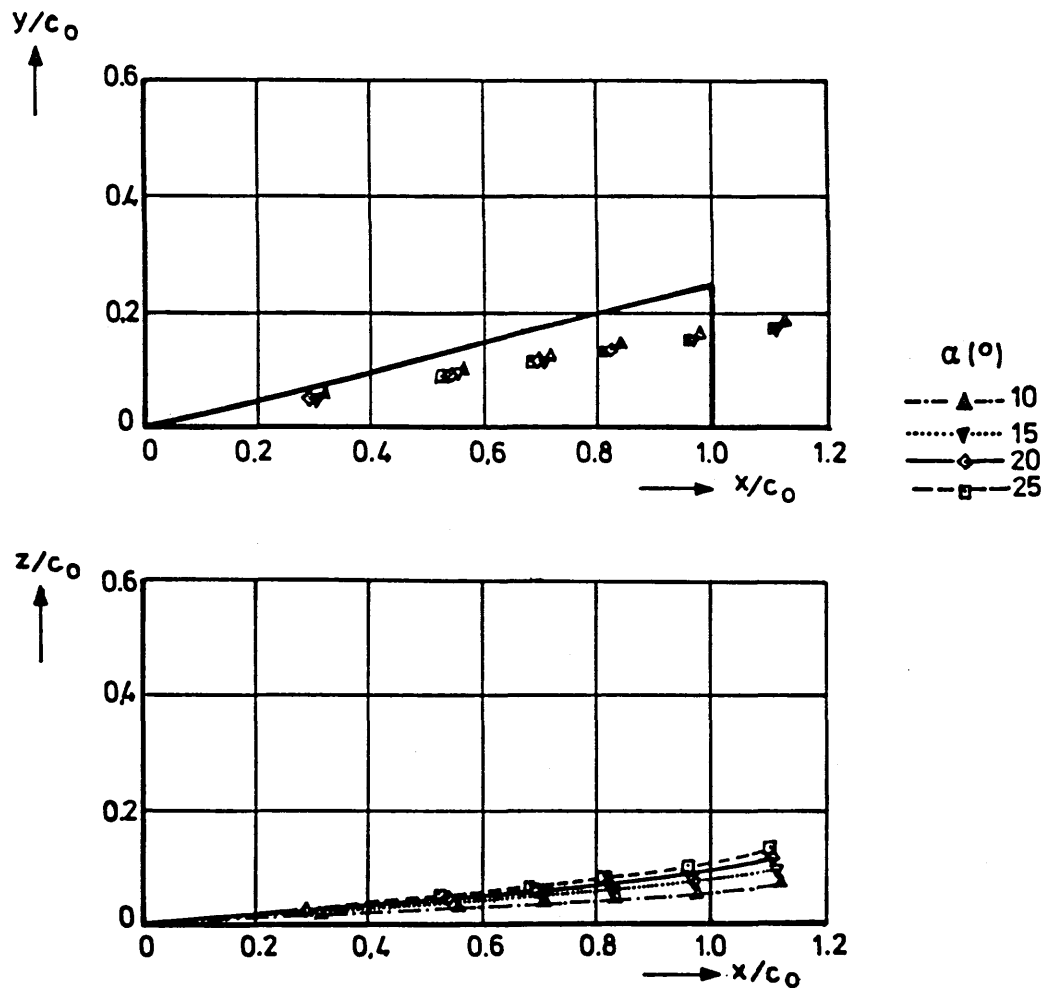


Fig.4.5 Experimental Variation of Vortex Core Location with α^5

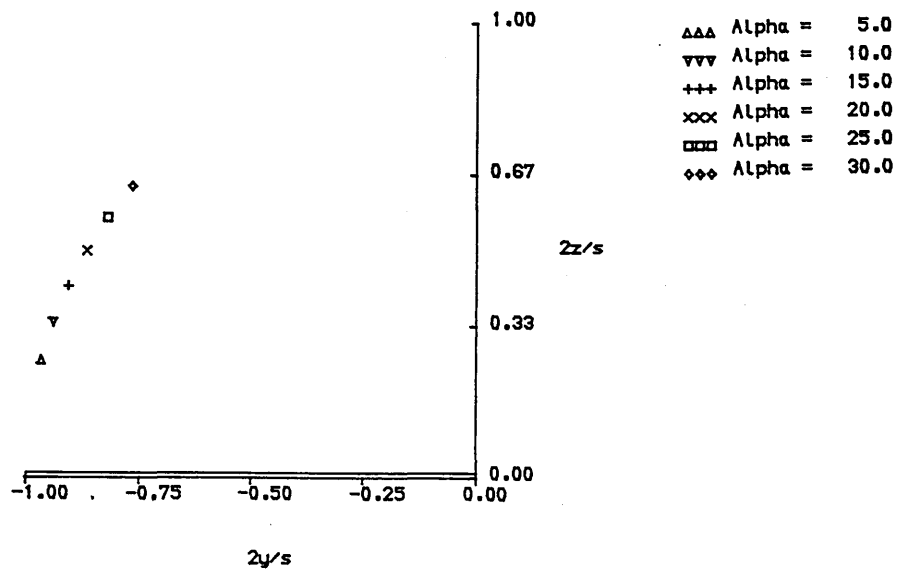


Fig.4.6 MODEL3D Variation of Initial Vortex-Sink Location with α

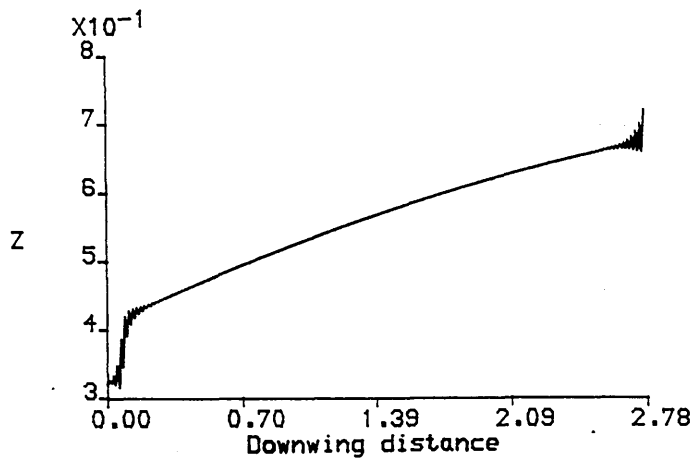


Fig.4.7(a)

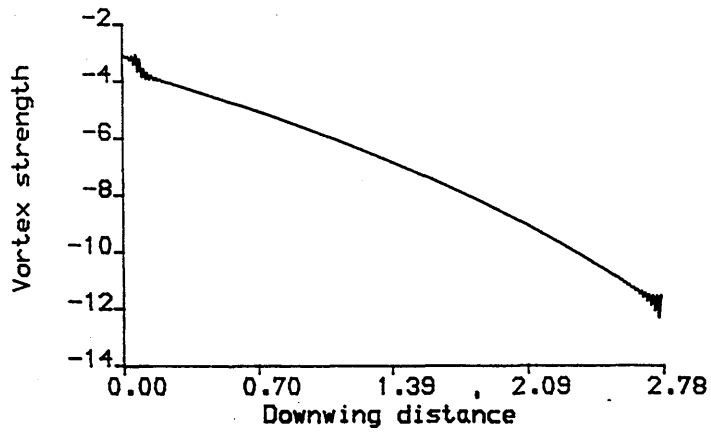


Fig.4.7(b)

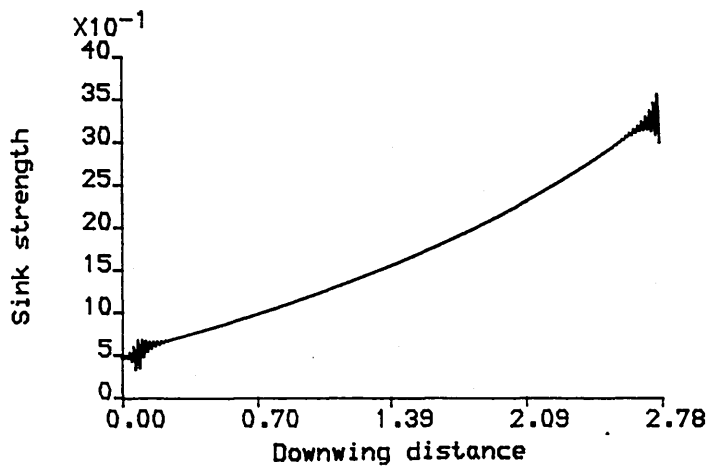


Fig.4.7(c)

Figs.4.7(a-c) Oscillatory Solution Behaviour for $U = 1.0$ m/s $s_1 = 1.0$ m
 $\alpha = 30^\circ$ $\Lambda = 80^\circ$ $b_1 = -0.15$ $C_1 = 1.4$

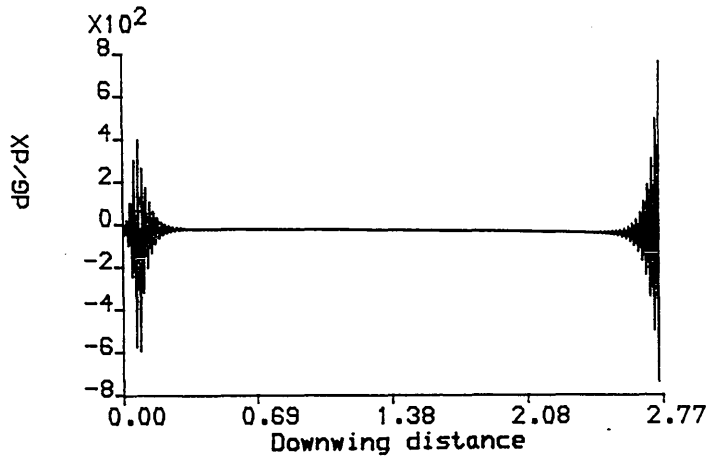


Fig.4.7(d)

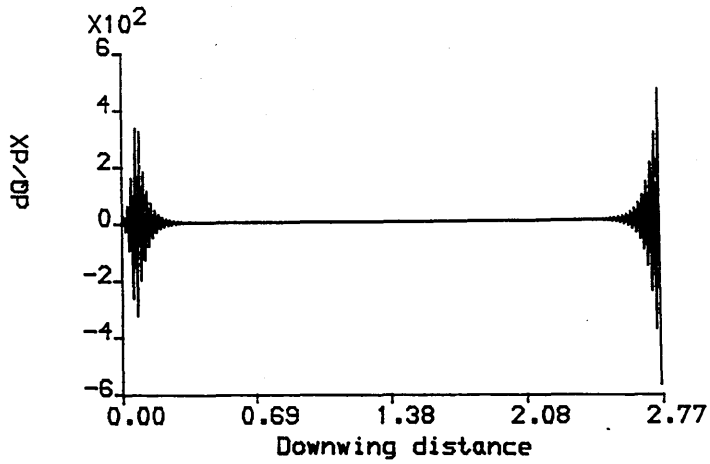


Fig.4.7(e)

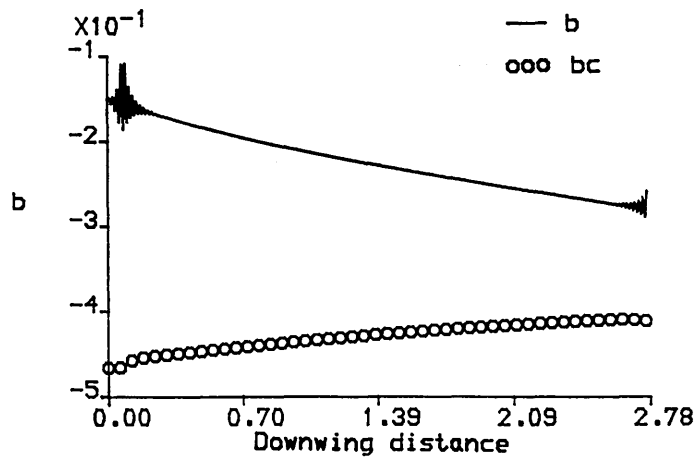


Fig.4.7(f)

Figs.4.7(d-f) Oscillatory Solution Behaviour for $U = 1.0$ m/s $s_i = 1.0$ m
 $\alpha = 30^\circ$ $\Lambda = 80^\circ$ $b_1 = -0.15$ $C_1 = 1.4$

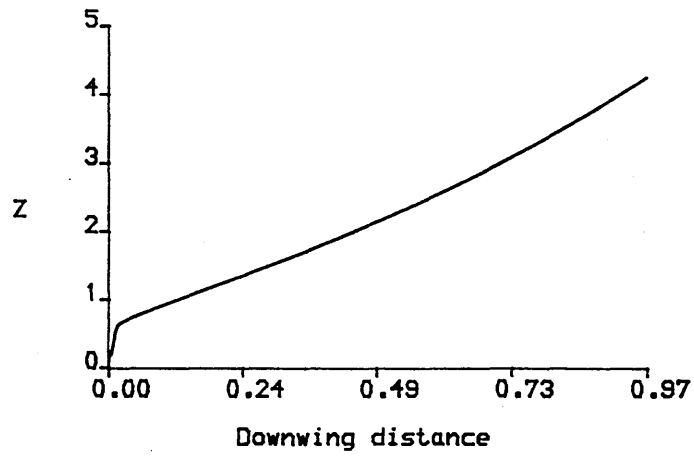


Fig.4.8(a)

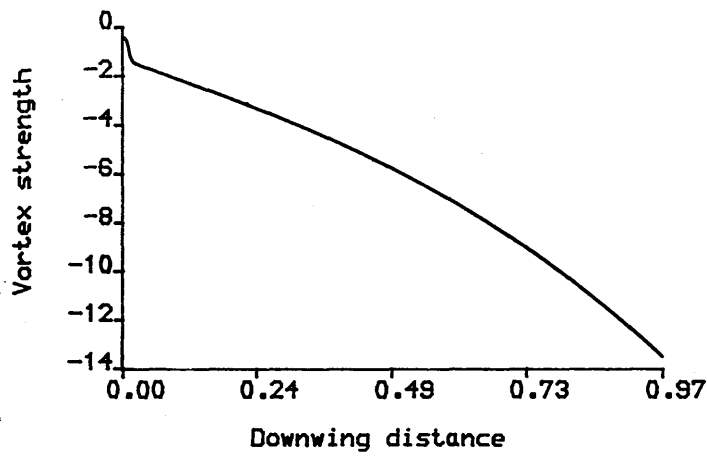


Fig.4.8(b)

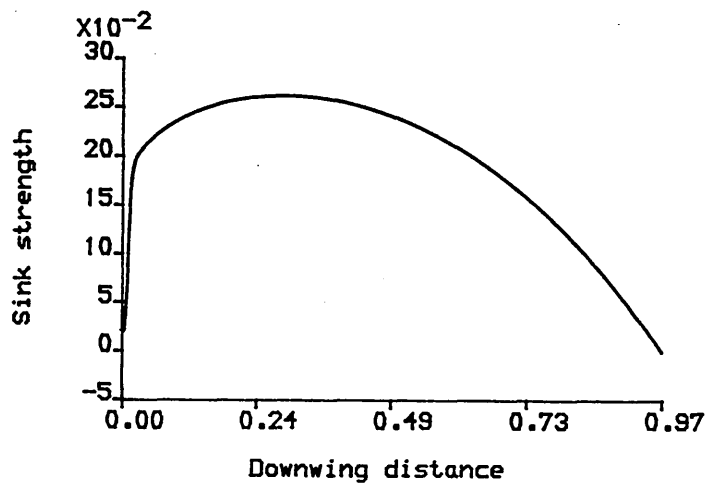


Fig.4.8(c)

Figs.4.8(a-c) Solution Type 1 for $U = 1.0 \text{ m/s}$ $s_i = 1.0 \text{ m}$
 $\alpha = 10^\circ$ $\Lambda = 70^\circ$ $b_i = -0.05$ $C_1 = 1.0$

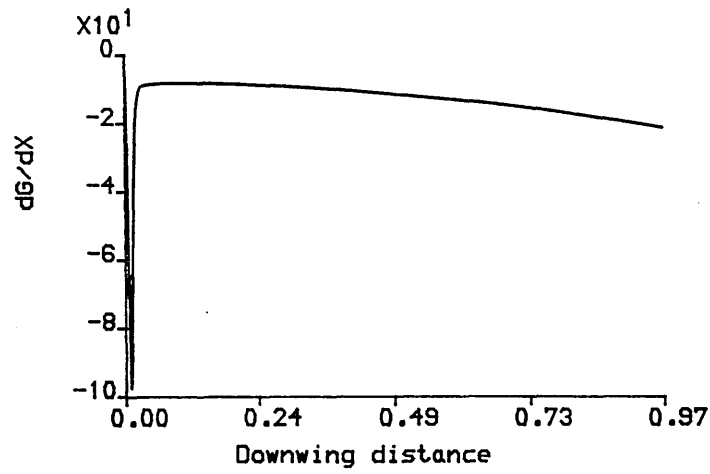


Fig.4.8(d)

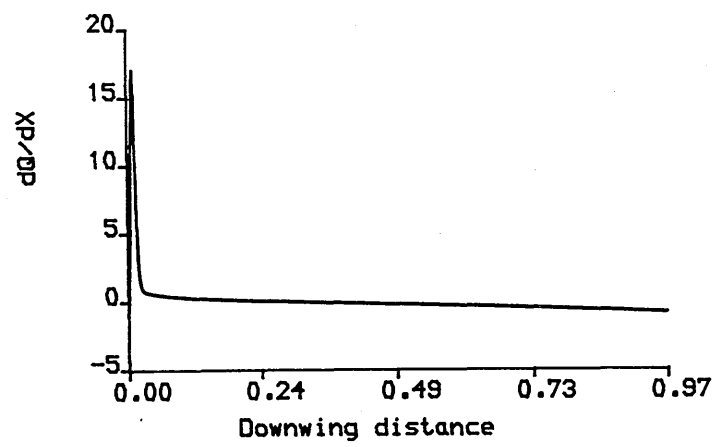


Fig.4.8(e)

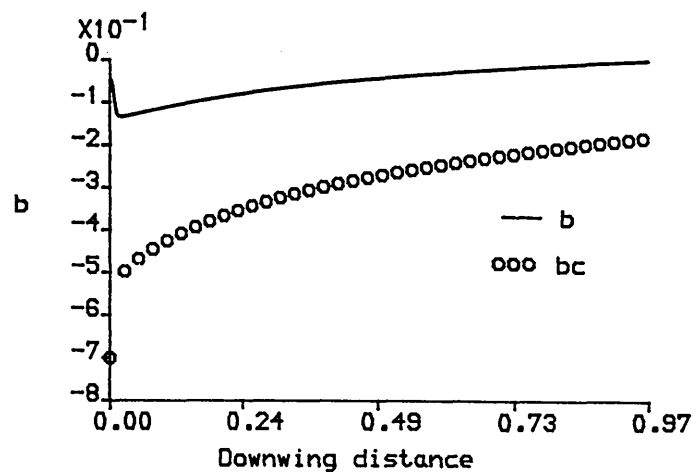


Fig.4.8(f)

Figs.4.8(d-f) Solution Type 1 for $U = 1.0 \text{ m/s}$ $s_i = 1.0 \text{ m}$
 $\alpha = 10^\circ$ $\Lambda = 70^\circ$ $b_i = -0.05$ $C_i = 1.0$

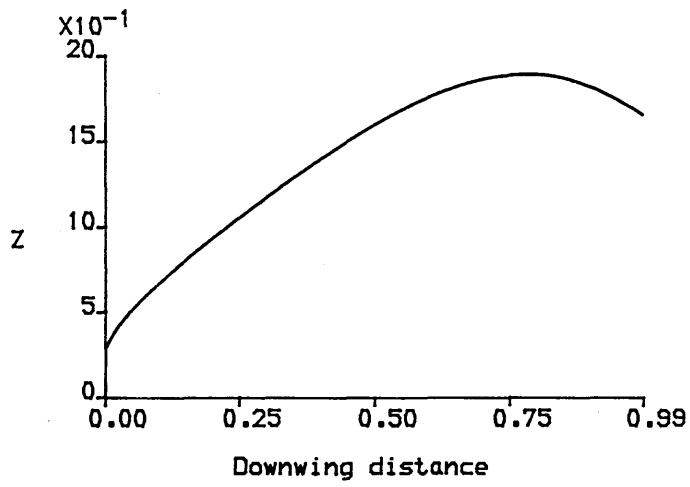


Fig.4.9(a)

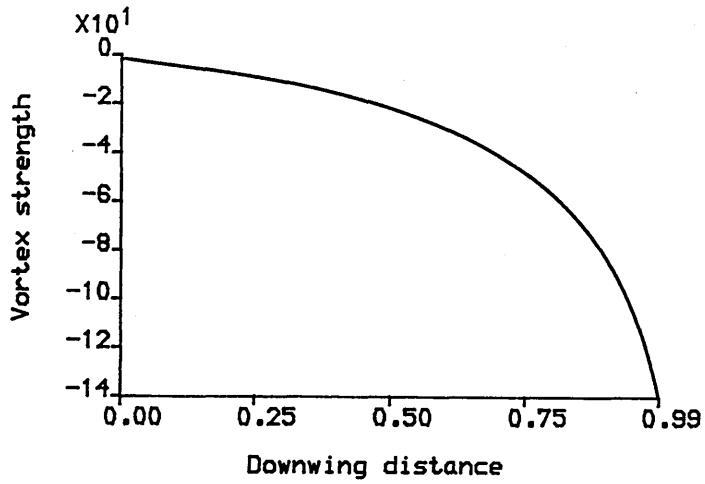


Fig.4.9(b)

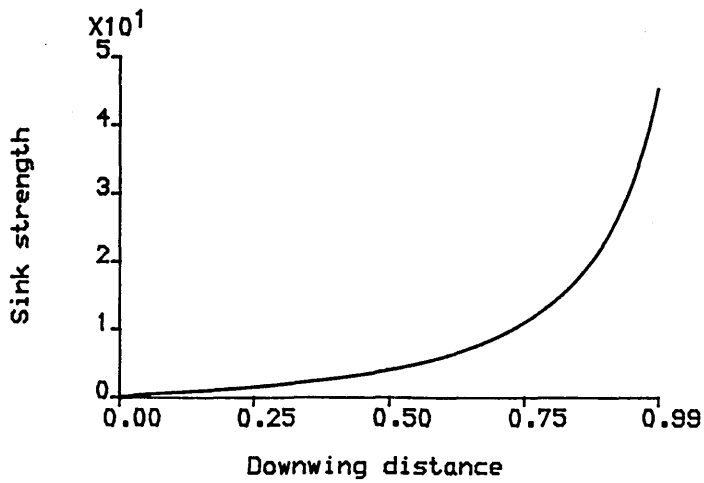


Fig.4.9(c)

Figs.4.9(a-c) Solution Type 2 for $U = 1.0 \text{ m/s}$ $s_i = 1.0 \text{ m}$
 $\alpha = 25^\circ$ $\Lambda = 70^\circ$ $b_i = -0.05$ $C_1 = 1.0$

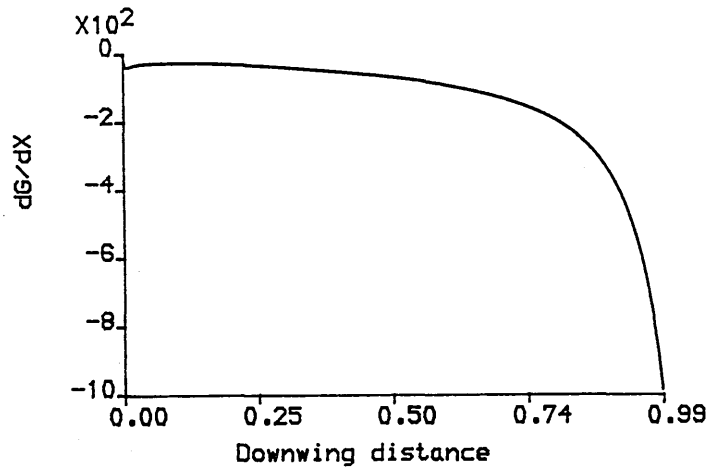


Fig. 4.9(d)

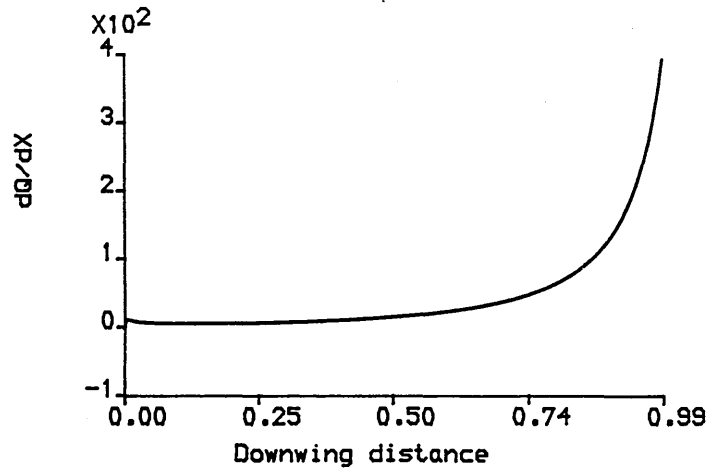


Fig. 4.9(e)

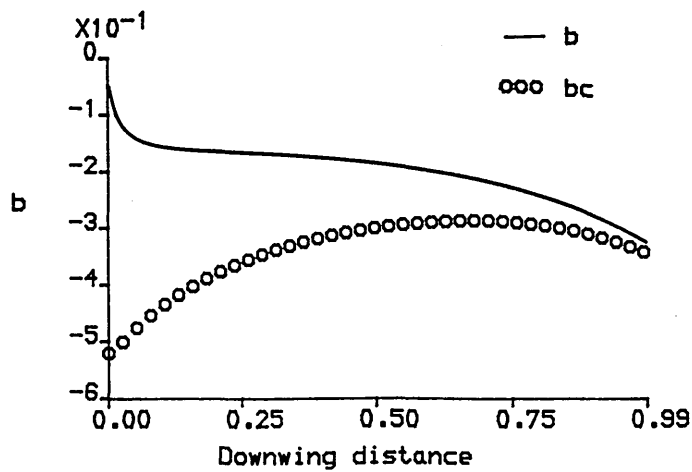


Fig. 4.9(f)

Figs. 4.9(d-f) Solution Type 2 for $U = 1.0 \text{ m/s}$ $s_i = 1.0 \text{ m}$
 $\alpha = 25^\circ$ $\lambda = 70^\circ$ $b_i = -0.05$ $C_l = 1.0$

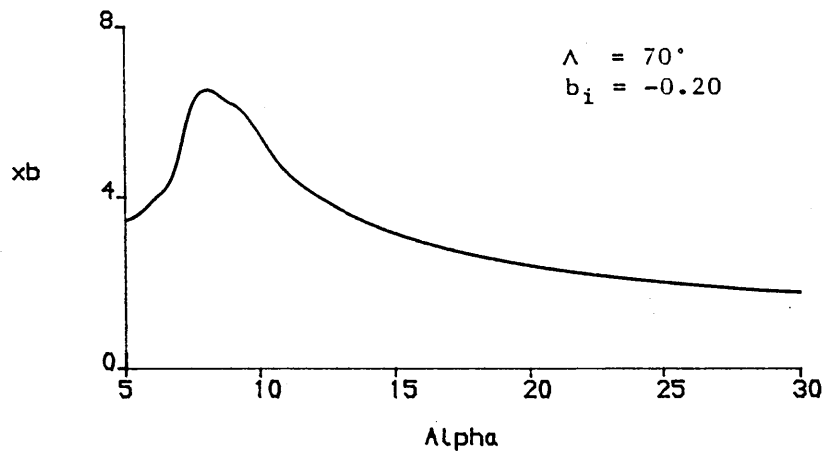


Fig.4.10(a)

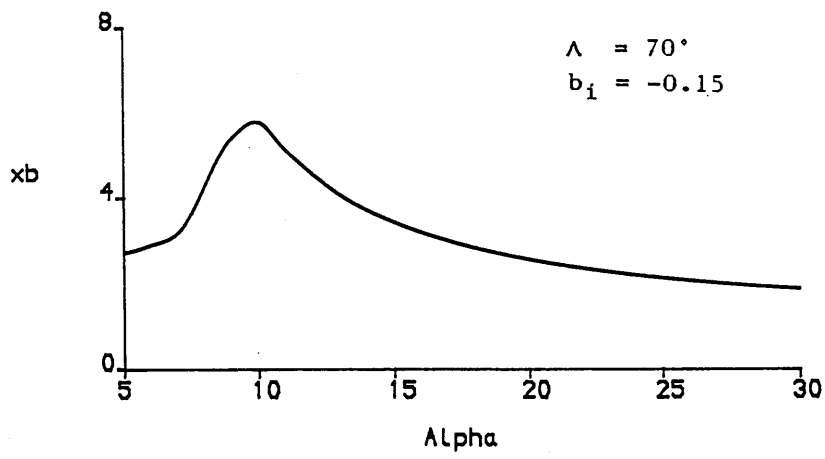


Fig.4.10(b)

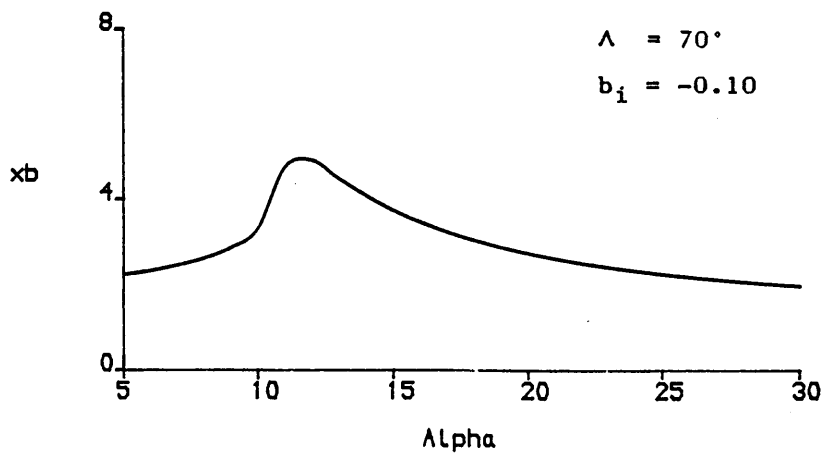


Fig.4.10(c)

Figs.4.10(a-c) Variation of x_b with α for Three Values of b_i

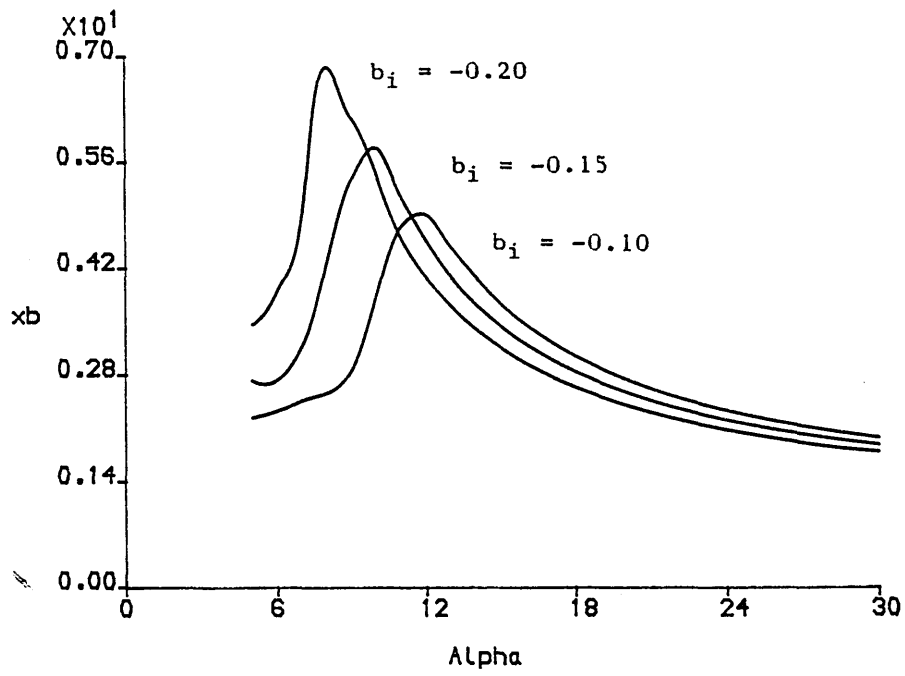


Fig.4.11 Superposition of figs.4.10(a-c)

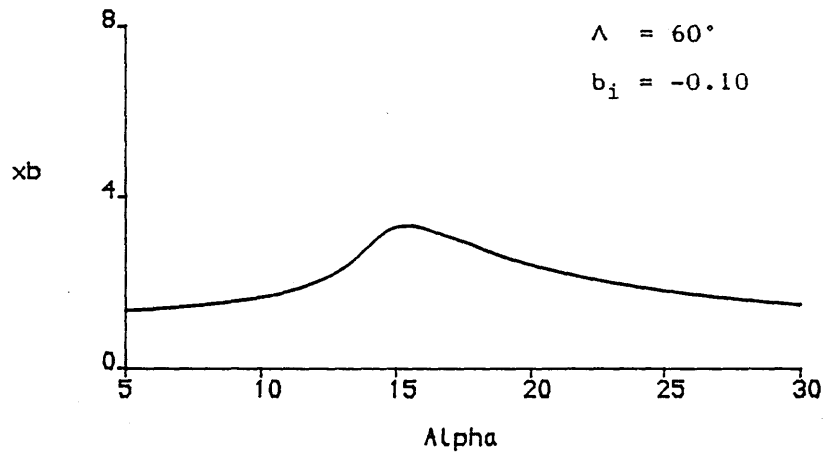


Fig.4.12(a)

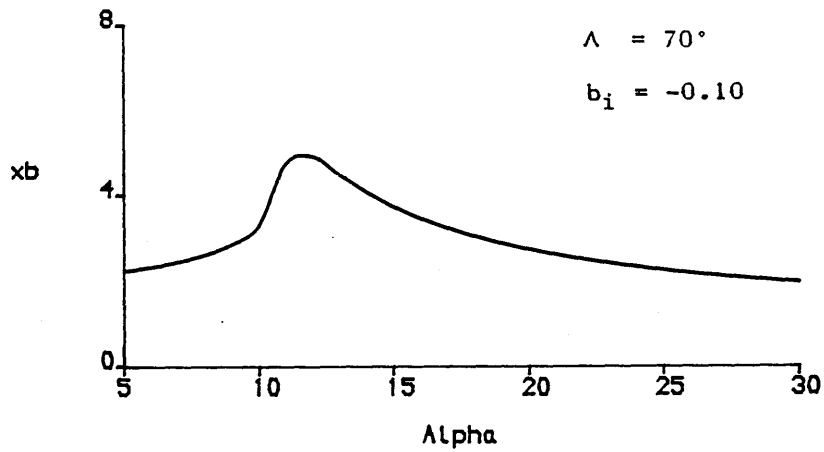


Fig.4.12(b)

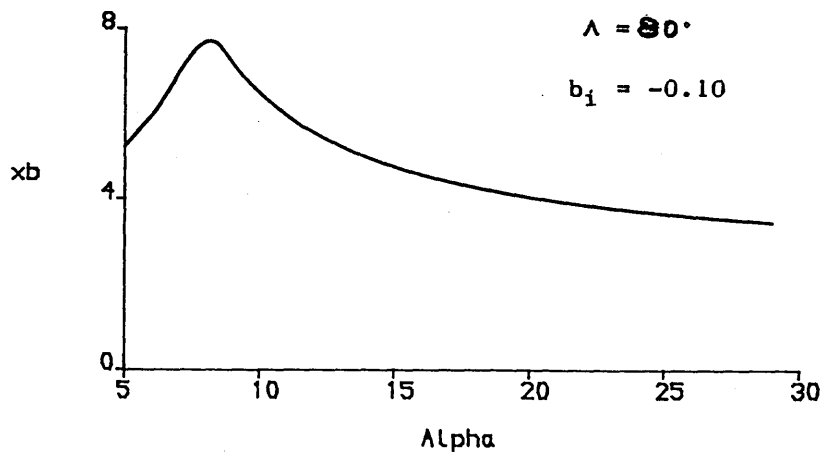


Fig.4.12(c)

Figs.4.12(a-c) Variation of x_b with α for Three Values of Λ

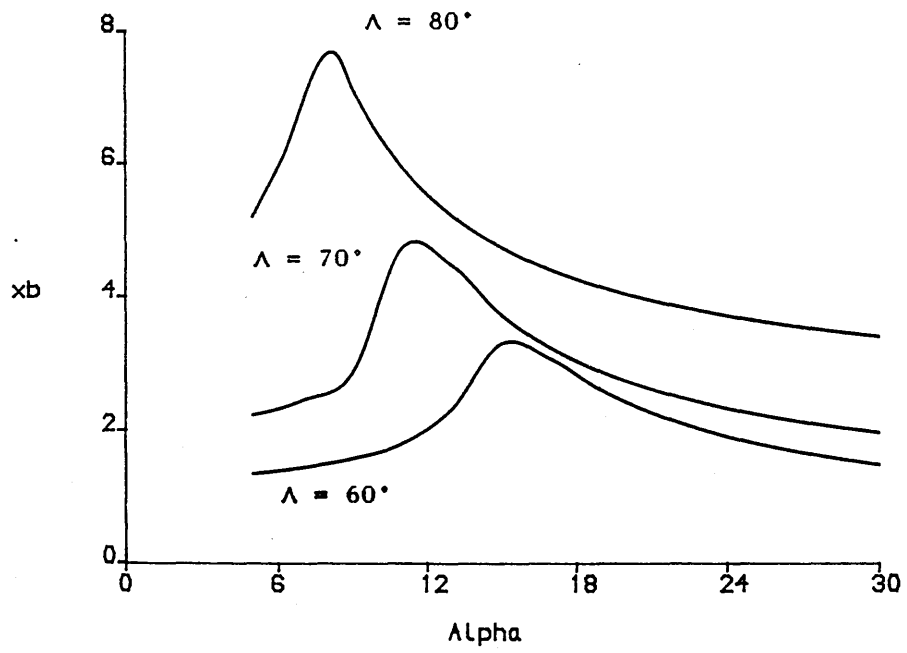


Fig.4.13 Superposition of figs.4.12(a-c)

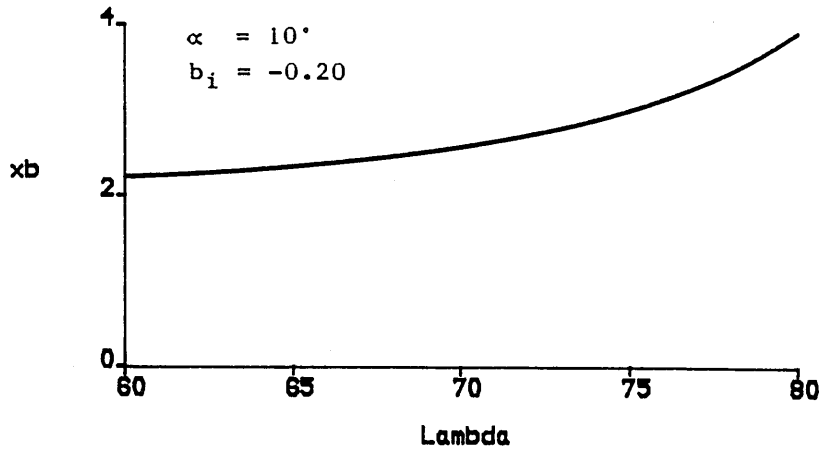


Fig.4.14(a)

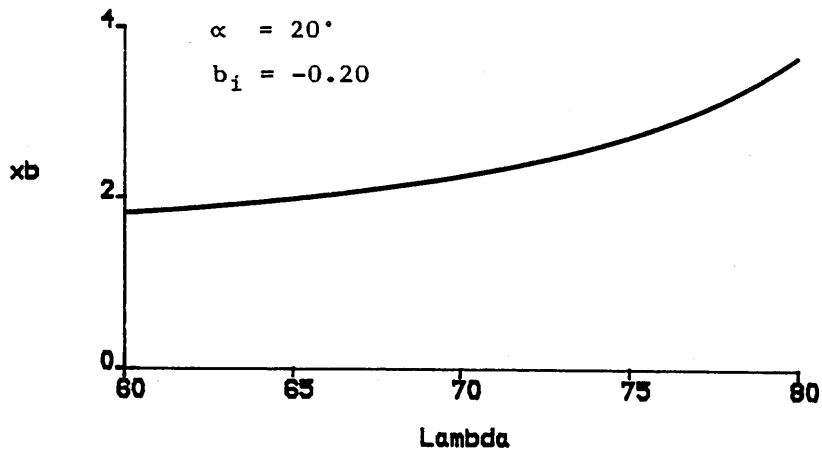


Fig.4.14(b)

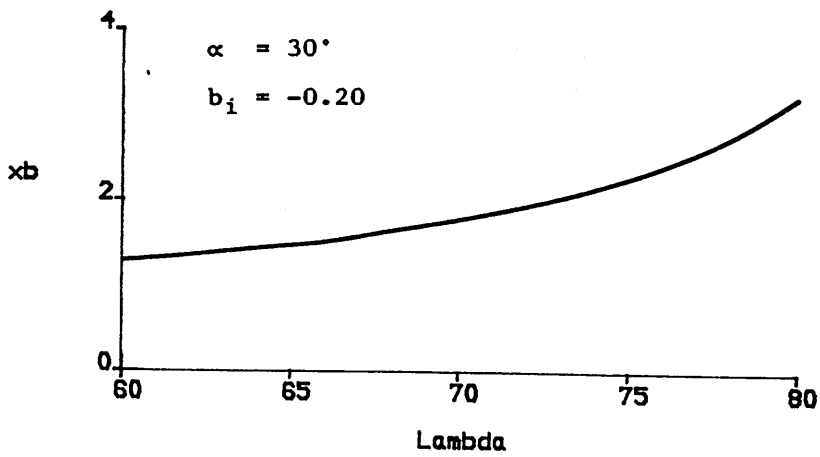


Fig.4.14(c)

Figs.4.14(a-c) Variation of x_b with Λ for Three Values of α

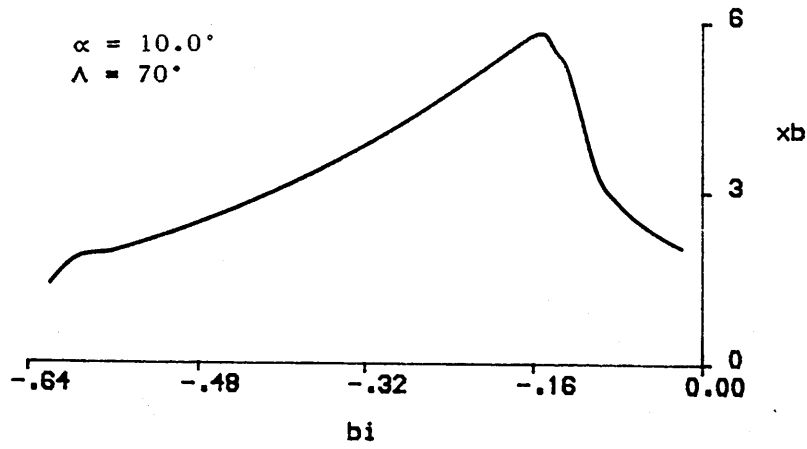


Fig.4.15(a)

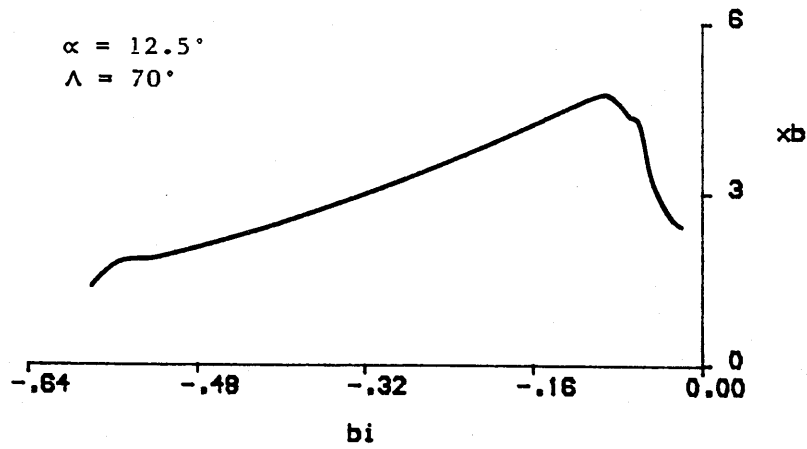


Fig.4.15(b)

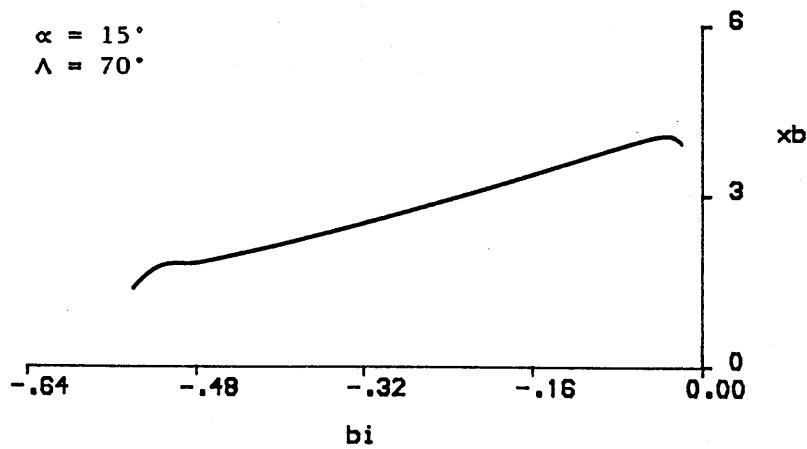


Fig.4.15(c)

Figs.4.15(a-c) Variation of x_b with b_i for Three Values of α

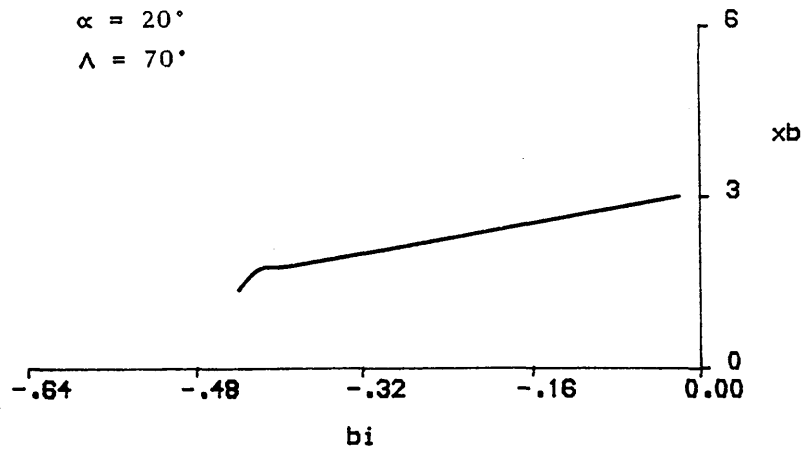


Fig.4.15(d)

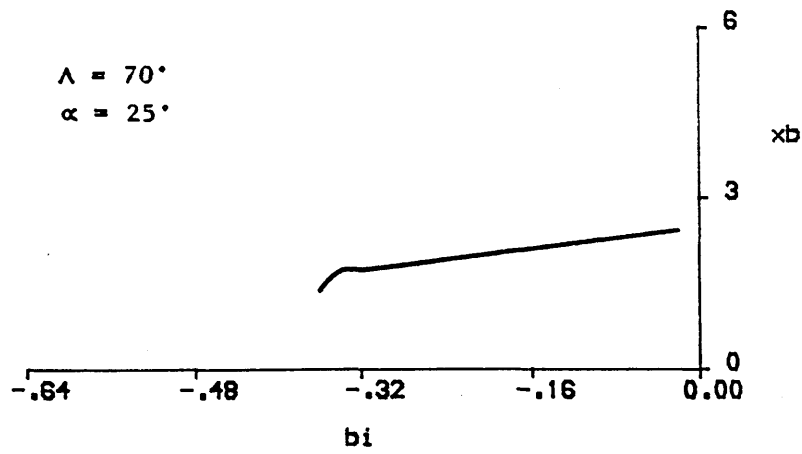


Fig.4.15(e)

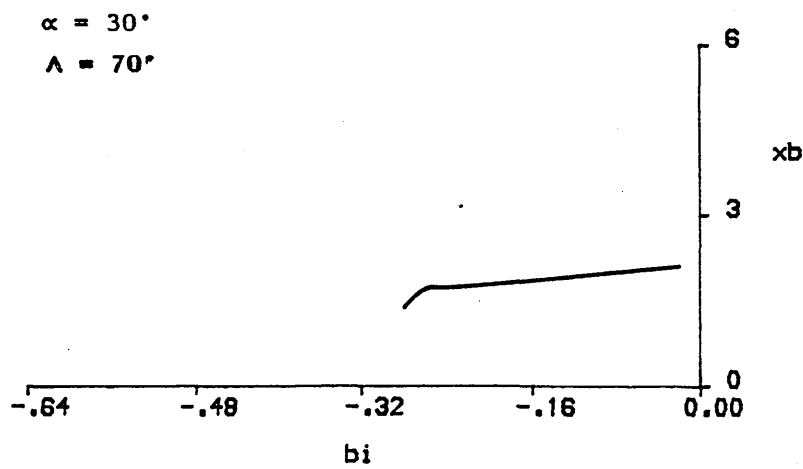


Fig.4.15(f)

Figs.4.15(d-f) Variation of x_b with b_i for Three Values of α

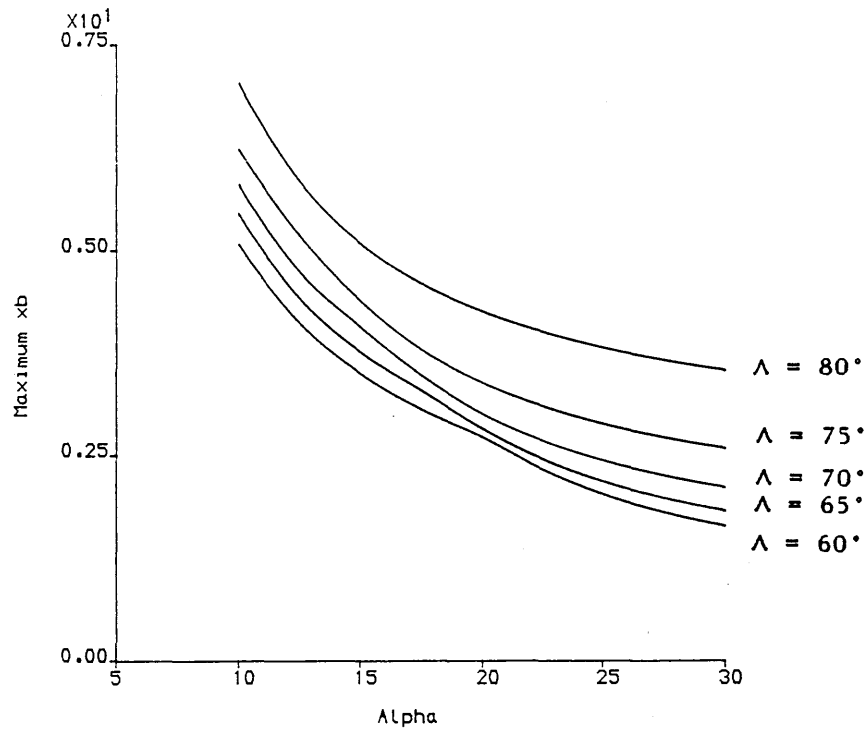


Fig.4.16 Maximum Values of x_b for Five Values of Λ

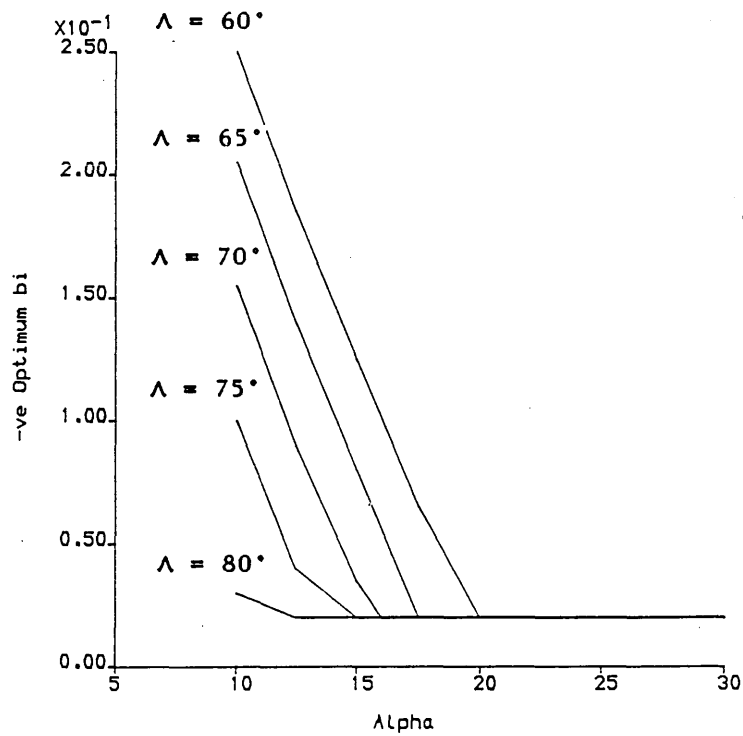


Fig.4.17 Required Values of b_i to Maximise x_b

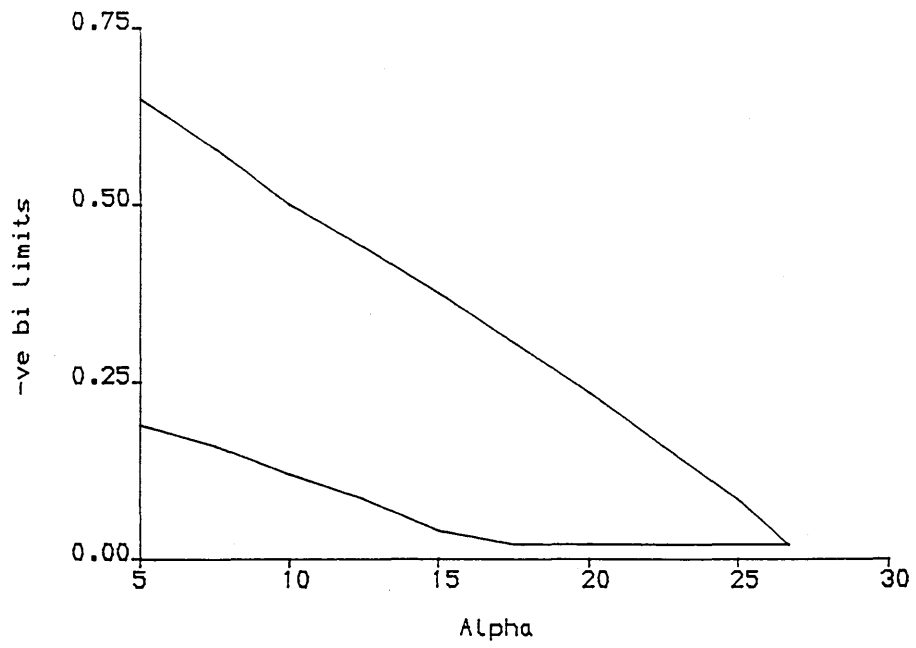


Fig.5.1 b_i - vs - α Envelope for $\Lambda = 60^\circ$

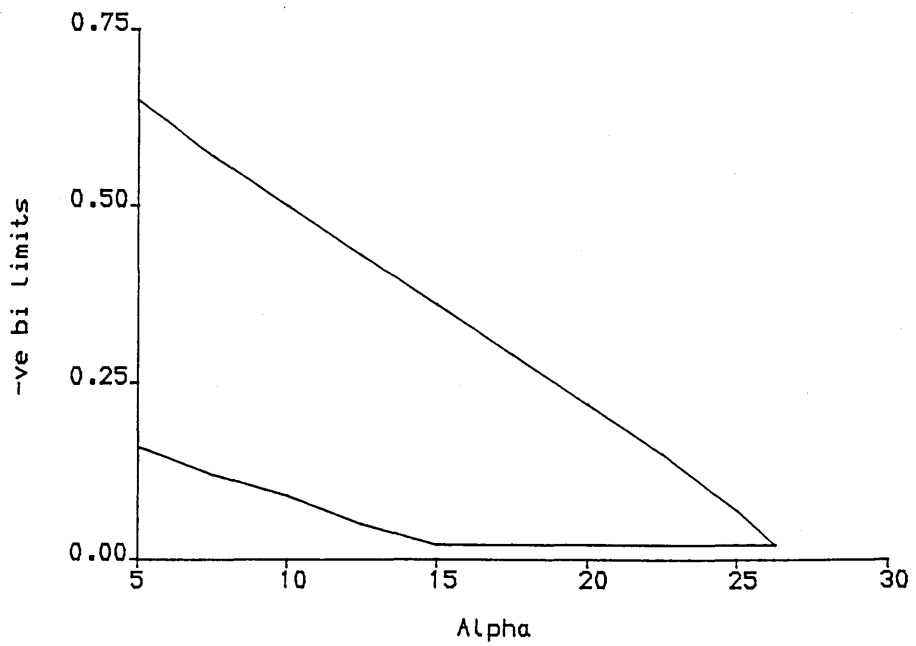


Fig.5.2 b_i - vs - α Envelope for $\Lambda = 65^\circ$

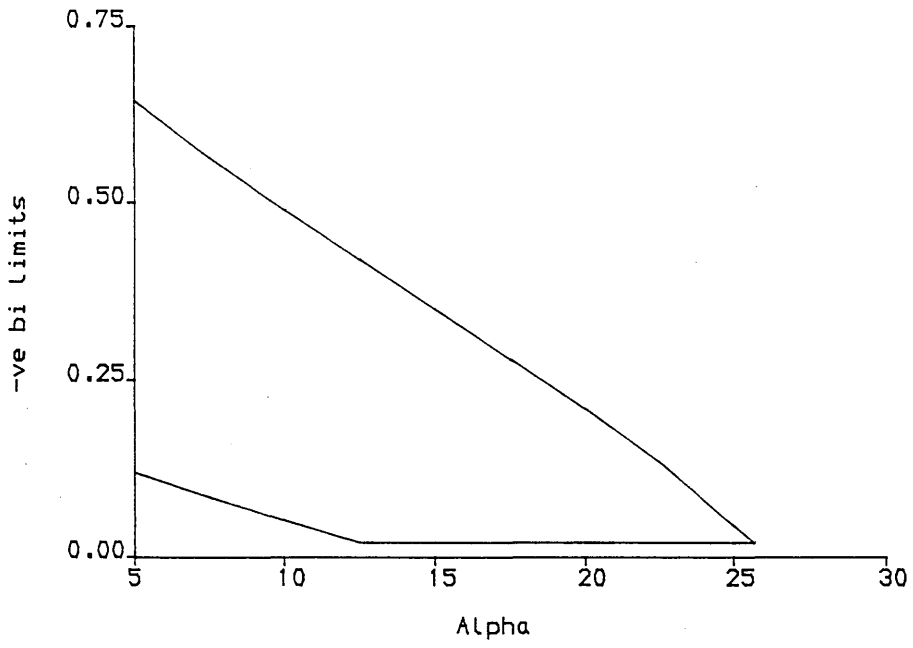


Fig.5.3 b_i - vs - α Envelope for $\Lambda = 70^\circ$

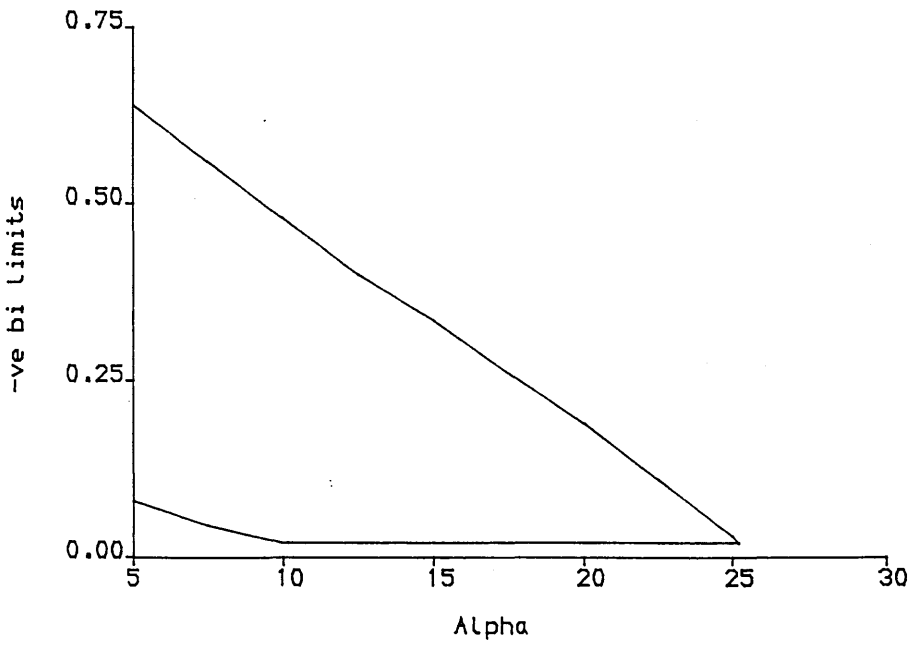


Fig.5.4 b_i - vs - α Envelope for $\Lambda = 75^\circ$

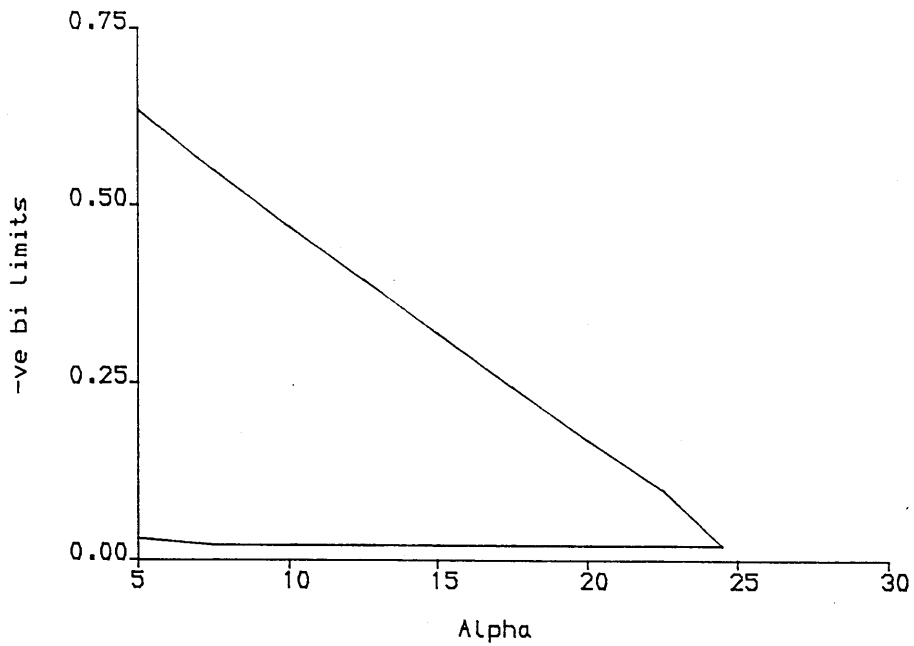


Fig.5.5 b_i - vs - α Envelope for $\Lambda = 80^\circ$

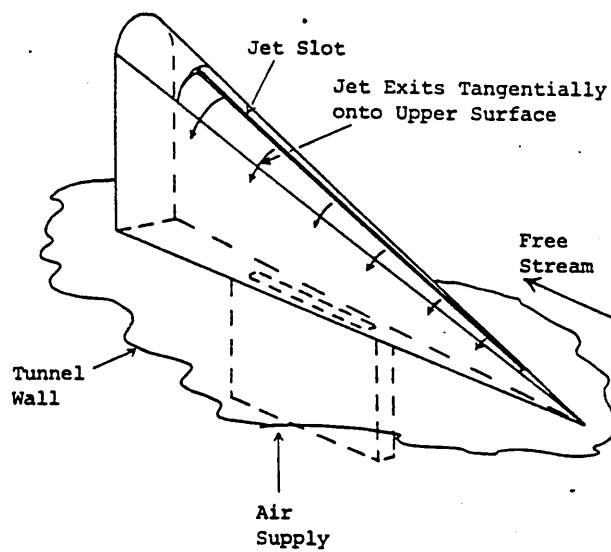


Fig.5.6 Tangential Leading Edge Blowing (TLEB) 72

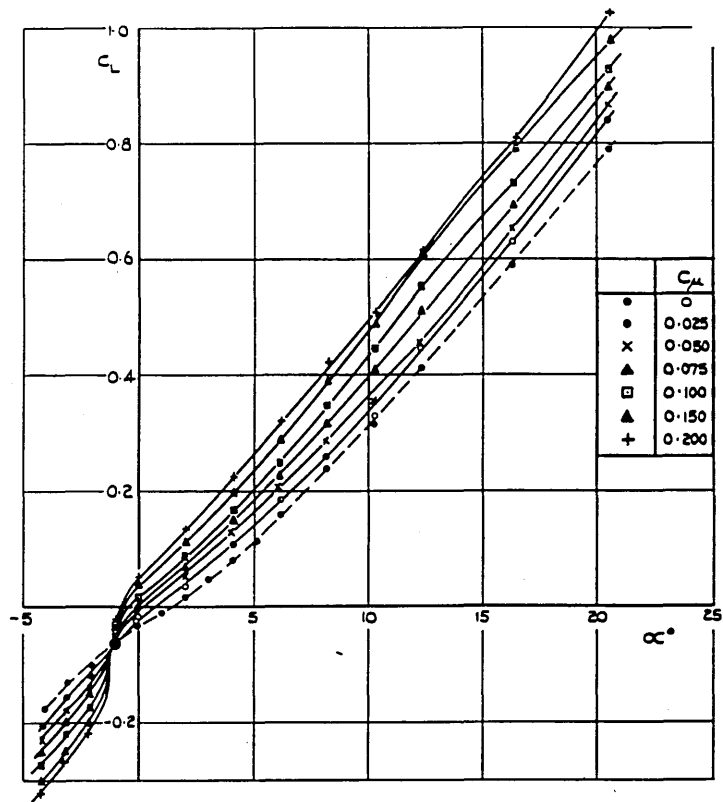


Fig.5.7 Enhancement of $C_L - \alpha$ Curve by Leading Edge Blowing ⁶⁹

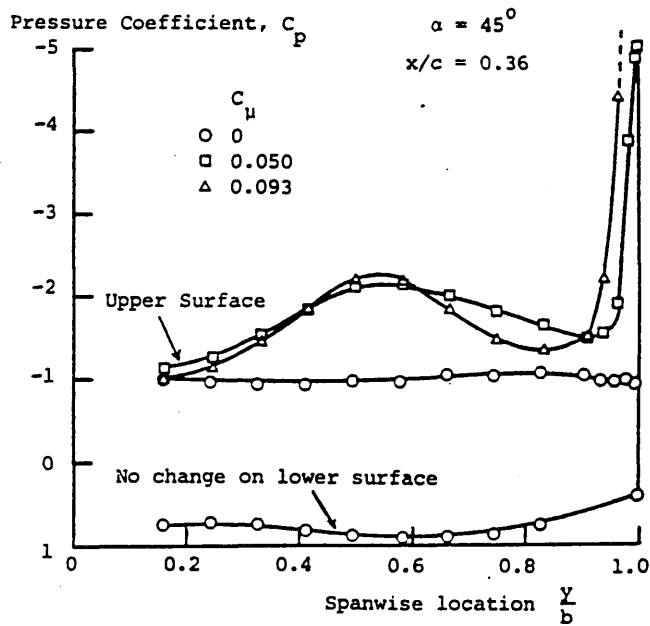


Fig.5.8 Re-establishment of Vortical Flow by TLEB⁷²

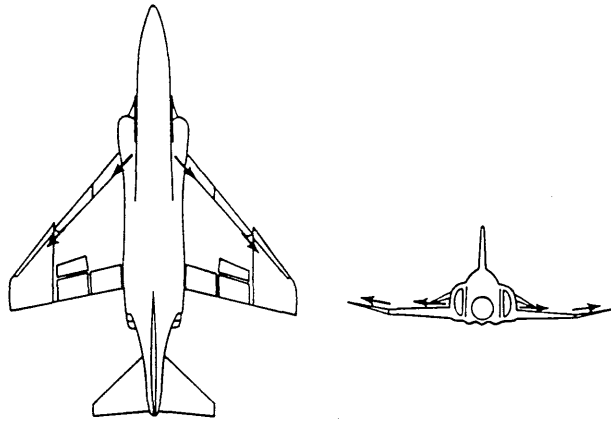


Fig. 5.9(a) General Spanwise Blowing Arrangement for F4-C ⁷⁴

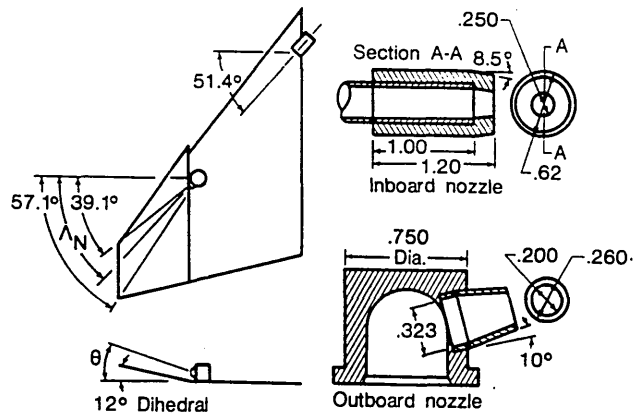


Fig. 5.9(b) Nozzle Detail ⁷⁴

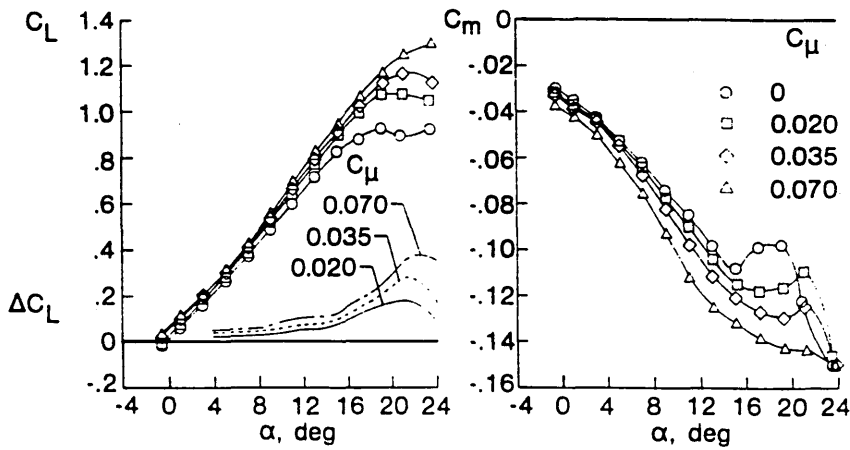


Fig. 5.10 Enhancement of C_L and $C_M - \alpha$ Curves by Spanwise Blowing ⁷⁴

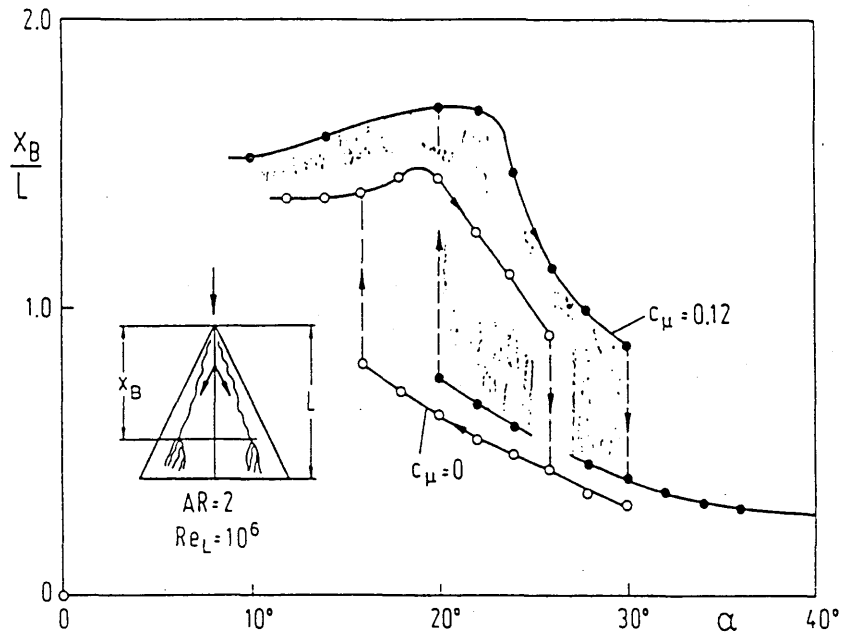


Fig.5.11 Bimodality of Vortex Breakdown Location ³⁵

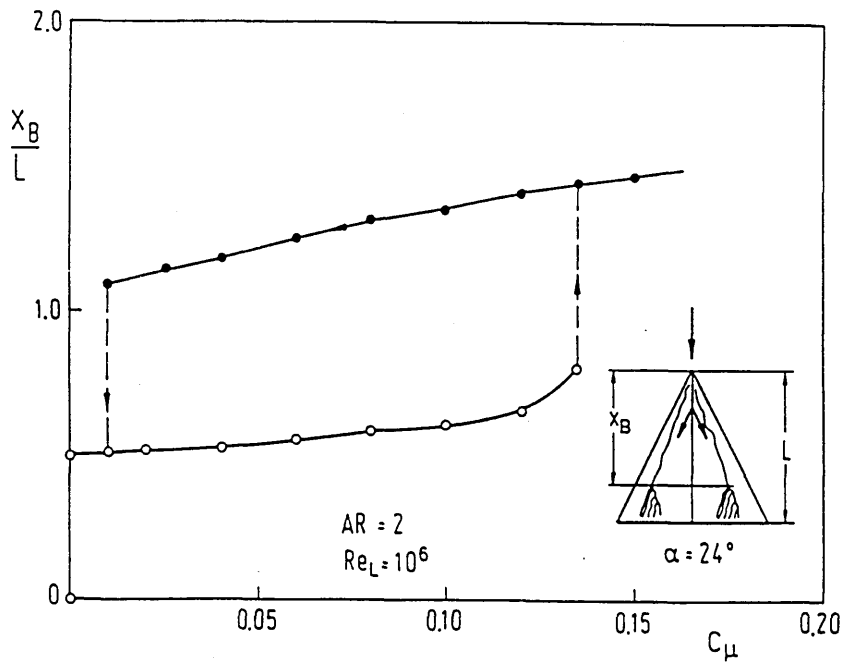


Fig.5.12 Control of Hysteresis by Spanwise Blowing ³⁵

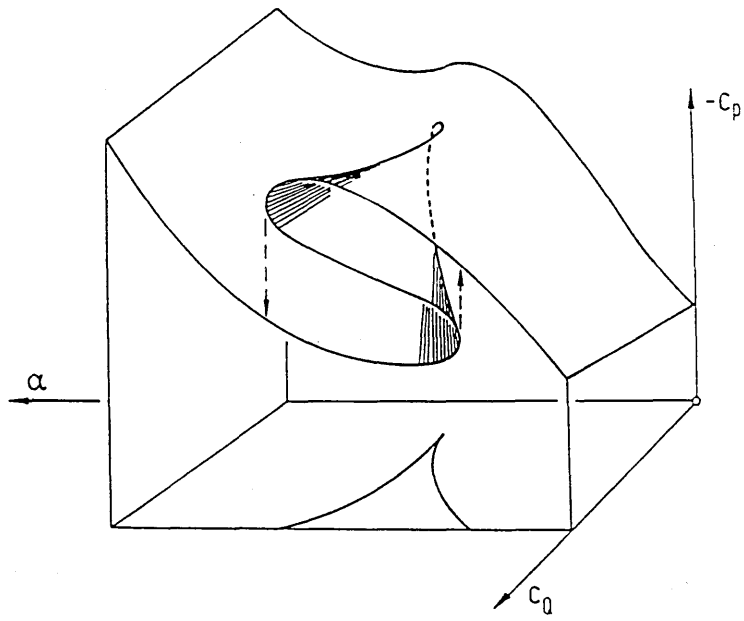


Fig.5.13 Catastrophe Surface with Control Parameters α and C_Q ³⁵



Fig.A2.1 Form of Governing Potential, Showing the Effect of a Control Parameter Variation 33

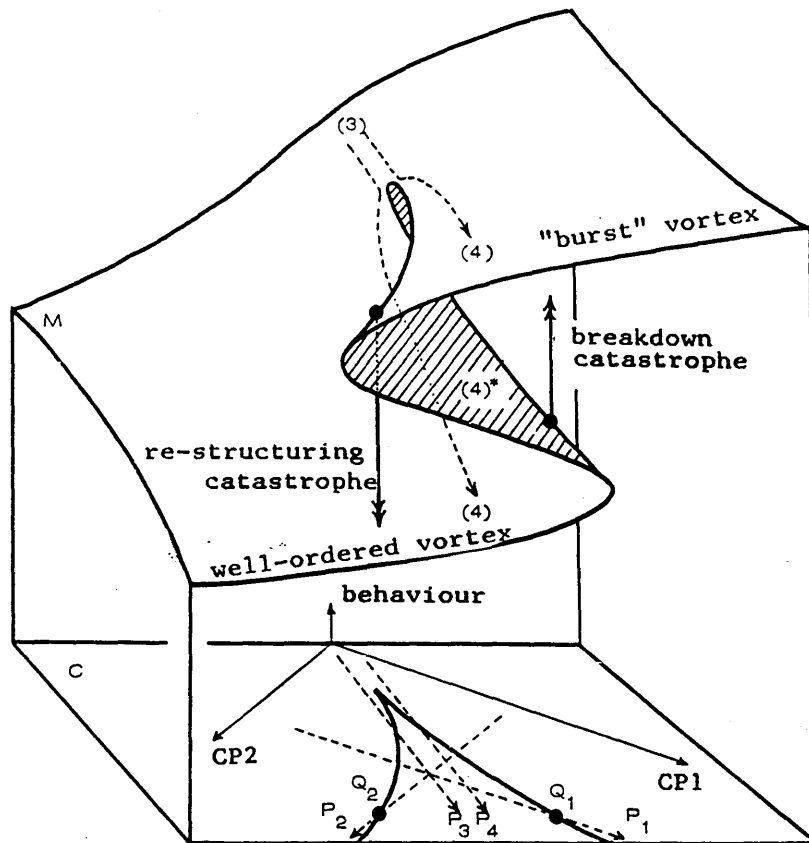


Fig.A2.2 Hypothesised Three-Dimensional Cusp Catastrophe for Vortex Breakdown

GLASGOW
UNIVERSITY
LIBRARY